

# RECLAMATION

*Managing Water in the West*

Technical Memorandum TM-85-833000-2017-10

## **Trends of Induced Seismicity and Pressures Following the 2013 Change in Injection Operations at the Paradox Valley Unit, Colorado**



## **Mission Statements**

The mission of the Department of the Interior is to protect and provide access to our Nation's natural and cultural heritage and honor our trust responsibilities to Indian Tribes and our commitments to island communities.

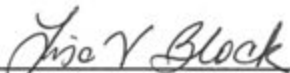
The mission of the Bureau of Reclamation is to manage, develop, and protect water and related resources in an environmentally and economically sound manner in the interest of the American public.

**BUREAU OF RECLAMATION**  
**Technical Service Center, Denver, Colorado**  
**Seismology, Geomorphology, and Geophysics Group**

**Technical Memorandum TM-85-833000-2017-10**

**Trends of Induced Seismicity Following the 2013  
Change in Injection Operations at the  
Paradox Valley Unit, Colorado**

**Prepared by:**

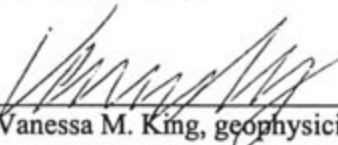
  
\_\_\_\_\_  
Lisa V. Block, geophysicist

7/12/2017  
\_\_\_\_\_  
Date

**Peer Review Certification**

This report has been reviewed and is believed to be in accordance with the service agreement and standards of the profession.

**Peer reviewed by:**

  
\_\_\_\_\_  
Vanessa M. King, geophysicist

7/12/17  
\_\_\_\_\_  
Date



# Executive Summary

In early 2013, changes in PVU injection operations were implemented in response to an induced earthquake with local magnitude ( $M_L$ ) 4.4 that occurred 8.2 km northwest of the PVU injection well. Immediately following this earthquake in January, PVU ceased injection operations for nearly three months. Injection resumed on April 17, 2013, with the same nominal flow rate as prior to the earthquake, 230 gpm, but with a 36-hour shut-in every week. On June 6, 2013, following the acquisition of new plungers for the injection pumps, the flow rate was reduced to 200 gpm and the length of the weekly shut-ins was reduced to 18 hours.

Injection pressures, subsurface pore pressures, and rates of induced seismicity decreased substantially following the injection well shut-in and change in injection protocol. Injection pressures have remained several hundred psi lower since injection resumed, compared to the peak value reached just prior to the January 2013 earthquake. Pressure diffusion modeling indicates that pore pressures decreased to a distance of roughly 4 to 7 km from the well following the changes in injection operations. Rates of induced earthquakes within 10 km of the injection well began decreasing approximately 4 to 6 months after the injection well was shut in. Rates of earthquakes within 5 km of the well decreased 72% after mid-2013, compared to the previous 2.5 years. Rates of earthquakes occurring 5 to 10 km from the well decreased 81%. Within 5 km of the injection well, this decline in seismicity rate continued a gradual decrease that had begun three years earlier. At distances of 5 to 10 km from the well, the seismicity rates had been generally increasing for three years prior to 2013 and this trend abruptly reversed. The decline in seismicity rates within 10 km of the injection well since 2013 is likely due to a combination of the extended injection well shut-down, the decreased injection flow rate and weekly shut-ins implemented in April 2013, re-distribution of stress in the vicinity of the January 2013  $M_L$  4.4 earthquake, and longer-term variations in pore pressure and stress due to the 25-year history of injection at PVU.

Recent trends of pressures and seismicity rates indicate that the beneficial effects of the operational changes made in 2013 are diminishing. Wellhead pressures, which had fluctuated in 2014-15 with little steady increase, have been increasing more consistently and more steeply since early 2016. Pressure diffusion modeling indicates that pore pressures were increasing at all distances from the well by late 2013. By the end of 2016, pore pressures at distances greater than ~0.3 – 1.4 km from the well had fully recovered and exceeded their previous maximum values by 30 to 100 psi. The rates of induced seismicity within 5 km of the well abruptly rebounded in early 2016, and the average seismicity rate for the year was comparable to that experienced during the two years prior to the 2013 change in injection operations (2011-2012). Similarly, rates of induced earthquakes 5 to 10 km from the well substantially increased in mid-2016, and rates for the second half of the year were comparable to those experienced prior to 2013. In addition, new seismicity clusters formed in this distance range during 2016, most notably two clusters within Paradox Valley, 5 to 7 km north of the injection well. The rebound in pressures and induced seismicity beginning in early 2016 is consistent with patterns observed after previous major operational changes, which also display rebounds 2.5 to 3 years after the change was implemented.

Rates of induced earthquakes occurring at distances greater than 10 km from the well showed no response to the 2013 operational changes. In addition, the geographical extent of the seismicity induced by PVU injection continued to evolve during this time. The distant seismicity expanded in some azimuthal directions, especially to the southeast, and seismicity is now occurring up to 17-20 km from the well in most directions. Some areas that were experiencing scattered seismicity prior to 2013 developed distinct seismicity clusters, such as within and north of Paradox Valley. The continued evolution of the distant induced seismicity and its insensitivity to operational changes at the well were anticipated. Pressure perturbations introduced at the injection well by operational changes are modulated with distance, and the effects of modest changes become negligible at distances beyond ~10 km. Pore pressures and associated deformational strains and stresses at these large distances will continue to increase over time as injection continues, and the distant seismicity could continue to evolve and expand for several years even if injection were to cease.

# Contents

	Page
1 Introduction .....	1
2 Seismicity Trends .....	7
2.1 Total Seismicity Rates .....	7
2.2 Seismicity Rates by Distance.....	11
2.2.1 0 to 5 km .....	11
2.2.2 5 to 10 km .....	16
2.2.3 Greater than 10 km.....	20
2.2.4 Summary .....	24
2.3 Geographical Distribution of Induced Seismicity.....	25
3 Pressure Trends.....	33
3.1 Injection Pressures .....	33
3.2 Pore Pressures .....	39
3.2.1 Initial Model.....	39
3.2.2 Additional Models .....	49
3.2.2.1 Varying Effective Borehole Radius.....	50
3.2.2.2 Varying Diffusivity.....	54
3.3 Summary.....	59
4 Conclusions .....	61
5 References .....	63
Pressure Modeling Methods .....	Appendix A

# Figures

	Page
Figure 1-1: Location of the deep injection well at Reclamation's Paradox Valley Unit in western Colorado.....	2
Figure 1-2: Location of the Paradox Valley Unit extraction wells and injection well .....	3
Figure 1-3: Lower plot: scatter plot of earthquakes with magnitudes $\geq 0.5$ and depths $< 8.5$ km (relative to the ground surface elevation at the injection wellhead), plotted as a function of date and distance from the PVU injection well. Upper plot: daily average injection flow rate. ....	4
Figure 1-4: Map of shallow earthquakes (depth $\leq 8.5$ km) recorded since the start of PVU fluid injection (through 12/31/2016).....	5
Figure 2-1: 2011 – 2016 occurrence rates of earthquakes (at all distances from the injection well) with depths $< 10$ km and duration magnitudes $\geq 0.5$ . (a) monthly event counts (b) quarterly event counts (c) one-sided (backward) 12-month event counts.....	9

Figure 2-2: 2011 – 2016 occurrence rates of earthquakes (at all distances from the injection well) with depths < 10 km and duration magnitudes  $\geq 1.5$ . (a) monthly event counts (b) quarterly event counts (c) one-sided (backward) 12-month event counts..... 10

Figure 2-3: 2011 – 2016 occurrence rates of earthquakes  $\leq 5$  km from the injection well, with depths < 10 km and duration magnitudes  $\geq 0.5$ . (a) monthly event counts (b) quarterly event counts (c) one-sided (backward) 12-month event counts ..... 13

Figure 2-4: 2005 – 2016 occurrence rates of earthquakes  $\leq 5$  km from the injection well, with depths < 10 km and duration magnitudes  $\geq 0.5$ . (a) monthly event counts (b) quarterly event counts (c) one-sided (backward) 12-month event counts ..... 14

Figure 2-5: 2005 – 2016 occurrence rates of earthquakes  $\leq 5$  km from the injection well, with depths < 10 km and duration magnitudes  $\geq 1.5$ . (a) monthly event counts (b) quarterly event counts (c) one-sided (backward) 12-month event counts ..... 15

Figure 2-6: 2011 – 2016 occurrence rates of earthquakes > 5 km and  $\leq 10$  km from the injection well, with depths < 10 km and duration magnitudes  $\geq 0.5$ . (a) monthly event counts (b) quarterly event counts (c) one-sided (backward) 12-month event counts..... 17

Figure 2-7: 2005 – 2016 occurrence rates of earthquakes > 5 km and  $\leq 10$  km from the injection well, with depths < 10 km and duration magnitudes  $\geq 0.5$ . (a) monthly event counts (b) quarterly event counts (c) one-sided (backward) 12-month event counts..... 18

Figure 2-8: 2005 – 2016 occurrence rates of earthquakes > 5 km and  $\leq 10$  km from the injection well, with depths < 10 km and duration magnitudes  $\geq 1.5$ . (a) monthly event counts (b) quarterly event counts (c) one-sided (backward) 12-month event counts..... 19

Figure 2-9: 2011 – 2016 occurrence rates of earthquakes > 10 km from the injection well, with depths < 10 km and duration magnitudes  $\geq 0.5$ . (a) monthly event counts (b) quarterly event counts (c) one-sided (backward) 12-month event counts ..... 21

Figure 2-10: 2005 – 2016 occurrence rates of earthquakes > 10 km from the injection well, with depths < 10 km and duration magnitudes  $\geq 0.5$ . (a) monthly event counts (b) quarterly event counts (c) one-sided (backward) 12-month event counts. .... 22

Figure 2-11: 2005 – 2016 occurrence rates of earthquakes > 10 km from the injection well, with depths < 10 km and duration magnitudes  $\geq 1.5$ . (a) monthly event counts (b) quarterly event counts (c) one-sided (backward) 12-month event counts. .... 23

Figure 2-12: Maps showing the geographical distribution of seismicity induced by PVU fluid injection over time: (a) 1991 – 1995 (b) 1996 – 2000 (c) 2001 – 2004 (d) 2005 – 2008 (e) 2009 – 2012 (f) 2013 – 2016..... 26

Figure 2-13: Maps showing the geographical distribution of seismicity induced by PVU fluid injection in recent years: (a) 2013 (b) 2014 (c) 2015 (d) 2016..... 30

Figure 3-1: Daily average injection flow rate, daily average surface injection pressure, daily average downhole pressure at 4.3 km depth, and cumulative volume of fluid injected from 1991 to 2016. .... 35

Figure 3-2: Daily average injection flow rate, daily average surface injection pressure, daily average downhole pressure at 4.3 km depth, and cumulative volume of brine injected from 2011 to 2016. .... 36

Figure 3-3: Daily average surface and downhole pressures and 91-day centered moving averages of the pressures from April 2013 to December 2016..... 37

Figure 3-4: PVU injection well downhole pressures averaged over daily, 6-month, 18-month, and 30-month time periods (top) and occurrence of shallow seismicity as a function of date and magnitude: within 5 km of the injection well, at distances of 5 to 10 km from the well, and at distances greater than 10 km from the injection well ..... 38

Figure 3-5: Pore-pressure variation over time at the PVU injection well (upper plot) and at multiple distances ( $r$ ) from the well (lower plot). These pressure trends represent the increase in pore pressure due to injection ..... 40

Figure 3-6: Pore-pressure variations over time at six radial distances from the well, computed using the initial diffusion model with  $D = 0.115 \text{ m}^2/\text{s}$  and  $r_w = 10 \text{ cm}$ ..... 41

Figure 3-7: Summary plots of the results from the initial pressure diffusion model with  $D = 0.115 \text{ m}^2/\text{s}$  and  $r_w = 10 \text{ cm}$  for the time period following the injection well shut-in and reduced flow rate implemented in 2013. The left plot shows the dates when pore pressures began decreasing following the injection well shut-in, as a function of distance from the well, and the dates when the pressures recovered to their previous maximum values. The right plot shows the size of the largest pressure decrease as a function of distance from the injection well. .... 42

Figure 3-8: Pore pressures as a function of distance from the well on the day before the January 2013 injection well shut-in (1/22/2013) and on the day before injection resumed (4/16/2013) (upper plot) and the difference between these two curves (lower plot). These results are from the initial diffusion model with  $D = 0.115 \text{ m}^2/\text{s}$  and  $r_w = 10 \text{ cm}$ . .... 44

Figure 3-9: Pore pressures as a function of distance from the well on the day before the January 2013 injection well shut-in (1/22/2013) and on 12/31/2013 (upper plot) and the difference between these two curves (lower plot). These results are from the initial diffusion model with  $D = 0.115 \text{ m}^2/\text{s}$  and  $r_w = 10 \text{ cm}$ . .... 45

Figure 3-10: Pore pressures as a function of distance from the well on the day before the January 2013 injection well shut-in (1/22/2013) and on 6/30/2014 (upper plot) and the difference between these two curves (lower plot). These results are from the initial diffusion model with  $D = 0.115 \text{ m}^2/\text{s}$  and  $r_w = 10 \text{ cm}$ . .... 46

Figure 3-11: Pore pressures as a function of distance from the well on the day before the January 2013 injection well shut-in (1/22/2013) and on 12/31/2014 (upper plot) and the difference

between these two curves (lower plot). These results are from the initial diffusion model with  $D = 0.115 \text{ m}^2/\text{s}$  and  $r_w = 10 \text{ cm}$ . ..... 47

Figure 3-12: Pore pressures as a function of distance from the well on the day before the January 2013 injection well shut-in (1/22/2013) and on 12/31/2015 (upper plot) and the difference between these two curves (lower plot). These results are from the initial diffusion model with  $D = 0.115 \text{ m}^2/\text{s}$  and  $r_w = 10 \text{ cm}$ . ..... 48

Figure 3-13: Pore pressures as a function of distance from the well on the day before the January 2013 injection well shut-in (1/22/2013) and on 12/31/2016 (upper plot) and the difference between these two curves (lower plot). These results are from the initial diffusion model with  $D = 0.115 \text{ m}^2/\text{s}$  and  $r_w = 10 \text{ cm}$ . ..... 49

Figure 3-14: Summary plots of the results from pressure diffusion models with  $D = 0.115 \text{ m}^2/\text{s}$  and  $r_w = 10 \text{ cm}$ ,  $10 \text{ m}$ ,  $100 \text{ m}$ ,  $250 \text{ m}$ , and  $500 \text{ m}$  for the time period following the injection well shut-in and reduced flow rate implemented in 2013. The left plot shows the dates when pore pressures began decreasing following the injection well shut-in, as a function of distance from the well, and the dates when the pressures recovered to their previous maximum values. The right plot shows the size of the largest pressure decrease as a function of distance from the injection well for each model. .... 51

Figure 3-15: Pore pressures as a function of distance from the well on the day before the January 2013 injection well shut-in (1/22/2013) and on 12/31/2016 (upper plots) and the difference between these two curves (lower plots). Results are shown for pressure diffusion models using  $D = 0.115 \text{ m}^2/\text{s}$  and  $r_w = 10 \text{ cm}$  (left plots) and  $r_w = 500 \text{ m}$  (right plots). ..... 52

Figure 3-16: Differences in pore pressure, as a function of distance from the well, from the day before the injection well was shut in (1/22/2013) to (from top to bottom): the day before injection resumed (4/16/2013), 12/31/2013, 12/31/2014, 12/31/2015, and 12/31/2016. Results are shown for pore pressure diffusion models with  $r_w = 10 \text{ cm}$  and  $r_w = 500 \text{ m}$ . The diffusivity,  $D$ , is  $0.115 \text{ m}^2/\text{s}$  for all models. .... 53

Figure 3-17: Summary plots of the results from pressure diffusion models with  $D = 0.115 \text{ m}^2/\text{s}$  and  $D = 0.2 \text{ m}^2/\text{s}$  and  $r_w = 10 \text{ cm}$  and  $r_w = 500 \text{ m}$  for the time period following the injection well shut-in and reduced flow rate implemented in 2013. The left plot shows the dates when pore pressures began decreasing following the injection well shut-in, as a function of distance from the well, and the dates when the pressures recovered to their previous maximum values. The right plot shows the size of the largest pressure decrease as a function of distance from the injection well for each model. .... 54

Figure 3-18: Pore pressures as a function of distance from the well on the day before the January 2013 injection well shut-in (1/22/2013) and on 12/31/2016 (upper plots) and the difference between these two curves (lower plots). Results are shown for pressure diffusion models using  $r_w = 10 \text{ cm}$  and  $D = 0.115 \text{ m}^2/\text{s}$  (left plots) and  $D = 0.2 \text{ m}^2/\text{s}$  (right plots). .... 56

Figure 3-19: Pore pressures as a function of distance from the well on the day before the January 2013 injection well shut-in (1/22/2013) and on 12/31/2016 (upper plots) and the difference

between these two curves (lower plots). Results are shown for pressure diffusion models using  $r_w = 500$  m and  $D = 0.115$  m<sup>2</sup>/s (left plots) and  $D = 0.2$  m<sup>2</sup>/s (right plots). ..... 56

Figure 3-20: Differences in pore pressure, as a function of distance from the well, from the day before the injection well was shut in (1/22/2013) to (from top to bottom): the day before injection resumed (4/16/2013), 12/31/2013, 12/31/2014, 12/31/2015, and 12/31/2016. Results are shown for pore pressure diffusion models with  $D = 0.115$  m<sup>2</sup>/s and  $D = 0.2$  m<sup>2</sup>/s. The effective borehole radius,  $r_w$ , is 10 cm for all models. .... 57

Figure 3-21: Differences in pore pressure, as a function of distance from the well, from the day before the injection well was shut in (1/22/2013) to (from top to bottom): the day before injection resumed (4/16/2013), 12/31/2013, 12/31/2014, 12/31/2015, and 12/31/2016. Results are shown for pore pressure diffusion models with  $D = 0.115$  m<sup>2</sup>/s and  $D = 0.2$  m<sup>2</sup>/s. The effective borehole radius,  $r_w$ , is 500 m for all models. .... 58

## Tables

Table 2-1: Summary of the decreases in seismicity rates following the 2013 injection well shut-in and subsequent change in injection protocol. .... 25

Table 2-2: Summary of recent increases in seismicity rates. .... 25



# 1 Introduction

The Bureau of Reclamation (Reclamation) operates a deep injection well in western Colorado as part of the Paradox Valley Unit (PVU), a component of the Colorado River Basin Salinity Control Project (Figure 1-1). PVU intercepts salt brine that would otherwise flow into the Dolores River, a tributary of the Colorado River. The brine is intercepted with a series of shallow extraction wells along the Dolores River (Figure 1-2). The diverted brine is injected at high pressure into a deep disposal well, designated PVU Salinity Control Well No. 1. Injection began in July, 1991, with a series of injection tests that continued into 1995. In mid-1996, Reclamation began nearly continuous, long-term brine disposal.

Relatively shallow (mostly 2.5- to 6.5-km-deep) earthquakes are induced in response to the brine injection at PVU. Reclamation maintains and operates the 20-station Paradox Valley Seismic Network (PVSN) to monitor this induced seismicity. The initial earthquakes, detected four days after the start of the first injection test in July 1991, occurred within 300 m of the injection well. As injection continued, earthquakes occurred at progressively increasing radial distances. To date, earthquakes interpreted to be related to PVU fluid injection have been observed at distances up to about 20 km from the injection well (Figure 1-3).

Nearly all of the more than 6000 earthquakes that PVSN has recorded since the start of PVU fluid injection have duration magnitudes ( $M_D$  or  $M$ ) less than 2.5, the approximate threshold for human detection in the area. However, 75 earthquakes with  $M_D \geq 2.5$  have occurred (through 12/31/2016), including five earthquakes with magnitude  $\geq 3.5$  (Figure 1-4). Reclamation has changed injection operations three times in response to these larger events: in mid-1999, two 20-day injection well shut-ins each year were implemented; in mid-2000, the injection flow rate was decreased by about one-third; and in early 2013, the nominal flow rate was decreased an additional 13% and weekly shut-ins replaced the bi-annual shut-ins (for a decrease in effective flow rate of ~9%).

The operational changes implemented in 2013 were made in response to an induced earthquake with local magnitude ( $M_L$ ) 4.4 that occurred 8.2 km northwest of the PVU injection well in January of that year. The earthquake occurred at 4:46 on January 24 in Coordinated Universal Time (UTC), the time system in which the earthquake data are recorded, or at 9:46 p.m. on January 23 in Mountain Standard Time (MST), which is the time system used when recording the injection data at the well. (More information about this earthquake can be found in Wood et al., 2016 and Block et al., 2014.) Immediately following this earthquake (at 9:50 p.m.), PVU ceased injection operations for nearly three months. Injection resumed on April 17, 2013, with the same nominal flow rate as prior to the earthquake, 230 gallons per minute (gpm), but with a 36-hour shut-in every week. On June 6, 2013, following the acquisition of new plungers for the injection pumps, the flow rate was reduced to 200 gpm and the length of the weekly shut-ins was reduced to 18 hours. The decrease in flow rate and change from bi-annual to weekly shut-ins was based on modeling of the pressure-flow data at the injection well (Wood et al., 2016) and the observation that lower long-term average injection pressures were correlated with decreased rates and magnitudes of near-well induced seismicity (Block and Wood, 2009).

In this report, we review the trends of induced seismicity that have been observed since the 3-month injection well shut down and subsequent change in PVU injection protocol implemented in 2013. We compare the trends from recent years (2013 – 2016) to historical seismicity patterns to evaluate the

effectiveness of the most recent operational change in reducing the rates and magnitudes of induced earthquakes.

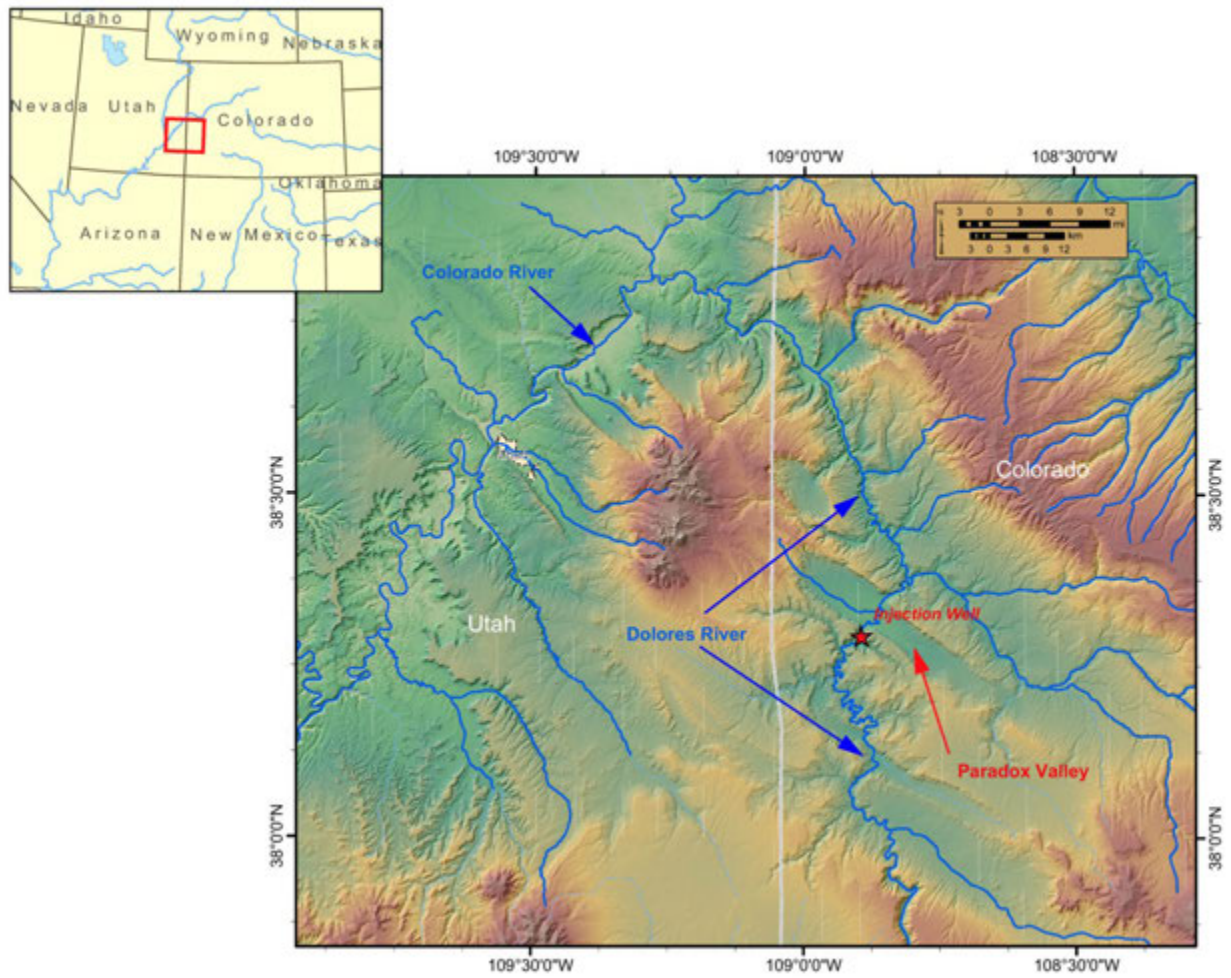


**Figure 1-1: Location of the deep injection well at Reclamation's Paradox Valley Unit in western Colorado.**

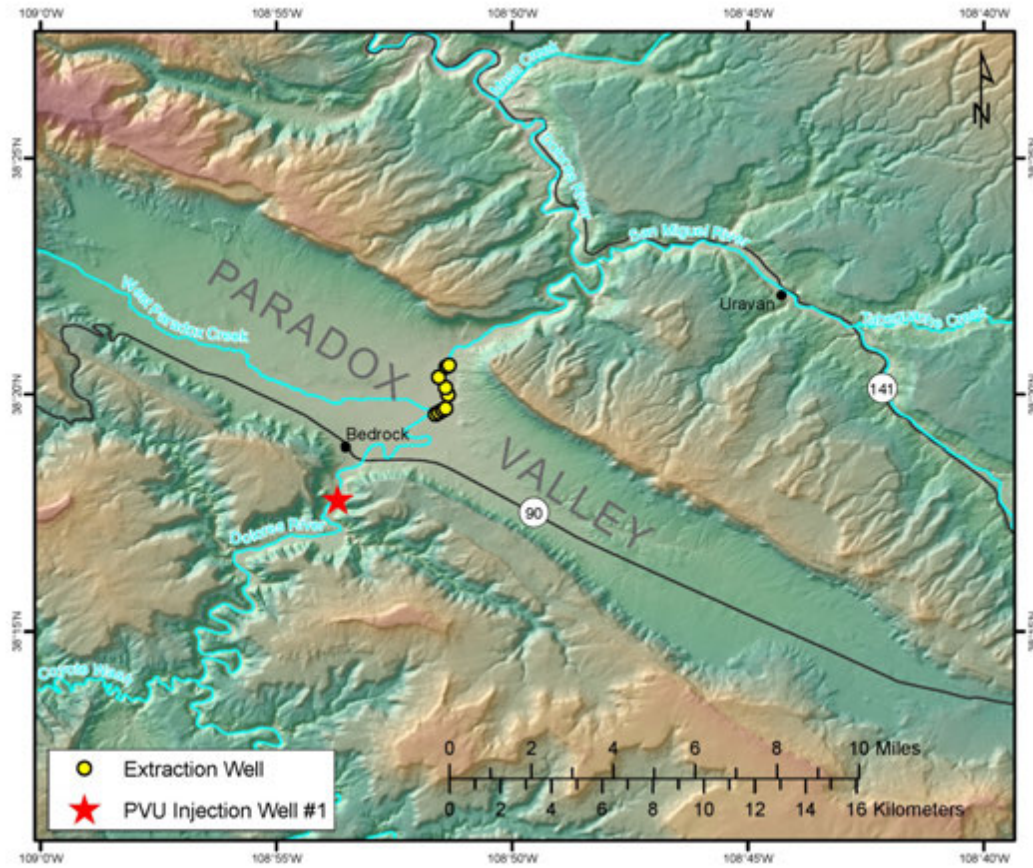
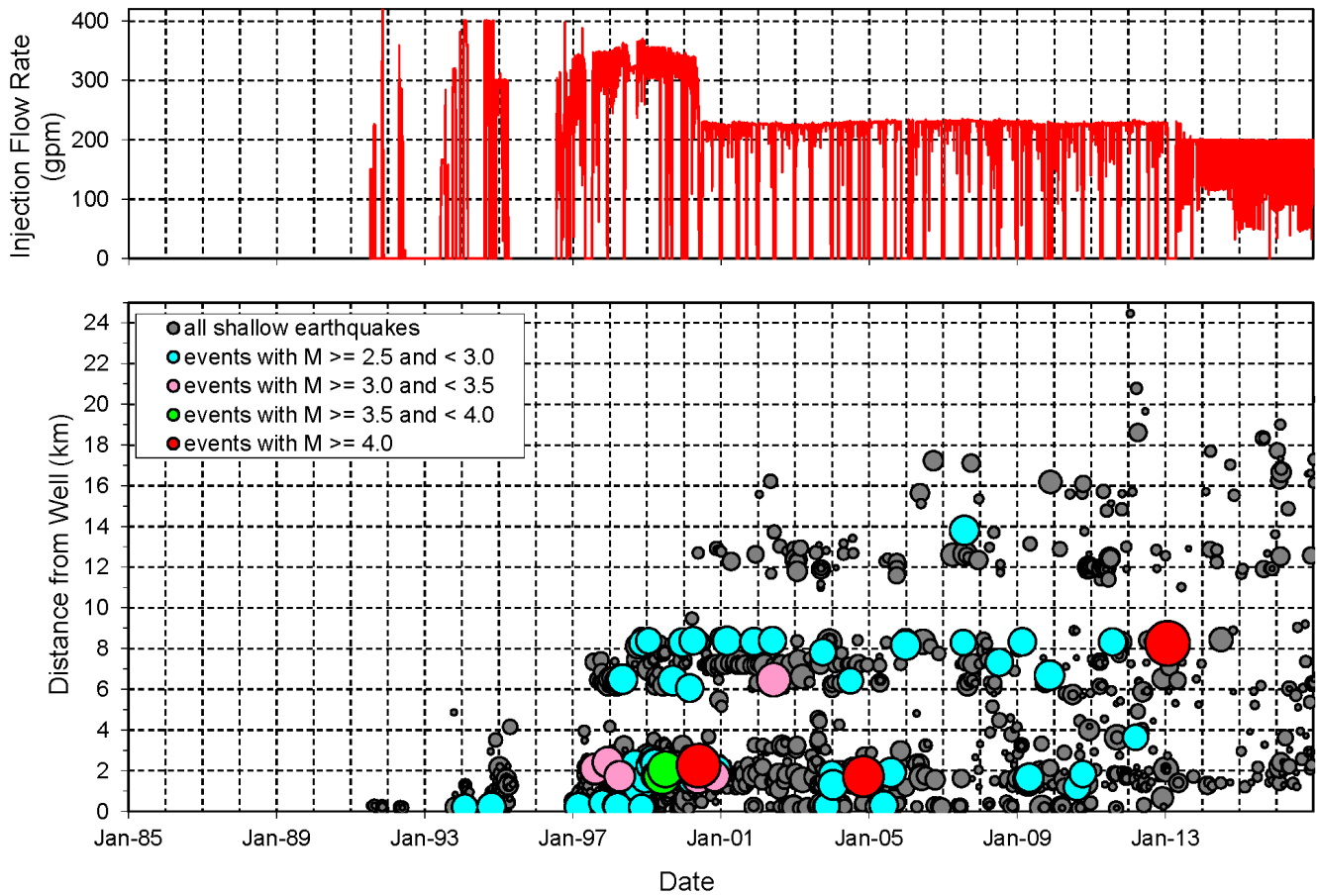


Figure 1-2: Location of the Paradox Valley Unit extraction wells (yellow circles) and injection well (red star).



**Figure 1-3: Lower plot: scatter plot of earthquakes with magnitudes  $\geq 0.5$  and depths  $< 8.5$  km (relative to the ground surface elevation at the injection wellhead), plotted as a function of date and distance from the PVU injection well. Each circle represents a single earthquake, with the width of the circle scaled by the event magnitude. Upper plot: daily average injection flow rate.**

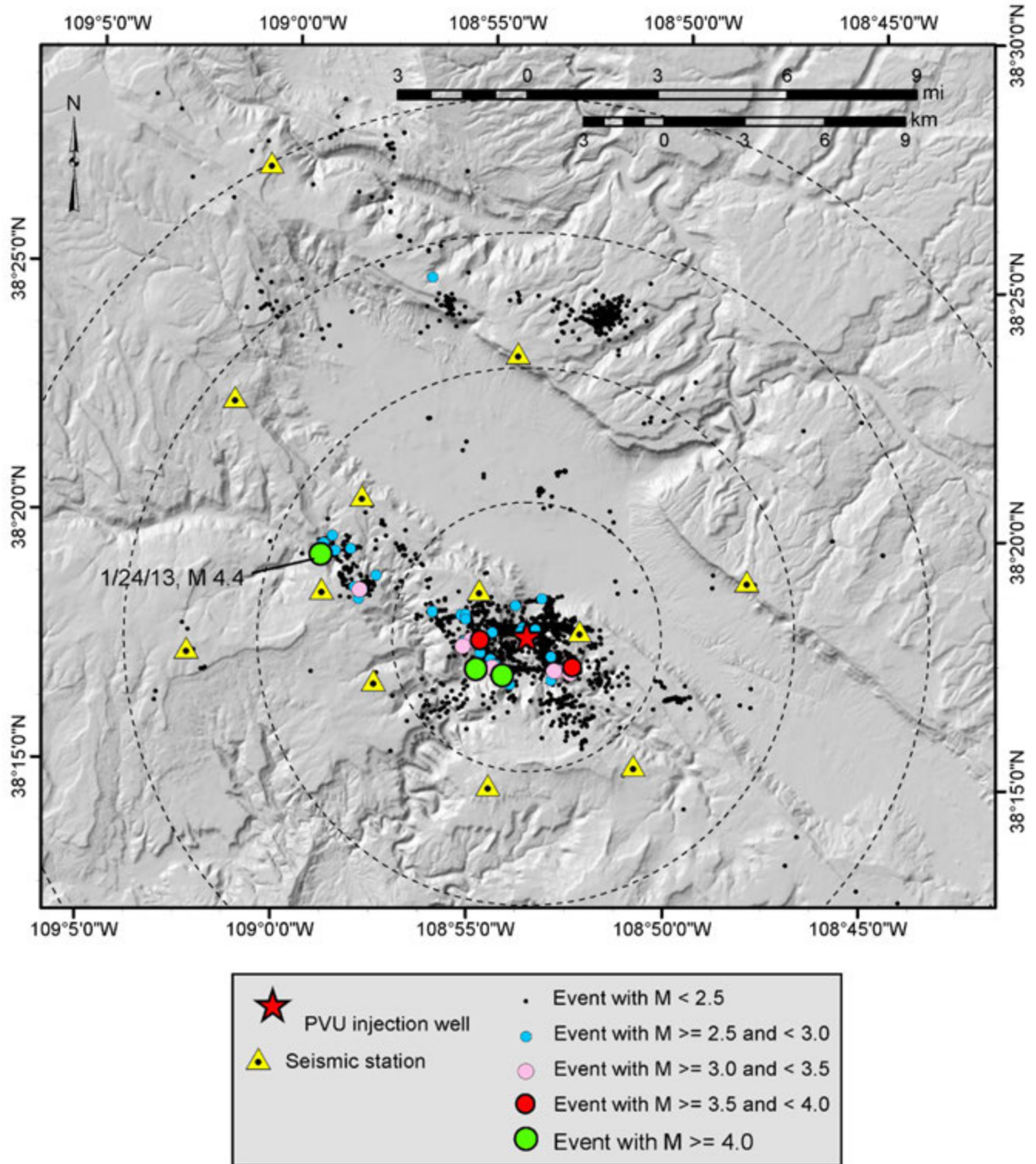


Figure 1-4: Map of shallow earthquakes (depth  $\leq 8.5$  km) recorded since the start of PVU fluid injection (through 12/31/2016). Symbol sizes and colors indicate event magnitudes. The  $M_L$  4.4 earthquake that occurred on January 24, 2013 is labeled. The large dashed circles mark distances of 5, 10, 15, and 20 km from the injection well.



## 2 Seismicity Trends

### 2.1 Total Seismicity Rates

Rates of PVU-induced seismicity decreased substantially following the 3-month injection well shut-down in early 2013 and subsequent resumption of injection at a lower flow rate (on April 17, 2013). The plots presented in Figure 2-1 show the decreased seismicity rate in several ways. These plots show the number of shallow earthquakes having duration magnitude  $\geq 0.5$  recorded from January 2011 (two years before the shut-down) through December 2016 (three years and eight months after resumption of injection). Shallow earthquakes are defined as those having depth  $< 10$  km, relative to the ground surface elevation at the injection well. Only earthquakes shallower than 10 km are included because the few deeper events that have been recorded are considered naturally induced. Events with magnitude less than  $M_D 0.5$  are excluded from the analysis because detection of events smaller than this magnitude threshold is incomplete, and counts of these events are biased by temporal variations in the operating status of the seismic network. With the exception of August and September, 2016, when the magnitude completeness threshold of the seismic network temporarily increased to approximately  $M_D 1.5$  due to severely deteriorated radio data communications (Block et al., 2017), temporal variations in the number of events with  $M_D \geq 0.5$  is considered robust. The upper plot in Figure 2-1 shows the monthly event counts, the middle plot shows the quarterly counts, and the lower plot shows a one-sided (backward) 12-month running event count.

The monthly event counts show considerable variation from month to month (Figure 2-1a). This variation is reduced somewhat in the plot of quarterly event counts (Figure 2-1b). Each of these plots shows the data recorded for a given interval, either for one month or one quarter (three months). The curve shown in the lower plot (Figure 2-1c) is a running event count. For a given point on the curve, corresponding to a given date, the event count plotted on the y-axis corresponds to the number of events recorded during the 12-month period ending on that date. A new point is computed for each successive quarter. In this type of running curve, abrupt changes in event counts over time are significantly smoothed.

The monthly and quarterly plots in Figure 2-1 indicate that the event counts were substantially lower from mid-2013 to late 2015 (after the change in injection operations) than in 2011 to mid-2013. During the 2.5-year period from January 2011 to June 2013, 195 events with  $M_D \geq 0.5$  ( $M 0.5+$ ) were recorded, corresponding to an average rate of 19.5 events per quarter. In contrast, only 46  $M 0.5+$  events occurred during the subsequent 2.5-year period from July 2013 to December 2015, corresponding to an average rate of 4.6 events per quarter. This represents a decrease in the  $M 0.5+$  seismicity rate of 76%. The running event count curve in Figure 2-1c indicates that the decline in seismicity rate actually began at least a year prior to the January 2013 injection well shut-down and continued until mid-2014 before leveling off. Seismicity rates subsequently began to rebound in late 2015. Fifty-four  $M 0.5+$  events were detected during 2016, corresponding to an average rate of 13.5 events per quarter. This is 69% of the rate experienced

in 2011 to mid-2013. Because of PVSN's severely deteriorated event detection capabilities in August-September, 2016, the average rate of M 0.5+ events computed for 2016 is almost certainly underestimated. If we exclude the third quarter of 2016 from the calculations because of the deteriorated event detection capabilities, then the average quarterly rate of M 0.5+ events for 2016 is 15.3, corresponding to 78% of the rate experienced in 2011 to mid-2013.

The same types of plots showing only the rates of the larger events, those with  $M_D \geq 1.5$  are presented in Figure 2-2. The rate of occurrence of events with  $M_D \geq 1.5$  decreased markedly a few months after the injection well shut-down in 2013. During the 2.5-year period from January 2011 to June 2013, 32 events with  $M_D \geq 1.5$  were recorded, corresponding to an average rate of 3.2 events per quarter. In contrast, only four events in this magnitude range occurred during the subsequent 2.5-year period (after the change in injection operations) from July 2013 to December 2015, corresponding to an average rate of 0.4 events per quarter. This represents a decrease in the M 1.5+ seismicity rate of 88%. In early 2016, the rate of occurrence of events with  $M_D \geq 1.5$  abruptly increased, with seven such events occurring during the first quarter (Jan. – Mar., 2016). No M 1.5+ events occurred during the second or third quarters of 2016, but two additional M 1.5+ events were recorded during the last quarter. Hence, the total number of M 1.5+ events for 2016 was nine, corresponding to an average quarterly rate of 2.25. This is 70% of the average quarterly rate observed prior to mid-2013.

M 0.5+ Events at All Distances

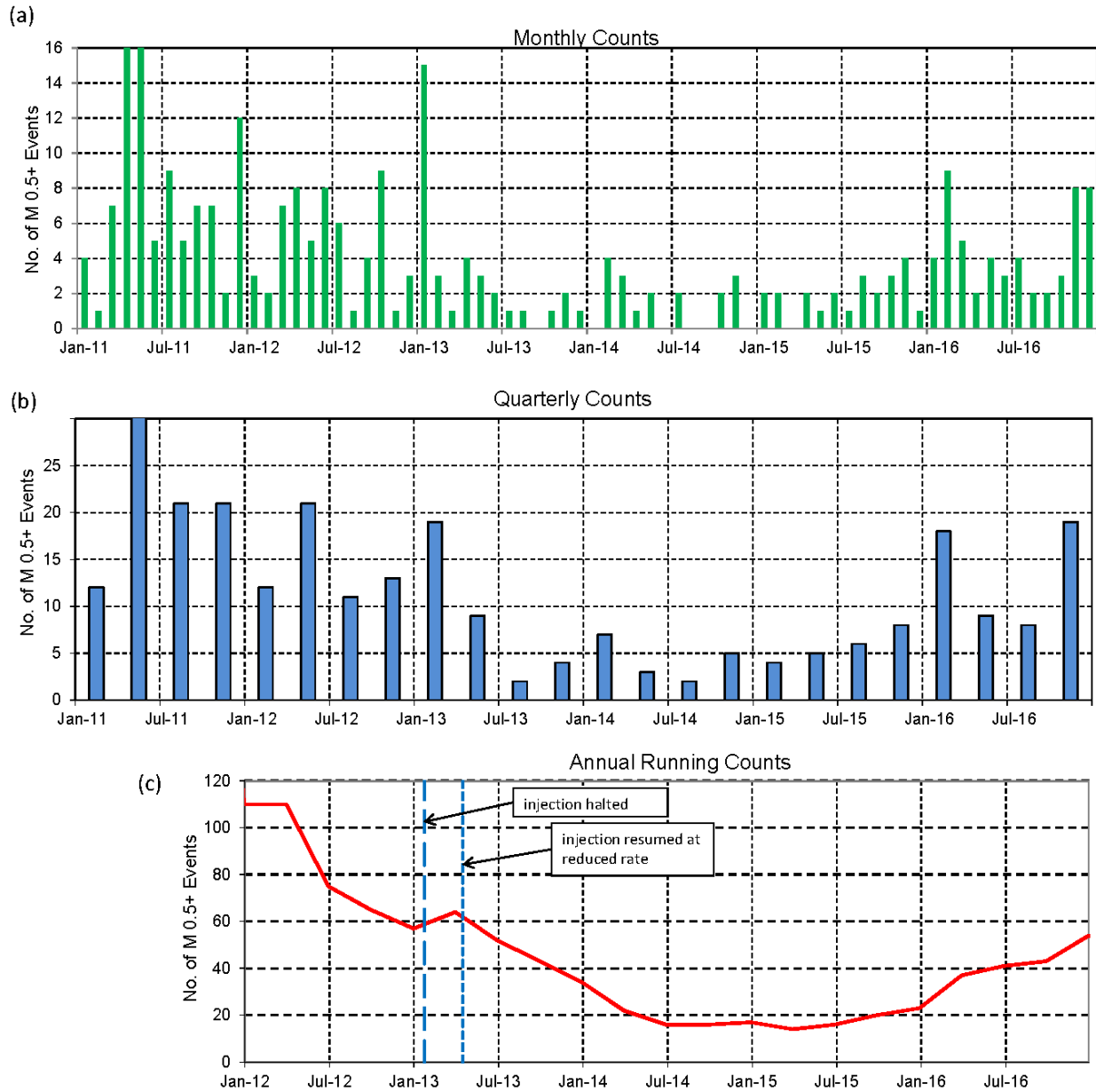


Figure 2-1: 2011 – 2016 occurrence rates of earthquakes (at all distances from the injection well) with depths < 10 km and duration magnitudes  $\geq 0.5$ . (a) monthly event counts (b) quarterly event counts (c) one-sided (backward) 12-month event counts. High event counts in 2011 are clipped.

### M 1.5+ Events at All Distances

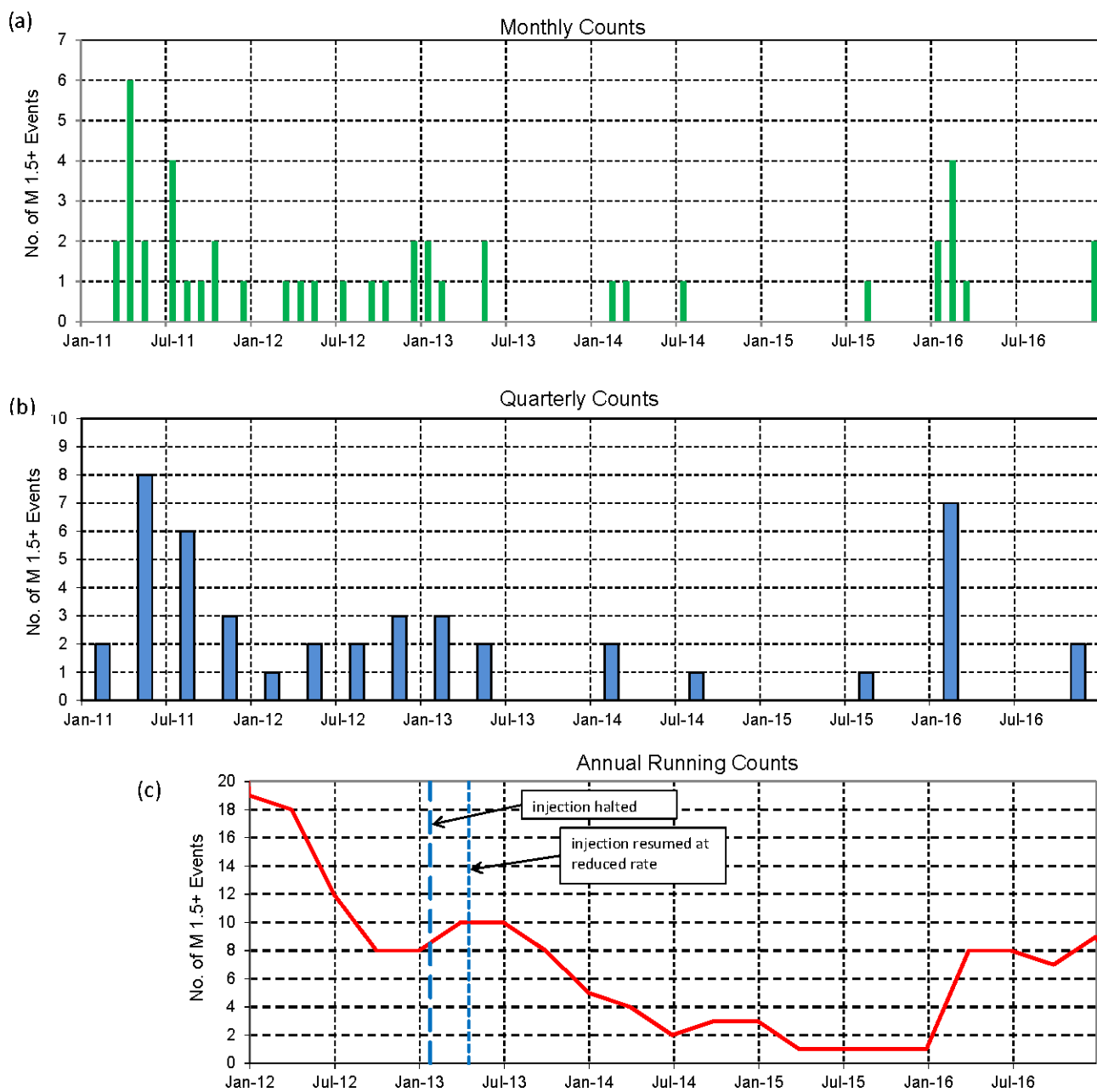


Figure 2-2: 2011 – 2016 occurrence rates of earthquakes (at all distances from the injection well) with depths < 10 km and duration magnitudes  $\geq 1.5$ . (a) monthly event counts (b) quarterly event counts (c) one-sided (backward) 12-month event counts.

## 2.2 Seismicity Rates by Distance

The time that it takes the induced seismicity to respond to changes in injection operations is expected to increase with distance from the injection well. Just as it took years after the start of injection for the induced seismicity to begin at distances of several km from the injection well (Figure 1-3), it could take years for the induced seismicity at large ( $> 10$  km) distances from the injection well to show a response to changes in injection operations. In this section we examine seismicity rates for three distance ranges: 0 to 5 km, 5 to 10 km, and greater than 10 km. For each region, we examine the changes in recent seismicity rates (2013 – 2016) in the context of longer-term variations in seismicity rates to evaluate how the extended injection well shut-down in 2013 and subsequent injection at a reduced flow rate may have affected the induced seismicity. Because it took at least a few months for seismicity rates to decline following the changes in injection operations implemented in early 2013, even at relatively small distances from the well, we use mid-2013 (July) as the starting date for evaluating seismicity rates after the changes in injection operations.

### 2.2.1 0 to 5 km

The plots presented in Figure 2-3 show that the rates of events (with  $M_D \geq 0.5$ ) within 5 km of the injection well peaked in mid-2011 to mid-2012 and subsequently began decreasing. Event counts decreased further after the change in injection operations in 2013 and remained very low through 2015. Near-well seismicity rates began increasing in early 2016.

To put these recent variations in near-well seismicity rates into perspective, Figure 2-4 shows the seismicity rate plots extending back to the beginning of 2005. This plot clearly shows that the decreasing near-well seismicity rates in recent years are part of a longer trend. The 12-month event counts peaked previously in early 2010 at a value of 66 (Figure 2-4c). These 12-month event counts had already decreased by 61%, to a value of 26, prior to the injection well shut-down in 2013. Following the shut-down and subsequent change to a lower flow rate, the 12-month event counts continued to decrease, reaching a minimum value of 5 in early 2015. This represents an additional 32% decrease in seismicity rate, relative to the peak value in 2010.

Near-well seismicity rates increased in early 2016 and are approaching rates that were more typical prior to 2013 (Figure 2-4a and b). The quarterly average rate of M 0.5+ near-well earthquakes during 2016 (excluding the third quarter because of deteriorated event detection capabilities) was 7.3, compared to an average quarterly rate of 6.5 during the 2.5-year period from January 2011 to June 2013 and an average quarterly rate of 12.5 in 2009-2010. In contrast, the average quarterly rate of M 0.5+ events following the change in injection operations, from July 2013 through December 2015, was only 1.8 events/quarter.

The rates of the larger-magnitude near-well events ( $M_D \geq 1.5$ ), from 2005 to early 2016, are shown in Figure 2-5. The trends are similar to those described above. The rates of near-well M 1.5+ events began decreasing in 2010, prior to the 2013 change in injection operations. Relative to the peak 12-month event count of 21 in early 2010, the annual rate of M 1.5+ events had already decreased 90%, to a value of only 2, by January 2013. Annual rates decreased an

additional 10%, to a value of 0, by early 2015. The rate of larger-magnitude near-well events increased in early 2016, with three such events occurring in the first quarter (Figure 2-5a and b). However, no additional M 1.5+ near-well earthquakes occurred during the rest of 2016.

While the rates of near-well induced seismicity have been lower since the 2013 change in injection operations than before, we cannot quantify how much of the decrease is attributable to the change in PVU operations and how much is a continuation of the previous long-term trend. One of the fundamental shortcomings of trying to evaluate the effectiveness of a change in injection operations from observations of induced seismicity is that we cannot know what induced seismicity would have occurred if the change had not been made. Assuming that at least part of the decreased rate of near-well seismicity observed since 2013 is due to the injection well shut-down and subsequent injection at a decreased flow rate, then the increase in near-well seismicity rates in the last year suggests that the effects of these changes are diminishing.

M 0.5+ Events within 5 km of the Injection Well

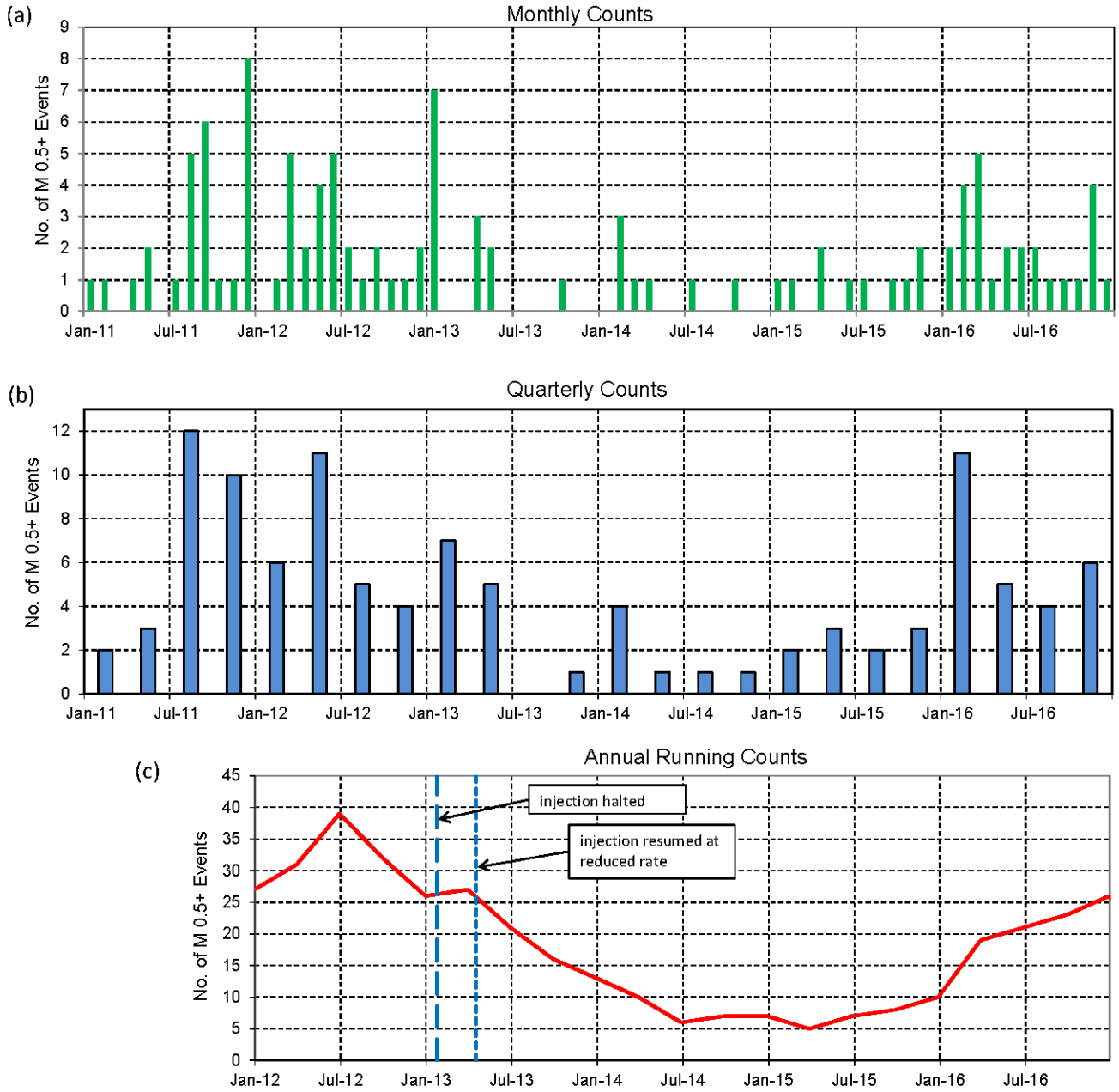
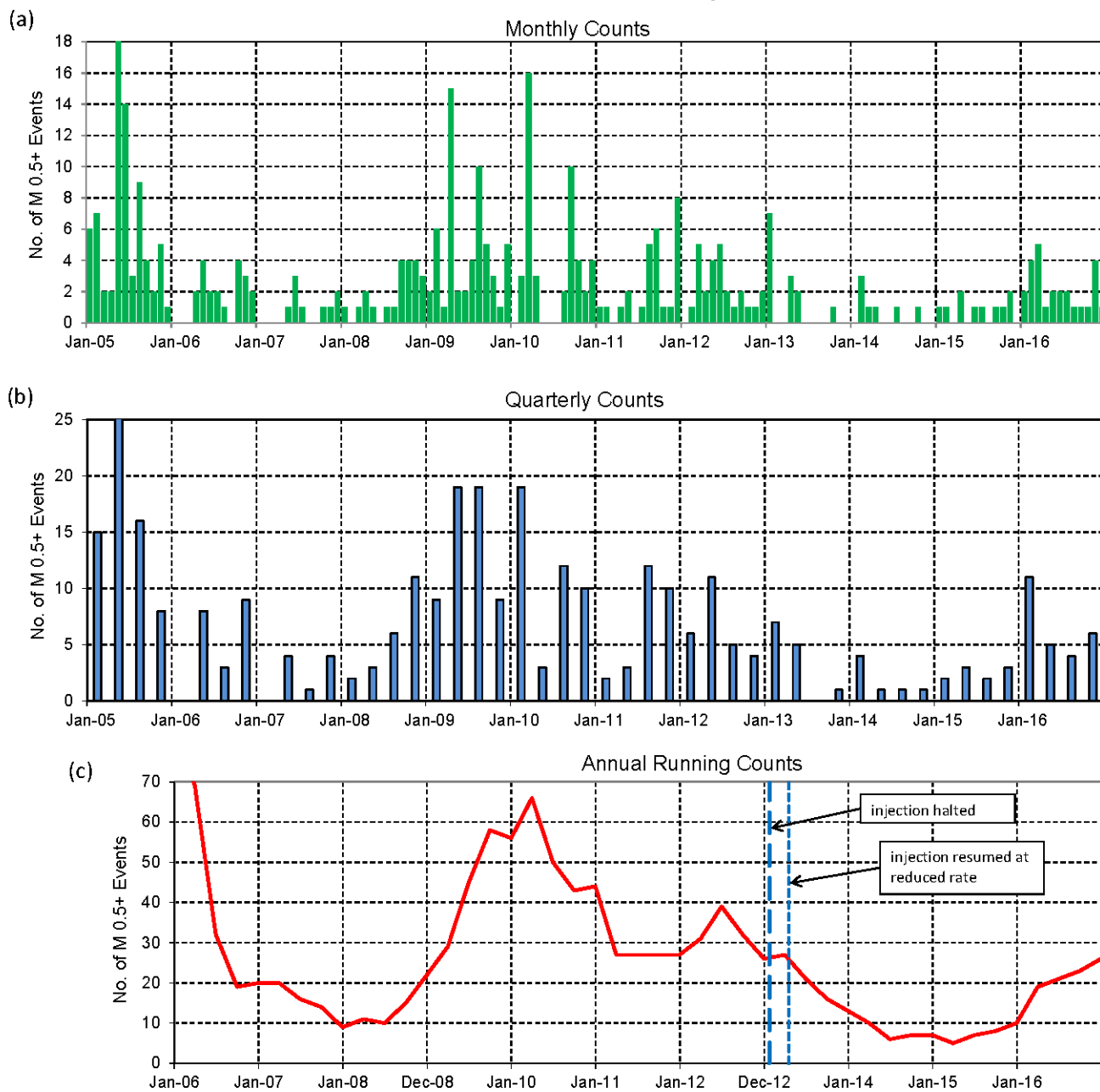


Figure 2-3: 2011 – 2016 occurrence rates of earthquakes  $\leq 5$  km from the injection well, with depths  $< 10$  km and duration magnitudes  $\geq 0.5$ . (a) monthly event counts (b) quarterly event counts (c) one-sided (backward) 12-month event counts.

### M 0.5+ Events within 5 km of the Injection Well



**Figure 2-4: 2005 – 2016 occurrence rates of earthquakes  $\leq 5$  km from the injection well, with depths  $< 10$  km and duration magnitudes  $\geq 0.5$ . (a) monthly event counts (b) quarterly event counts (c) one-sided (backward) 12-month event counts. High event counts in 2005 are clipped.**

M 1.5+ Events within 5 km of the Injection Well

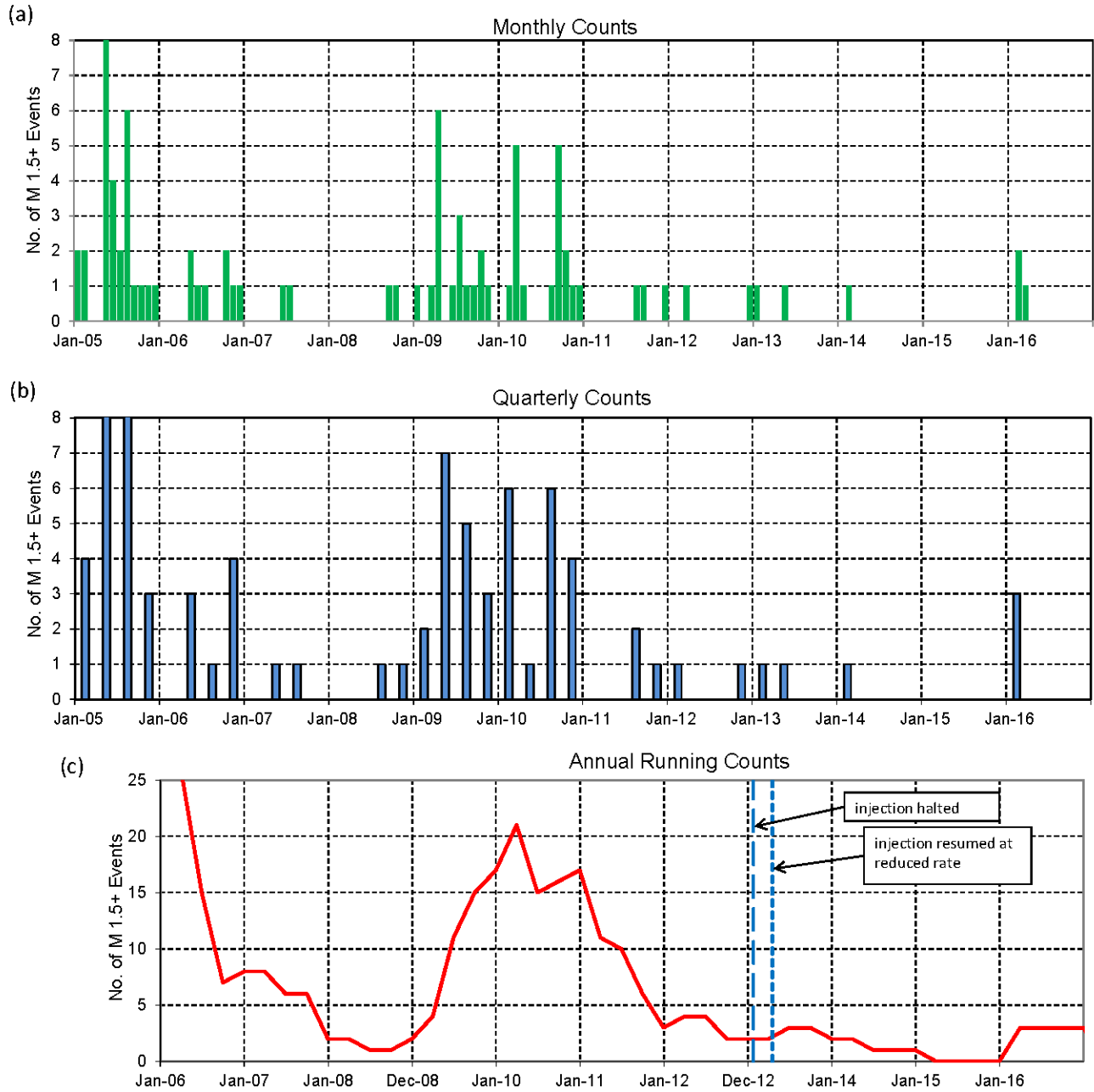


Figure 2-5: 2005 – 2016 occurrence rates of earthquakes  $\leq 5$  km from the injection well, with depths  $< 10$  km and duration magnitudes  $\geq 1.5$ . (a) monthly event counts (b) quarterly event counts (c) one-sided (backward) 12-month event counts. High event counts in 2005 are clipped.

### 2.2.2 5 to 10 km

The plots presented in Figure 2-6 show that the rates of events (with  $M_D \geq 0.5$ ) between 5 and 10 km from the injection well decreased substantially in mid-2013. Only 12 events with  $M_D \geq 0.5$  were recorded during the 12 quarters between July 2013 and June 2016 (an average rate of 1 event/quarter), compared to 54 such events during the 10 quarters from January 2011 to June 2013 (an average rate of 5.4 events/quarter), representing a decrease in seismicity rate of 81%.

In contrast to the low seismicity rates observed in mid-2013 to 2015, the historical 12-month event count curve presented in Figure 2-7c shows that the seismicity rates were generally increasing for three years prior to the occurrence of the  $M_L$  4.4 event in January 2013 (at a distance of 8.2 km from the injection well). The 81% decrease in seismicity rate following the  $M_L$  4.4 earthquake could be related to effects of the injection well shut-down and decreased flow rate. Alternatively, since many of the earthquakes observed during the three years prior to 2013 at distances of 5 to 10 km from the well occurred within 2 km of the January 2013 earthquake, the decreased seismicity rate could be due to the earthquake and its aftershocks changing the local stress field in such a way that the fault planes in this area are less critically loaded than they were prior to 2013.

Rates of M 0.5+ earthquakes at distances of 5 to 10 km from the well began increasing in mid-2016. Four such events were detected during the third quarter of 2016, and eight M 0.5+ events were detected during the fourth quarter, resulting in an average rate of 6 events/quarter for the second half of 2016. (Because of PVSN's decreased event detection capabilities during the third quarter of 2016, this rate may be underestimated.) This rate is comparable to the rate of 5.4 events/quarter observed prior to mid-2013. Hence, the rate of events observed in this distance range has rebounded to the rate observed prior to the extended shut-down of the injection well and subsequent change in flow rate. However, nine of the twelve M 0.5+ events observed during the second half of 2016 occurred in seismicity clusters that did not exist prior to the 2013 change in injection operations. Hence, the recent increase in seismicity rate in the 5-to-10-km distance range does not represent significantly increased activity in historical seismicity clusters, but instead is largely due to formation of new seismicity clusters. Changes in the spatial distribution of induced seismicity in recent years is described in detail in section 2.3.

The rates of events with  $M_D \geq 1.5$  also decreased substantially following the 2013 injection well shut-down and subsequent decrease in flow rate (Figure 2-8). Only one event with  $M_D \geq 1.5$  occurred at a distance of 5 to 10 km from the injection well between July 2013 and December 2015, compared to 13 such events during the previous 2.5 years (January 2011 to June 2013), corresponding to a 92% decrease in the M 1.5+ seismicity rate.

M 0.5+ Events 5 to 10 km from the Injection Well

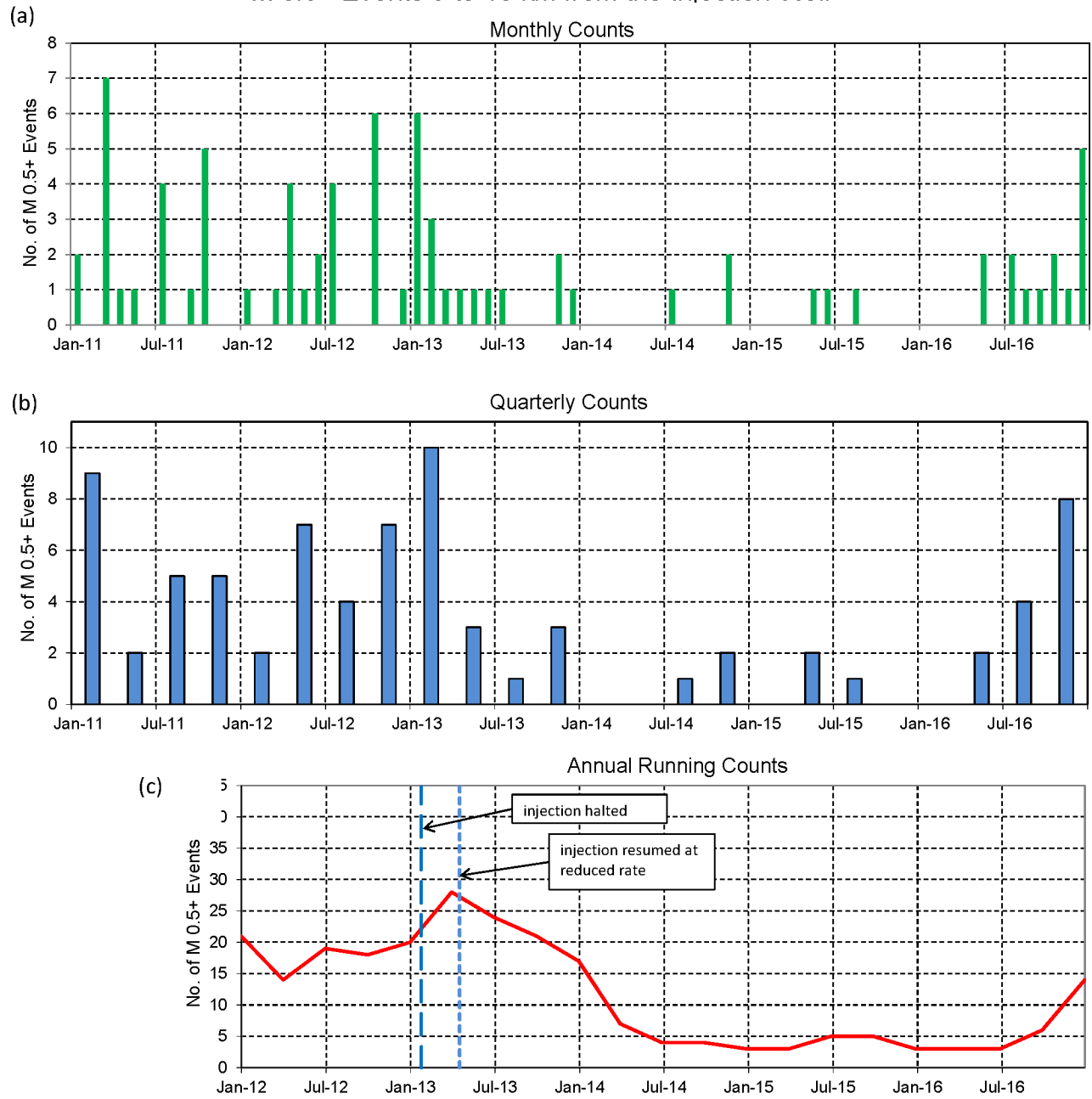


Figure 2-6: 2011 – 2016 occurrence rates of earthquakes > 5 km and ≤ 10 km from the injection well, with depths < 10 km and duration magnitudes ≥ 0.5. (a) monthly event counts (b) quarterly event counts (c) one-sided (backward) 12-month event counts.

M 0.5+ Events 5 to 10 km from the Injection Well

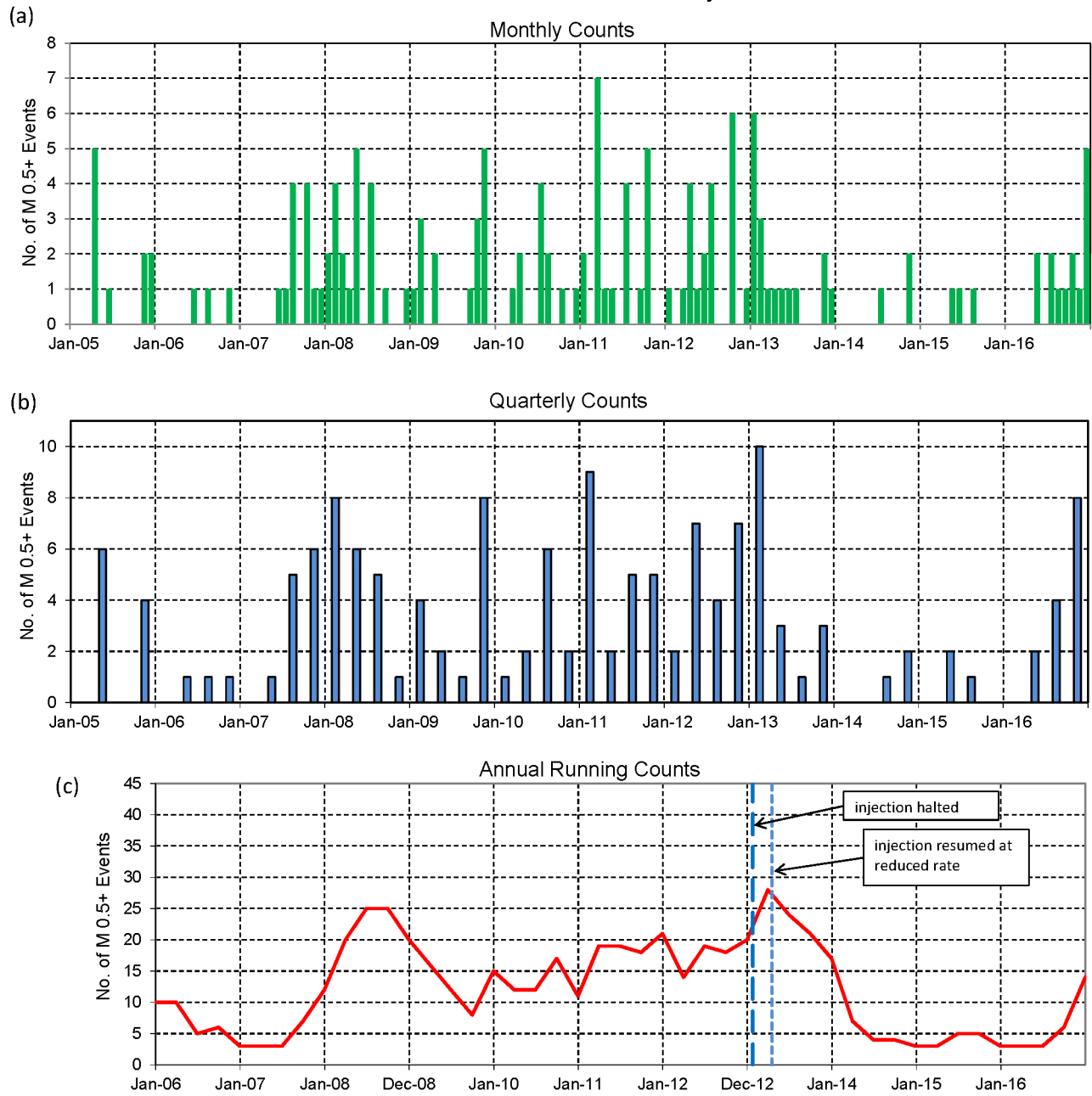


Figure 2-7: 2005 – 2016 occurrence rates of earthquakes > 5 km and ≤ 10 km from the injection well, with depths < 10 km and duration magnitudes ≥ 0.5. (a) monthly event counts (b) quarterly event counts (c) one-sided (backward) 12-month event counts.

M 1.5+ Events 5 to 10 km from the Injection Well

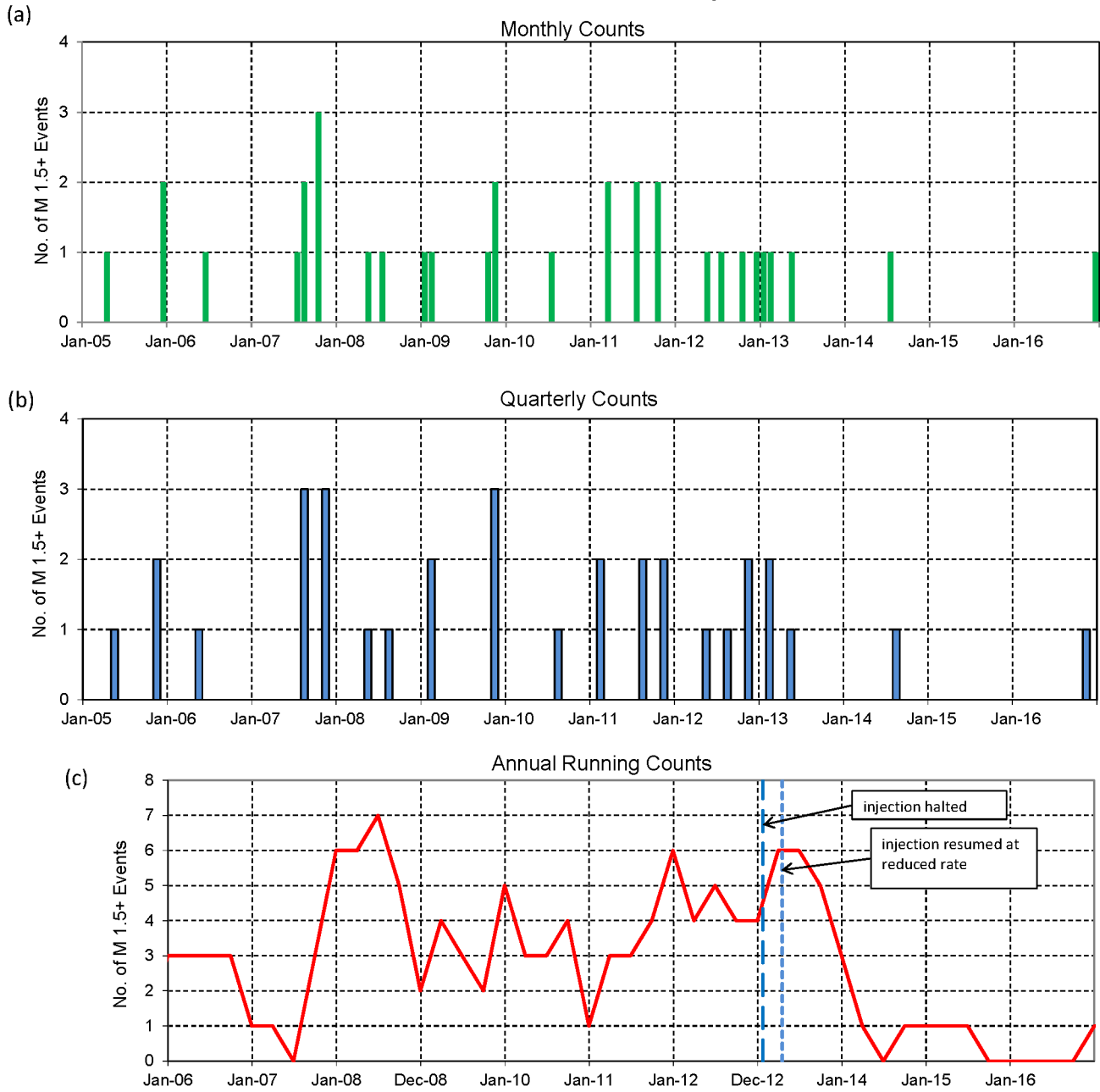


Figure 2-8: 2005 – 2016 occurrence rates of earthquakes > 5 km and ≤ 10 km from the injection well, with depths < 10 km and duration magnitudes ≥ 1.5. (a) monthly event counts (b) quarterly event counts (c) one-sided (backward) 12-month event counts.

### 2.2.3 Greater than 10 km

Rates of the distant seismicity show little correlation to the injection well shut-down and decreased flow rate implemented in 2013. The largest change in rates of events at distances greater than 10 km from the injection well occurred prior to 2013. Seismicity rates decreased sharply from mid-2011 to mid-2012 (Figure 2-9). Rates continued to decrease, but much more gradually, from mid-2012 to mid-2013. The seismicity rates were fairly constant from mid-2013 to mid-2015.

Rates of the earthquakes occurring more than 10 km from the injection well increased in mid-2015 to early 2016. Between July 2015 and December 2016, the average quarterly rate of distant M 0.5+ earthquakes was 3.7, compared to an average quarterly rate of only 1.25 from July 2013 to June 2015. The rate of M 1.5+ events has also increased. Six M 1.5+ distant earthquakes occurred between July 2015 and December 2016 (an average rate of 1 event/quarter), compared to only one earthquake from July 2013 to June 2015 (an average rate of 0.125 event/quarter).

Rates of distant seismicity have been highly variable during the last decade (Figure 2-10). Since 2005, quarterly rates of distant M 0.5+ earthquakes have ranged from 0 to 222 (Figure 2-10b; peak event count clipped). Similarly, quarterly rates of the larger-magnitude events, those with  $M_D \geq 1.5$ , have also varied significantly over time, ranging from 0 to 31 since 2005 (Figure 2-11b, peak event count clipped). Recent seismicity rates are moderate compared to these long-term historical trends.

M 0.5+ Events greater than 10 km from the Injection Well

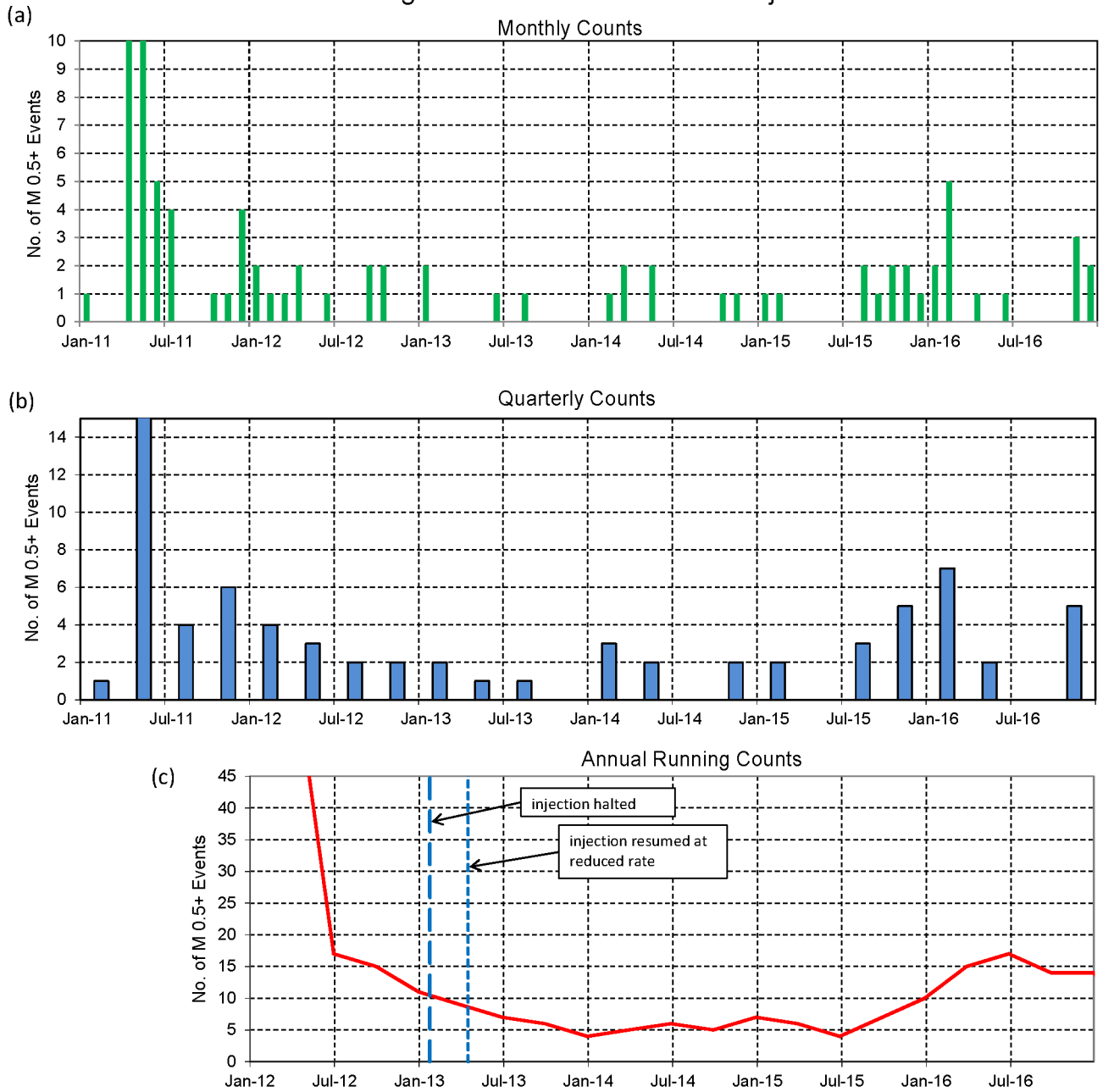
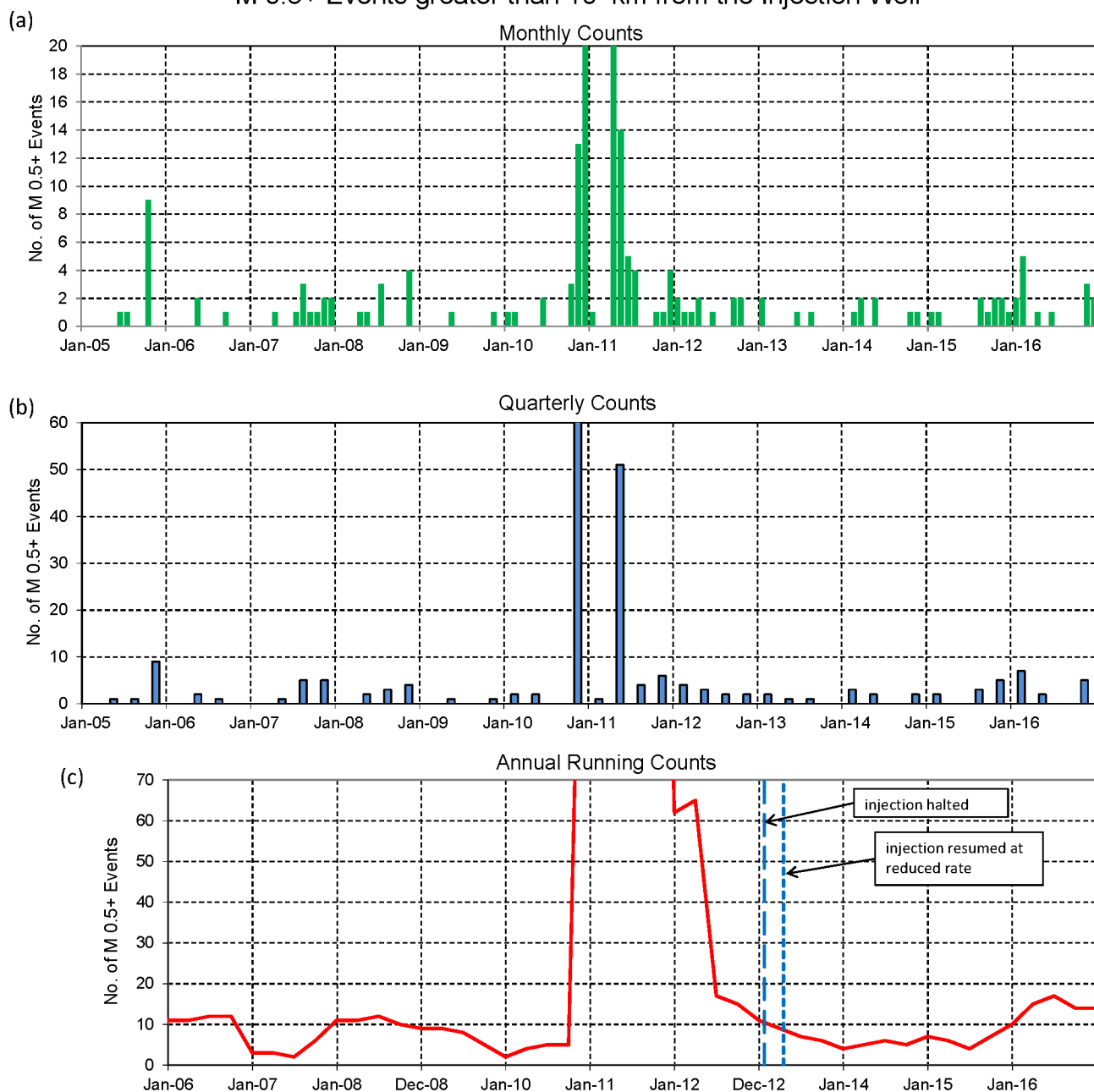


Figure 2-9: 2011 – 2016 occurrence rates of earthquakes > 10 km from the injection well, with depths < 10 km and duration magnitudes ≥ 0.5. (a) monthly event counts (b) quarterly event counts (c) one-sided (backward) 12-month event counts. High event counts in 2011 are clipped.

M 0.5+ Events greater than 10 km from the Injection Well



**Figure 2-10: 2005 – 2016 occurrence rates of earthquakes > 10 km from the injection well, with depths < 10 km and duration magnitudes  $\geq 0.5$ . (a) monthly event counts (b) quarterly event counts (c) one-sided (backward) 12-month event counts. High event counts in 2010 – 2011 are clipped. A peak quarterly event count of 222 was reached in late 2010.**

M 1.5+ Events greater than 10 km from the Injection Well

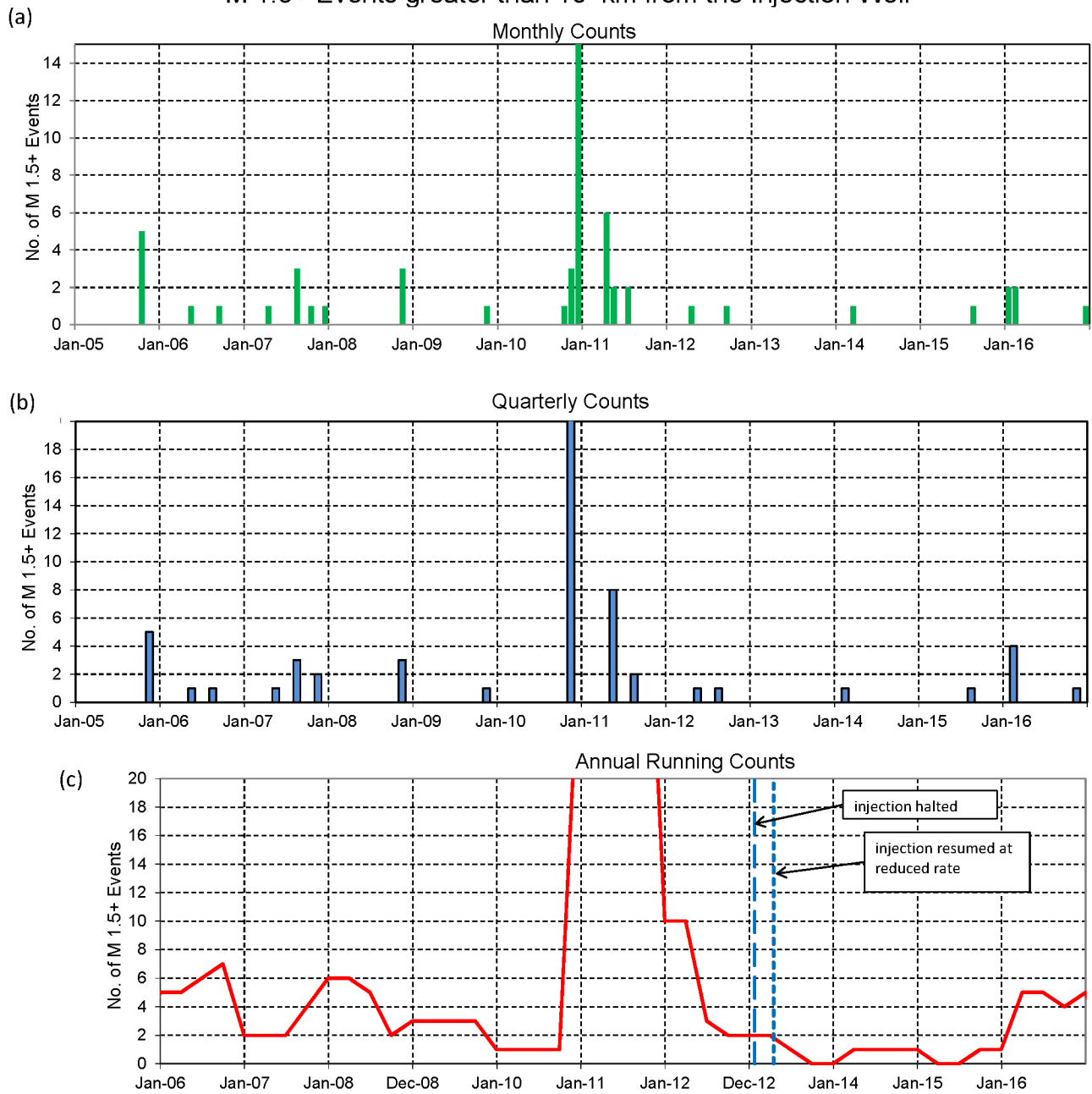


**Figure 2-11: 2005 – 2016 occurrence rates of earthquakes > 10 km from the injection well, with depths < 10 km and duration magnitudes  $\geq 1.5$ . (a) monthly event counts (b) quarterly event counts (c) one-sided (backward) 12-month event counts. High event counts in 2010 - 2011 are clipped. A peak quarterly event count of 31 was reached in late 2010.**

## 2.2.4 Summary

Rates of induced seismicity within 10 km of the PVU injection well declined following the January-April 2013 injection well shut-down and subsequent change in injection protocol. Within 5 km of the injection well, this decline in seismicity rate continued a gradual decrease that had begun three years earlier. At distances of 5 to 10 km from the well, the seismicity rates had been generally increasing for three years prior to 2013, and this trend abruptly reversed a few months following the January 2013  $M_L$  4.4 earthquake and subsequent changes in injection operations. The seismicity rates decreased by 72% to 81% after mid-2013, compared to the previous 2.5 years (Table 2-1). The decline in seismicity rates within 10 km of the injection well since 2013 is likely due to a combination of the extended injection well shut-down, the decreased injection flow rate and weekly shut-ins implemented in April 2013, re-distribution of stress in the vicinity of the January 2013  $M_L$  4.4 earthquake, and longer-term variations in pore pressure and stress due to the 25-year history of injection at PVU.

The induced seismicity at distances greater than 10 km from the injection well occurs much more sporadically than the seismicity closer to the injection well. Rates vary substantially over time, and much of the historical distant seismicity has occurred during short swarms of activity (lasting days to weeks). No substantial change in the rates of this distant seismicity was observed in response to the 2013 change in injection protocol.

Recent increases in the rates of induced seismicity have been observed at all distances from the injection well. The rates of induced seismicity within 5 km of the well began rebounding in early 2016, and the rates of induced seismicity 5 to 10 km from the well substantially increased beginning in mid-2016. At distances  $> 10$  km from the well, seismicity rates were higher from mid-2015 through 2016 than during the preceding two years. The recent increases in seismicity rates are summarized in Table 2-2.

Distance from the Injection Well	Date Range	Quarterly Rate of M 0.5+ Earthquakes	Percent Decrease in Seismicity Rate
0 – 5 km	Jan. 2011 – Jun. 2013	6.5	72%
	Jul. 2013 – Dec. 2015	1.8	
5 – 10 km	Jan. 2011 – Jun. 2013	5.4	81%
	Jul. 2013 – Jun. 2016	1.0	

**Table 2-1: Summary of the decreases in seismicity rates following the 2013 injection well shut-in and subsequent change in injection protocol.**

Distance from the Injection Well	Date Range	Quarterly Rate of M 0.5+ Earthquakes	Percent Increase in Seismicity Rate
0 – 5 km	Jul. 2013 – Dec. 2015	1.8	306%
	Jan. 2016 – Dec. 2016	7.3	
5 – 10 km	Jul. 2013 – Jun. 2016	1.0	500%
	Jul. 2016 – Dec. 2016	6.0	
>10 km	Jul. 2013 – Jun. 2015	1.25	196%
	Jul. 2015 – Dec. 2016	3.7	

**Table 2-2: Summary of recent increases in seismicity rates.**

### 2.3 Geographical Distribution of Induced Seismicity

Seismicity induced by PVU brine disposal has become more widespread and its spatial distribution more complex since injection initially began. During the injection tests performed between 1991 and 1995, induced seismicity was observed only in the immediate vicinity of the injection well, to radial distances of roughly 4 km (Figure 2-12a). For the first 4.5 years of long-term, near-continuous injection (July 1996 to 2000), the induced seismicity was mostly confined to a main cluster within 5 km of the injection well and secondary clusters 6 to 8 km northwest of the well (Figure 2-12b). A few events on the far side of Paradox Valley were recorded during 2000. Additional clusters of induced seismicity soon formed around the edges of northern Paradox Valley (Figure 2-12c), but then the geographical expansion largely ceased for several years (2001 – 2008; Figure 2-12c and d). In the last eight years (2009 – 2016), the induced seismicity at the northern end of Paradox Valley has begun expanding (Figure 2-12e and f). In addition, seismicity has occurred in many new areas, including: toward the southeast to a distance of ~18 km from the injection well, east toward Uravan to a distance of ~17 km from the well, west to a distance of ~14 km from the well, and at several locations within northern Paradox Valley (Figure 2-12f).

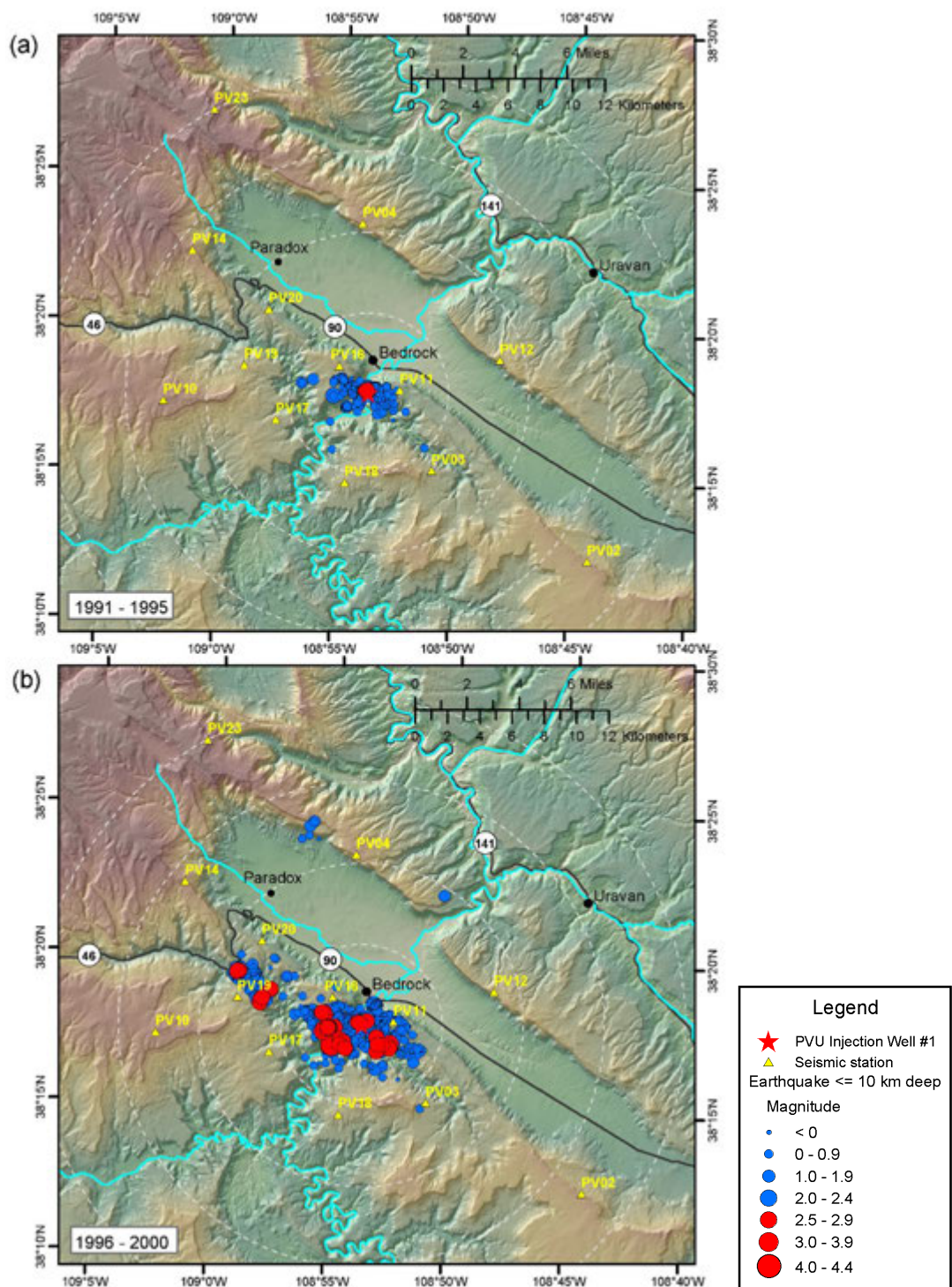


**Figure 2-12: Maps showing the geographical distribution of seismicity over time: (a) 1991 – 1995 (b) 1996 – 2000 (c) 2001 – 2004 (d) 2005 – 2008 (e) 2009 – 2012 (f) 2013 – 2016. Earthquakes (of all magnitudes) with depths  $\leq 10$  km with respect to the ground surface elevation at the injection well are included. The blue circles represent earthquakes with  $M_D < 2.5$ ; the red circles represent earthquakes with  $M_D \geq 2.5$ . The size of the circles is scaled by earthquake magnitude. The large dashed circles mark distances of 5, 10, 15, and 20 km from the injection well.**

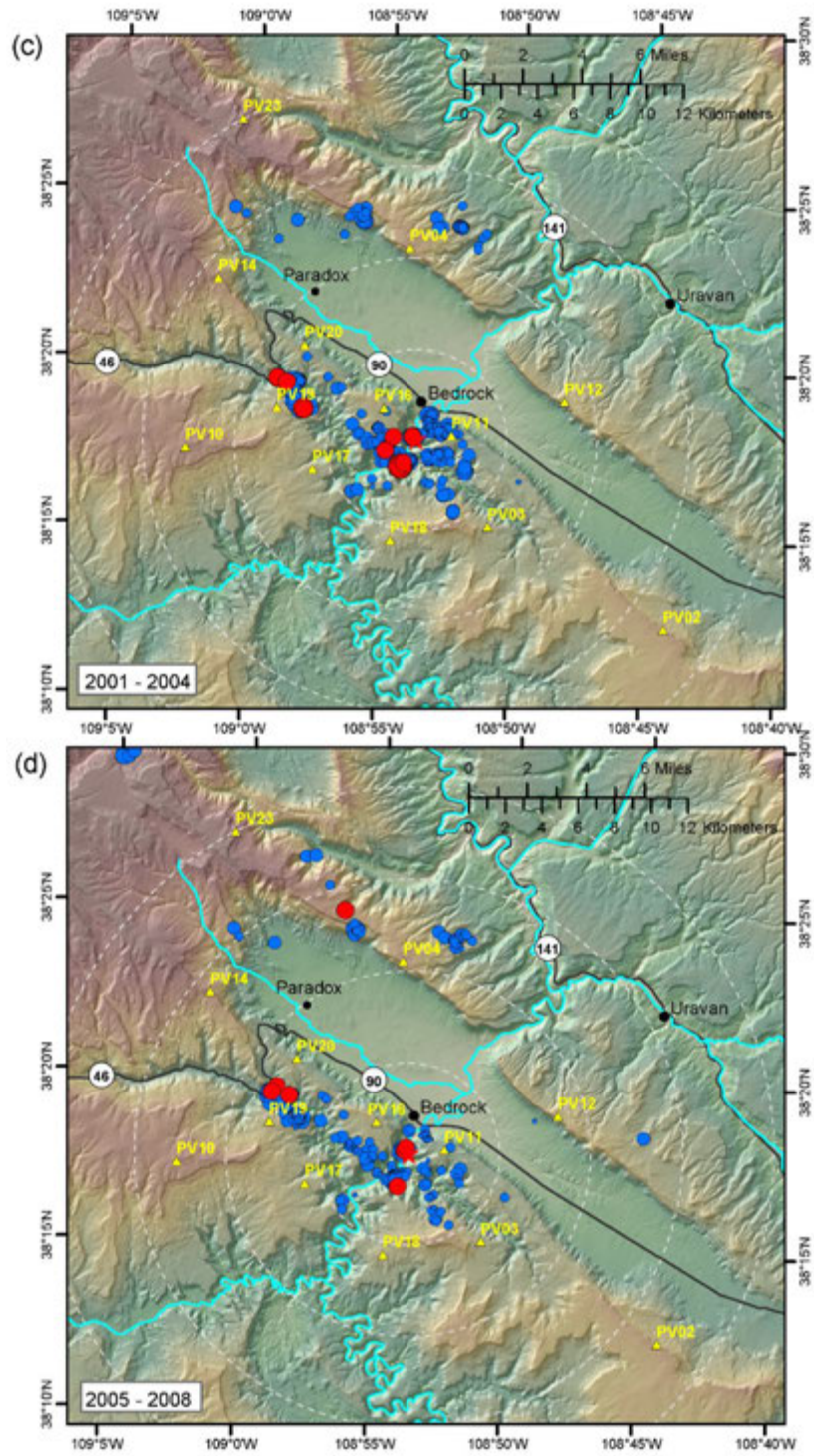


Figure 2-12, continued.

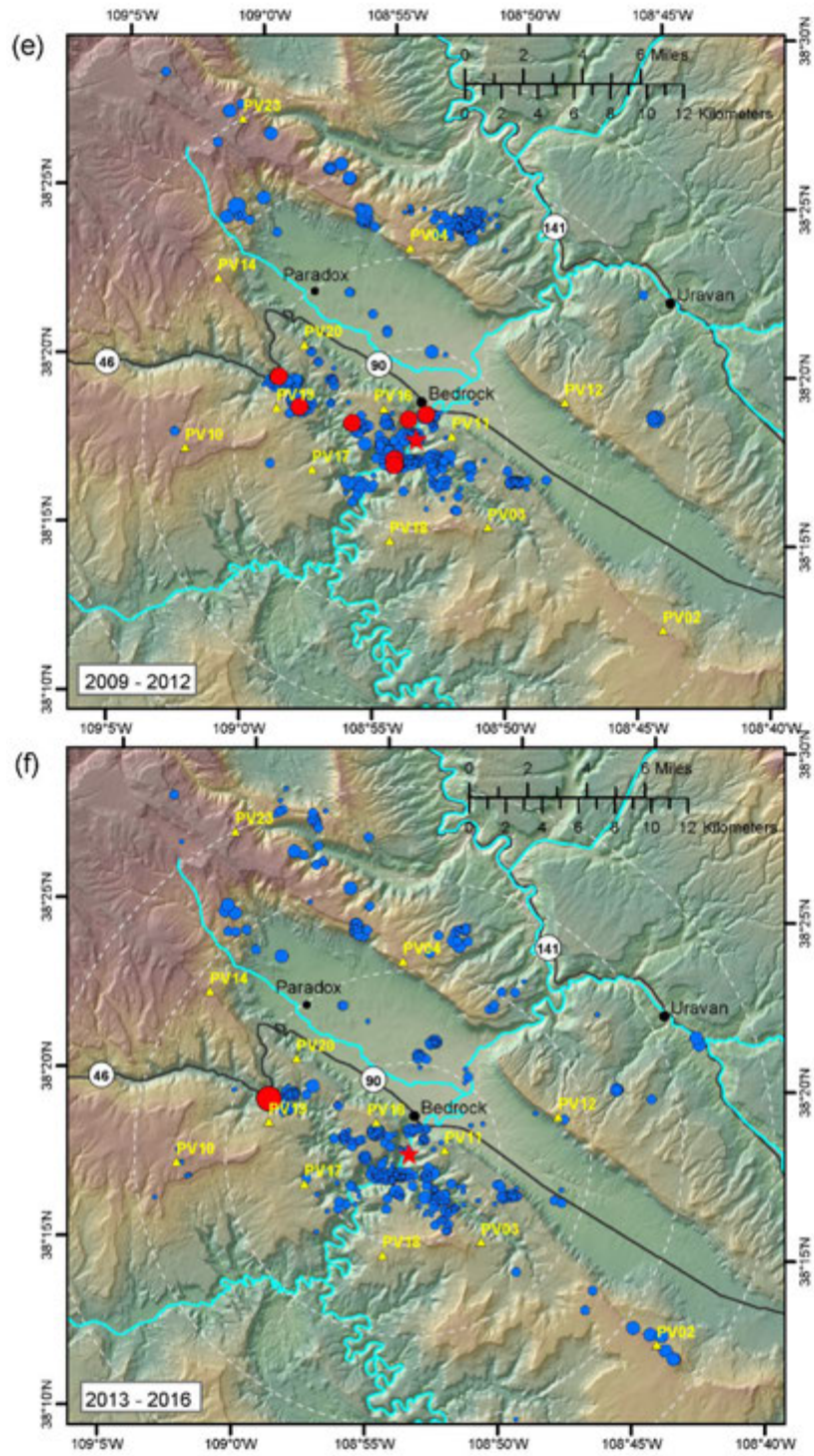
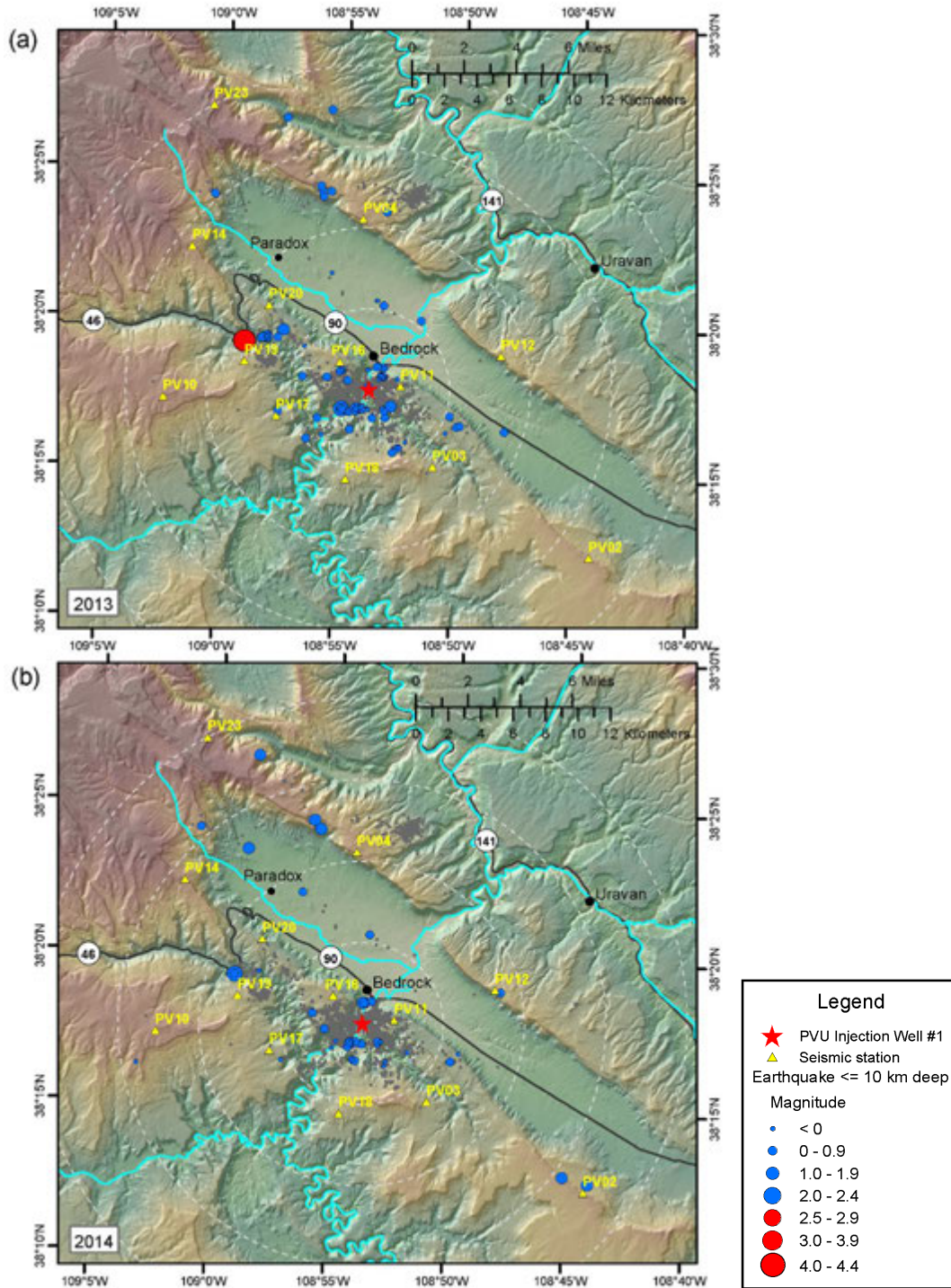


Figure 2-12, continued.

Figure 2-13 shows how the geographical distribution of induced seismicity has evolved since 2013 in more detail. During 2013, the year that the  $M_L$  4.4 earthquake occurred, induced seismicity mainly occurred around the edges of the main cluster of induced seismicity near the well and in a cluster 8 km northwest of the well (where the  $M_L$  4.4 earthquake occurred). A few earthquakes also occurred ~6 km southeast of the injection well, around the northern edges of Paradox Valley, and at a few isolated locations within northern Paradox Valley (Figure 2-13a). Seismicity rates in the near-well area and the cluster 8 km northwest of the well substantially decreased following the extended shut-in of the injection well and reduction in flow rate implemented in 2013, and remained low in 2014. Fewer earthquakes also occurred in the cluster ~6 km southeast of the injection well. Earthquakes occurred within and around the edges of northern Paradox Valley at about the same rate as in 2013. In addition, earthquakes occurred in three distant areas that were not active in 2013: ~9 km east of the well near seismic station PV12, 15-17 km southeast of the well near station PV02, and ~14 km west of the well near station PV10 (Figure 2-13b).

During 2015, seismicity rates along the northern edge of the near-well cluster and in the cluster 8 km northwest of the well remained low. However, seismicity rates along the southern edge of the near-well cluster and in the cluster ~6 km southeast of the well increased (Figure 2-13c). The character of the seismicity occurring within Paradox Valley also displayed subtle changes. Although the seismicity rate here was still relatively low, the seismicity began to show more clustering, with several events occurring 5 to 7 km north of the well. A dense seismicity cluster northeast of Paradox Valley (3-4 km northeast of station PV04), which had shown almost no activity in 2013 or 2014, experienced 15 earthquakes in 2015. The distant seismicity also showed continued expansion, with shallow earthquakes occurring as far as 13.5 km east of the well (near station PV12), 18.4 km southeast of the well (near station PV02), and 23.5 km northwest of the well (northwest of station PV23) (Figure 2-13c).

In 2016, seismicity rates in the southwestern half of the near-well cluster were relatively high, while the northeastern half of the cluster was largely inactive (Figure 2-13d). Rates increased in the seismicity cluster ~8 km northwest of the well and in the cluster ~6 km southeast of the well. In addition, seismicity rates increased in central Paradox Valley, with two distinct clusters forming 5 to 7 km north of the well. Rates of earthquakes occurring north of Paradox Valley increased substantially, and small new clusters formed in this area. Several earthquakes occurred in a previously aseismic area east of Paradox Valley, just north of the Dolores River (~5 to 7 km southeast of station PV04). Seismicity continued to occur at large distances from the injection well, such as near station PV10 to the west and station PV02 to the southeast. Two earthquakes also occurred 17 km east of the well near Uravan. However, these two earthquakes were somewhat deep (~9 km), and it is not clear whether these earthquakes are induced or naturally-occurring (Figure 2-13d).



**Figure 2-13: Maps showing the geographical distribution of seismicity in recent years: (a) 2013 (b) 2014 (c) 2015 (d) 2016. Earthquakes (of all magnitudes) with depths  $\leq 10$  km with respect to the ground surface elevation at the injection well are included. The blue circles represent earthquakes with  $M_D < 2.5$ ; the red circles represent earthquakes with  $M_D \geq 2.5$ . The size of the circles is scaled by earthquake magnitude. The gray dots indicate earthquakes that occurred prior to the specified year and are not scaled by magnitude. The large dashed circles mark distances of 5, 10, 15, and 20 km from the injection well.**

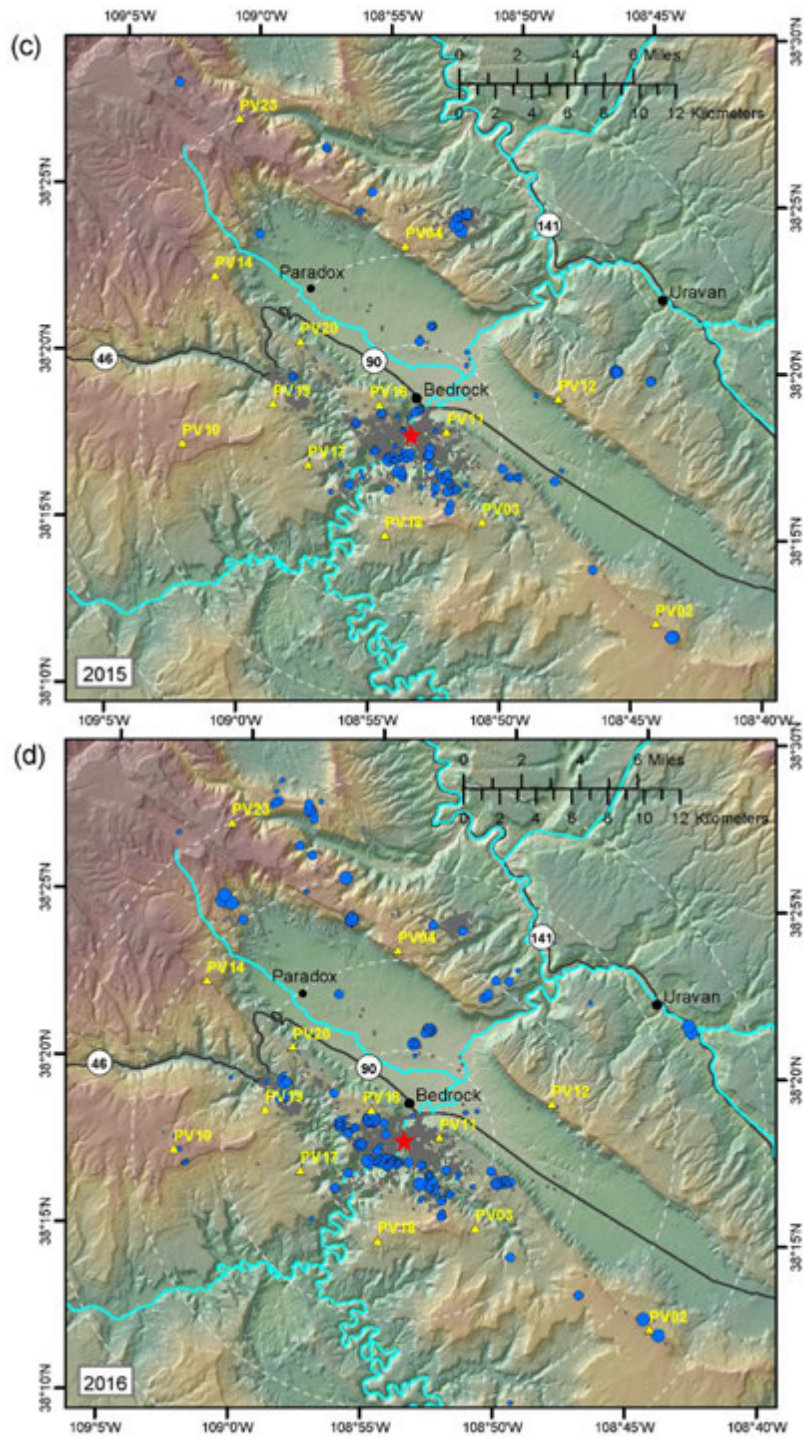


Figure 2-13, continued.

The above series of maps illustrate that the geographical extent of the seismicity induced by the PVU well has continued to evolve in recent years, despite the change in injection operations implemented in 2013. Induced earthquakes are occurring in more locations than prior to 2013. The seismicity has expanded in some azimuthal directions, especially to the southeast. Some areas that were experiencing scattered seismicity prior to 2013 now have distinct seismicity clusters, such as within and north of Paradox Valley. The continued geographical expansion of induced seismicity and the formation of new seismicity clusters suggests that the probability of having earthquakes at large distances from the injection well (up to ~20 km) that are large enough to be felt ( $\geq \sim M 2.5$ ) is higher now than in the past and will likely continue to increase.

## 3 Pressure Trends

### 3.1 Injection Pressures

Prior to the  $M_L$  4.4 earthquake in January, 2013, maximum surface and downhole pressures at the PVU injection well had been generally increasing for about eight years (Figure 3-1). Following the January 2013 earthquake, PVU ceased injection for 84 days. Injection resumed on April 17, 2013, with the same nominal flow rate as prior to the earthquake, 230 gpm, but with a 36-hour shut-in every week. On June 6, 2013, after new plungers for the injection pumps were installed, the flow rate was reduced to 200 gpm, and the length of the weekly shut-ins was reduced to 18 hours. Under this new injection protocol, the duration of any additional injection well shut-ins required for maintenance activities are tracked, and the total duration of these additional shut-ins is subtracted from the scheduled 18-hour weekly shut-ins. Hence, some weekly shut-ins are less than 18 hours, and in rare cases, the weekly shut-in is not implemented. Figure 3-2 shows the trends of injection flow rate, surface pressure, downhole pressure, and cumulative volume of injected fluid before, during, and after these operational changes.

The maximum daily average surface injection pressure at the PVU well, 5107 psi, was reached on January 22, 2013 (MST), the day before the  $M_L$  4.4 earthquake. This corresponds to a downhole pressure of 12,261 psi, computed using the density of brine in the well and ignoring the effects of frictional loss along the tubing. During the 84-day shut-in of the well, daily average injection pressures fell by about 4700 psi, to a minimum value of 400 psi for the surface pressure and 7554 psi for the downhole pressure (Figure 3-2). Within 5 months following the resumption of injection in April 2013, injection pressures rebounded by approximately 4200 psi, to within about 500 psi of their previous maximum values. Injection pressures have changed at a much slower rate since then. The maximum daily average surface pressure achieved since injection resumed (through the end of 2016) is 4797 psi and the maximum downhole pressure is 11,951 psi, which occurred on both Oct. 31 and Nov. 1, 2016. These maximum values are 310 psi lower than the maximum values reached prior to the change in injection operations.

To better understand the trends in surface and downhole pressures since injection resumed in April 2013, the daily average pressure data were smoothed by computing 91-day averages within centered moving windows (Figure 3-3). These smoothed curves show that pressures steeply increased for several months following the resumption of injection and then fluctuated for about two years. At least some of the fluctuation in the smoothed pressures appears to be due to longer than normal injection or shut-in periods. The pressures have increased more steadily since January 2016.

The new injection protocol implemented in 2013 was based in part on empirical observations indicating a general correlation between lower long-term average injection pressures and decreased rates and magnitudes of induced earthquakes occurring within 5 km of the injection well (Figure 3-4; Block and Wood, 2009). Pressure-flow modeling indicated that maximum and average injection pressures could be reduced by decreasing the flow rate and that less pressure

increase per unit volume of fluid injected could be achieved by having more frequent, shorter shut-ins rather than the 20-day shut-ins that had been implemented in the past (Wood et al., 2016).

The increase in rates and magnitudes of near-well induced earthquakes during 2016 (section 2.2.1) roughly correlates with increased injection pressures averaged over a time period of 2.5 years (Figure 3-4). These observations suggest that near-well pore pressures may be recovering from the effects of the operational changes implemented in 2013, despite the relatively low pressures measured at the well. To investigate the temporal and spatial variations in pore pressures within a few km of the injection well since 2013, we performed simple pressure diffusion calculations. These analyses are described in the next section.

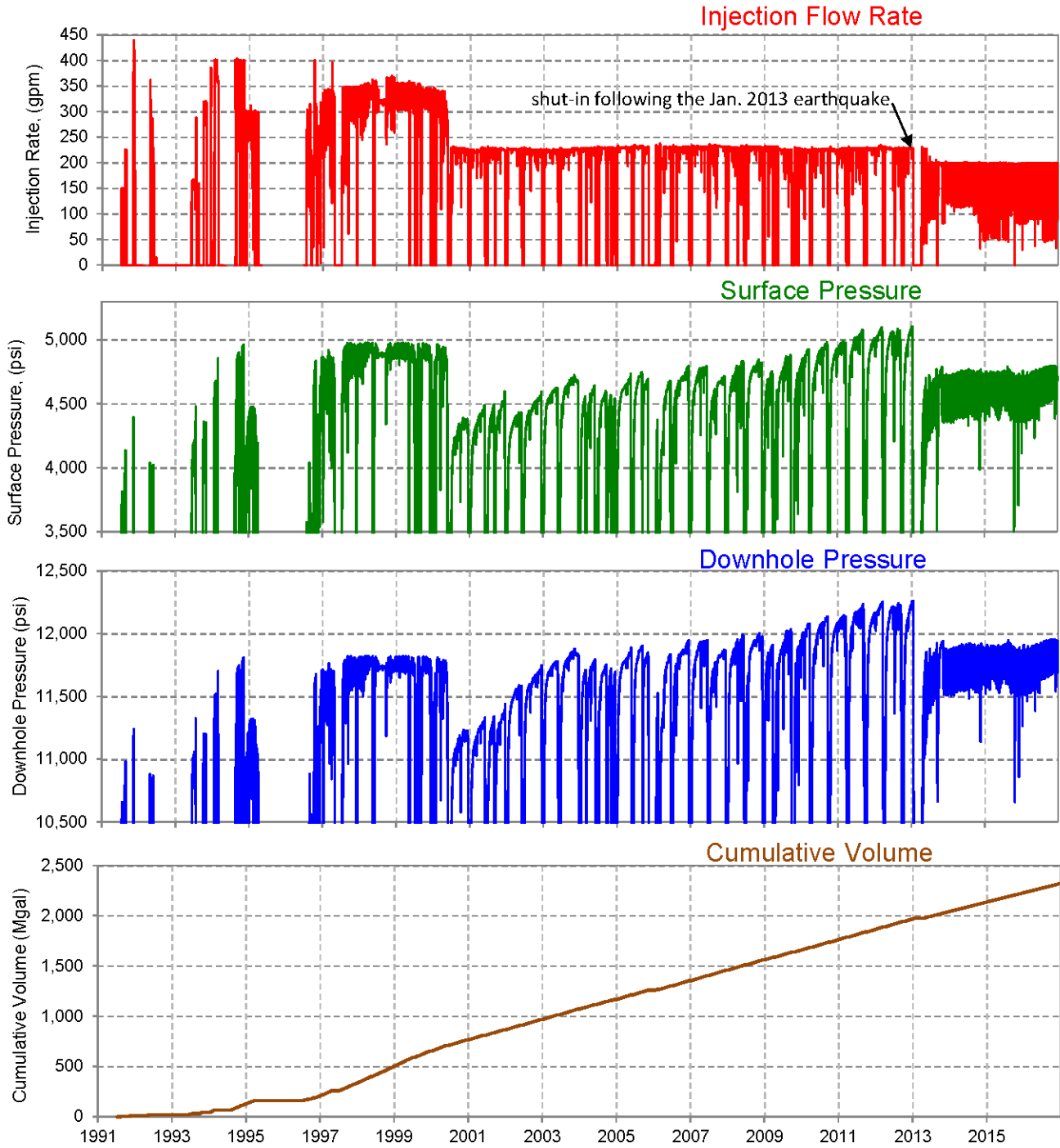


**Figure 3-1: Daily average injection flow rate, daily average surface injection pressure, daily average downhole pressure at 4.3 km depth, and cumulative volume of fluid injected from 1991 to 2016. The downhole pressures are computed from the measured surface pressures using the density of the brine in the well.**

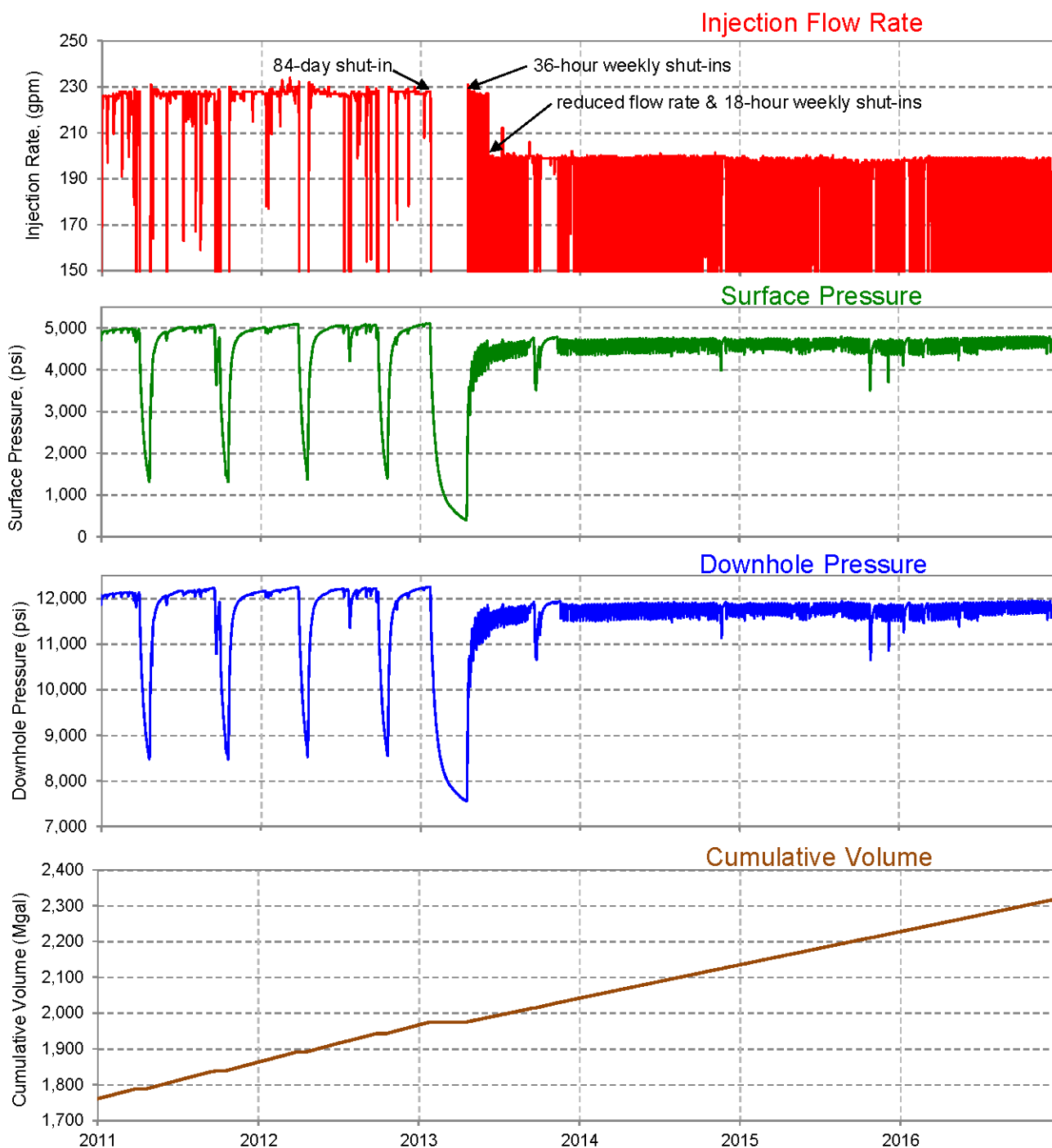


**Figure 3-2: Daily average injection flow rate, daily average surface injection pressure, daily average downhole pressure at 4.3 km depth, and cumulative volume of brine injected from 2011 to 2016. The downhole pressures are computed from the measured surface pressures using the density of the brine in the well. The injection well was shut in for 84 days following the  $M_L$  4.4 induced earthquake on Jan. 23, 2013 (MST). Injection resumed on April 17, 2013 (MST), with 36-hour weekly shut-ins. After new plungers were installed in early June 2013, the flow rate was reduced and the duration of the weekly shut-ins was decreased to 18 hours.**

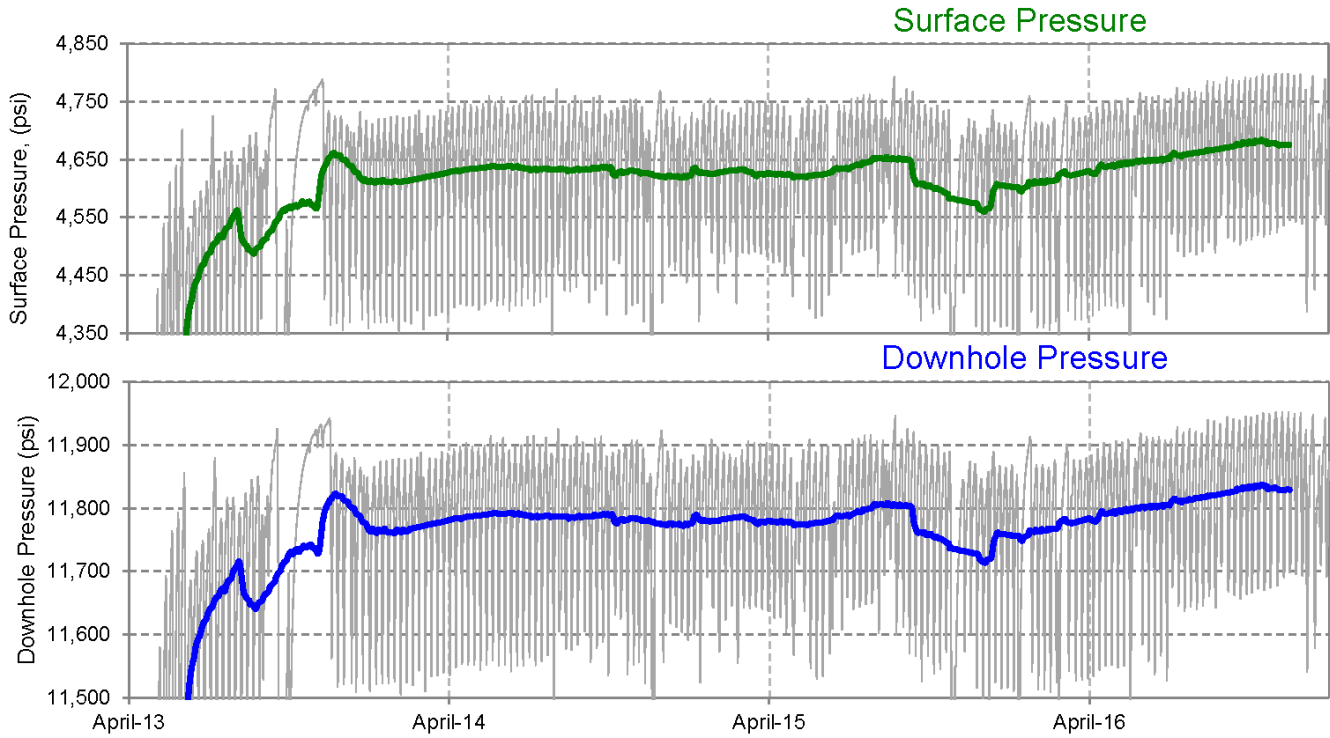


**Figure 3-3: Daily average surface and downhole pressures (gray lines) and 91-day centered moving averages of the pressures (green and blue lines) from April 2013 to December 2016. Prior to the resumption of injection on April 17, 2013, the surface and downhole pressures were at values of 400 and 7554 psi, respectively. To better observe the more recent pressure variations, these low pressure values are not shown in these plots.**

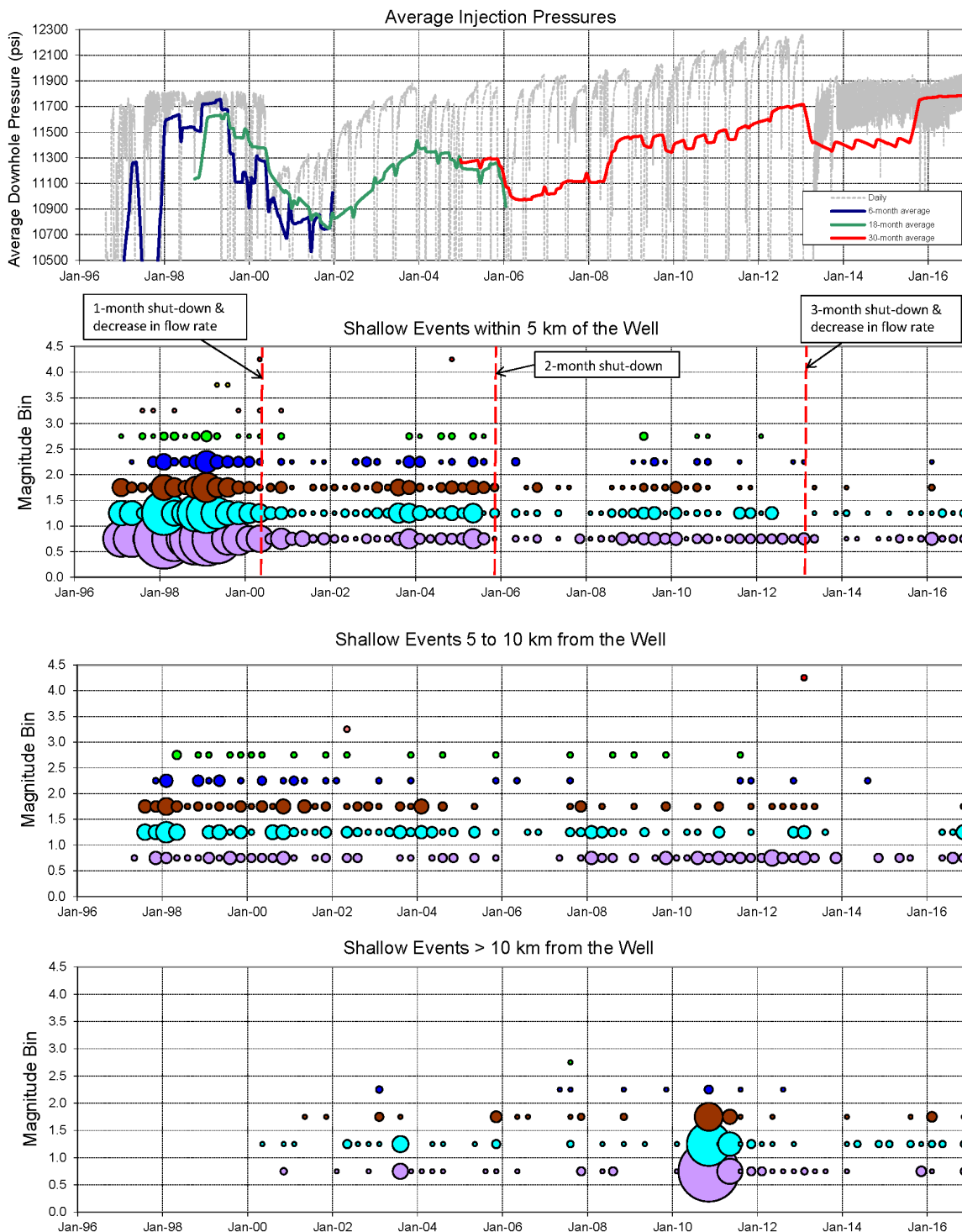


**Figure 3-4: PVU injection well downhole pressures averaged over daily, 6-month, 18-month, and 30-month time periods (top) and occurrence of shallow seismicity as a function of date and magnitude: within 5 km of the injection well, at distances of 5 to 10 km from the well, and at distances greater than 10 km from the injection well. In the seismicity plots, the area of each circle is scaled by the number of earthquakes occurring in a given quarter-year and magnitude range; each plot is scaled separately.**

## 3.2 Pore Pressures

We computed pore pressures as a function of time and distance from the injection well using the pressures observed at the well and a simple pore pressure diffusion model for an unbounded, single-layer homogenous reservoir. Details of the methodology used are presented in Appendix A. Although the geologic structure in the vicinity of the PVU well is complex and the presence of faults that act as impermeable barriers to fluid flow is suggested by other studies (King et al., 2014; Block et al., 2015; Excel Geophysical Services and International Reservoir Technologies Inc., 2017), this simple modeling is used to investigate the gross spatial and temporal variations in reservoir pore pressures related to changes in injection operations. Pore pressure variations introduced by the 2013 injection well shut-in and subsequent change in injection operations are specifically explored.

The pressure diffusion calculations require the specification of two input parameters: the hydraulic diffusivity  $D$  and the effective borehole radius  $r_w$ . The diffusivity is a property of the rock into which the fluids are injected and indicates how quickly pressure perturbations can diffuse through the rock. Previous analyses of the initial onset of seismicity as a function of distance from the injection well provided estimates for  $D$  of 0.1 to 0.2 m<sup>2</sup>/s (King and Block, 2016; King et al., 2016). These values of diffusivity are consistent with estimates of permeability derived from early injection tests in the PVU well (King and Block, 2016). The effective borehole radius,  $r_w$ , indicates the maximum distance from the well for which the modeled pore pressure is equal to the pressure in the well. In the simplest case, this is the radius of the wellbore. An effective borehole radius larger than the wellbore can be used to simulate an area of increased diffusivity immediately surrounding the well, such as a fractured zone.

Below we present the temporal and spatial variations in pores pressures estimated by an initial model with a diffusivity of 0.115 m<sup>2</sup>/s and a small effective wellbore radius of 10 cm. This value for  $D$  fits the move-out of the initial onset of induced seismicity to a distance of about 10 km from the well (King and Block, 2016), and this value of  $r_w$  approximately corresponds to the radius of the wellbore at the depth of the primary injection horizon, the Leadville Formation. We subsequently examine how the results change with variations in  $D$  and  $r_w$ .

### 3.2.1 Initial Model

The changes in pore pressure over time computed at multiple radial distances ( $r$ ) from the well are presented in the lower plot of Figure 3-5. The changes in pore pressure at the injection well are shown in the upper plot for reference. All curves indicate the changes in pore pressure with respect to the initial in-situ pressure prior to injection. The pressure perturbations at the injection well over time were computed from the measured surface injection pressures and the density of fluid in the wellbore. These pressure variations take into account the increase in fluid density in 2002 when injection of 100% brine began rather than the 70% brine: 30% fresh water mixture that had been used previously. The pore pressure changes at multiple distances from the well were then extrapolated from the pressure changes at the well using a pore pressure diffusion model with  $D = 0.115$  m<sup>2</sup>/s and  $r_w = 10$  cm.

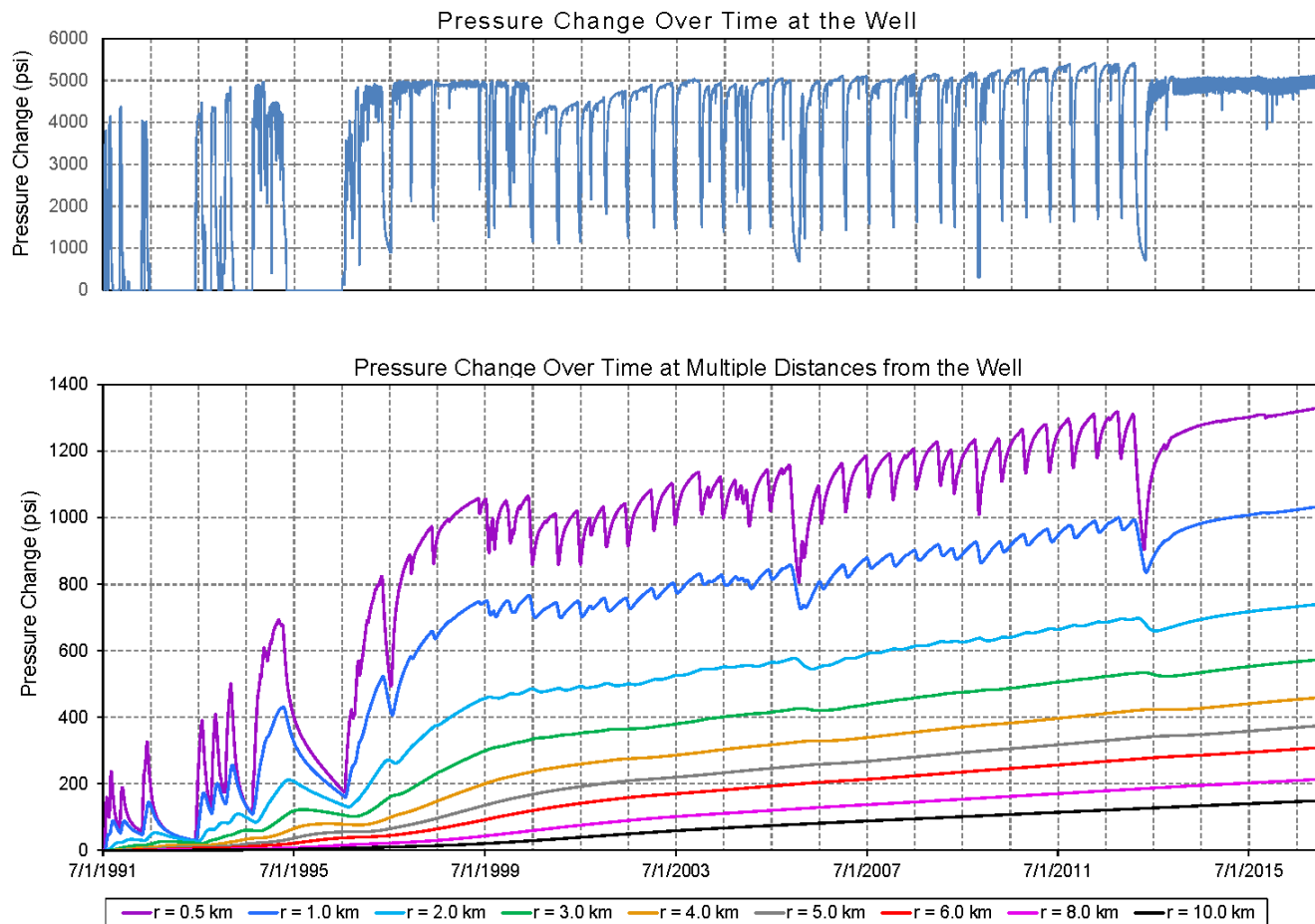


**Figure 3-5: Pore-pressure variation over time at the PVU injection well (upper plot) and at multiple distances (r) from the well (lower plot). These pressure trends represent the increase in pore pressure due to injection. The changes in pore pressure at the injection well were computed from the measured surface injection pressures and the density of brine in the borehole. The pore pressure changes at multiple distances from the well were extrapolated from the pressure changes at the well using a simple pore pressure diffusion model with  $D = 0.115 \text{ m}^2/\text{s}$  and  $r_w = 10 \text{ cm}$ .**

As demonstrated by the results presented in Figure 3-5, pressure perturbations at the injection well are modulated with distance from the well. The amplitudes of the pressure perturbations greatly decrease with increasing distance from the well. The pressure perturbations are also much smoother over time at greater distances. For example, the pressure variations due to the 20-day biannual shut-ins that were implemented between 1999 and 2012 are not seen in the pressure curves for distances greater than 2 to 3 km from the injection well. Even the extended shut-ins, such as the 73-day shut-in from Nov. 2005 to Jan. 2006 or the 84-day shut-in from Jan. to Apr. 2013, have negligible effect on the pressure trends at distances beyond about 4 km.

In order to better observe the pore pressure changes following the extended injection well shut-in and change in injection protocol implemented in 2013, the pressure curves for distances between 0.5 and 5.0 km are shown at an expanded scale in Figure 3-6. This initial model indicates that

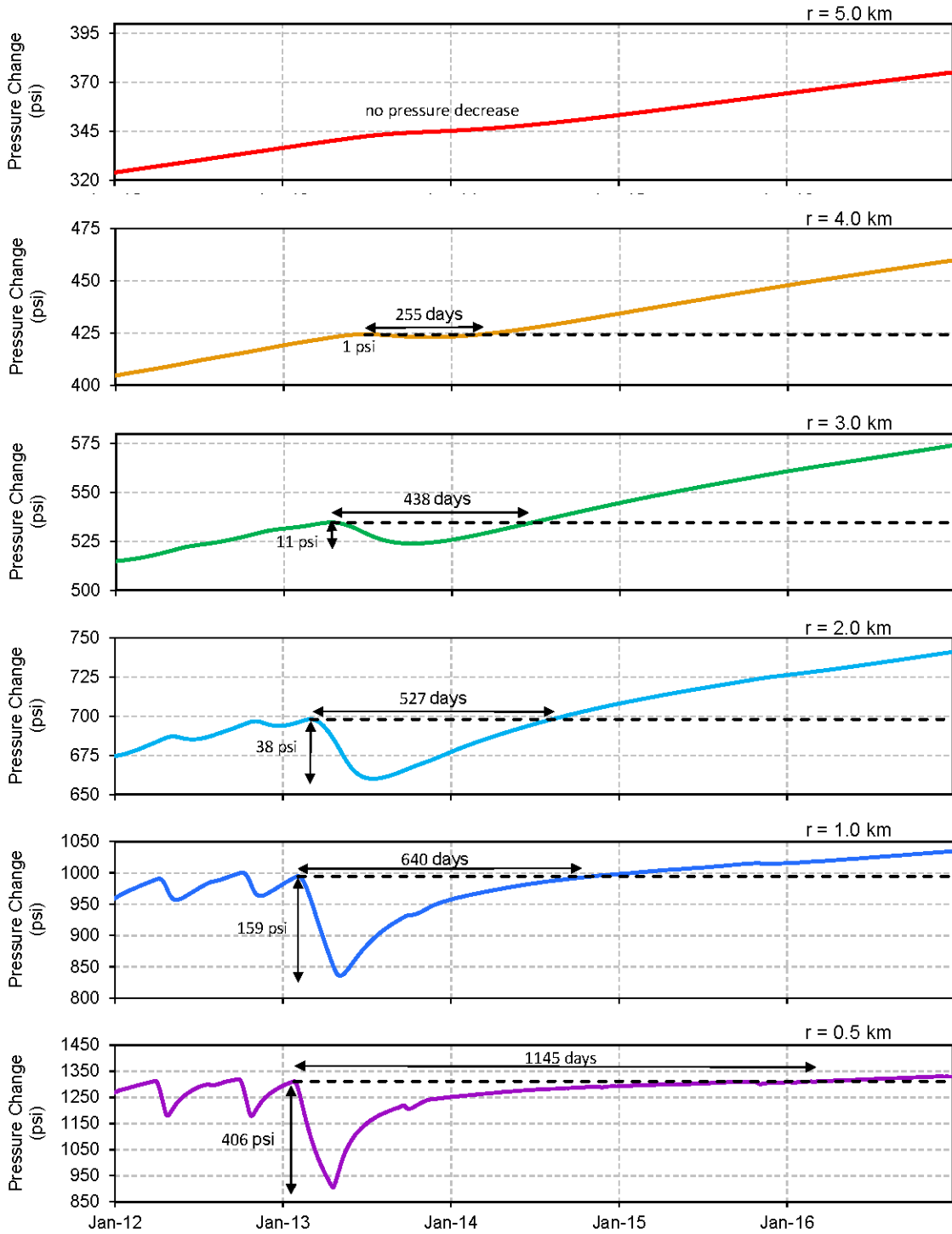


**Figure 3-6: Pore-pressure variations from 2012 to 2016 at six radial distances from the well, computed using the initial diffusion model with  $D = 0.115 \text{ m}^2/\text{s}$  and  $r_w = 10 \text{ cm}$ . The horizontal double arrows indicate the time periods when pore pressures were lower than those experienced immediately prior to the shut-in of the injection well in January 2013. The vertical double arrows indicate the largest magnitude of the pore-pressure decrease.**

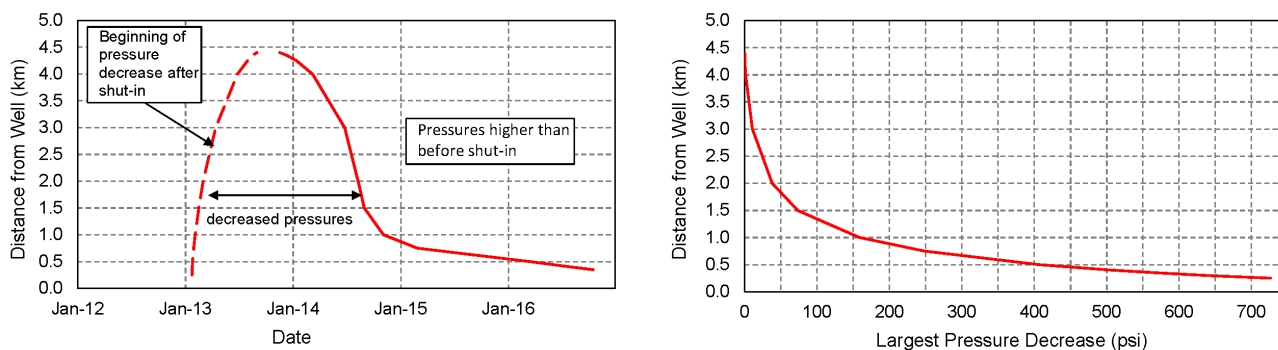


**Figure 3-7: Summary plots of the results from the initial pressure diffusion model with  $D = 0.115 \text{ m}^2/\text{s}$  and  $r_w = 10 \text{ cm}$  for the time period following the injection well shut-in and reduced flow rate implemented in 2013. The left plot shows the dates when pore pressures began decreasing following the injection well shut-in, as a function of distance from the well (dashed red line), and the dates when the pressures recovered to their previous maximum values (solid red line). For dates to the right of the solid red line, the model predicts that pressures are higher than they were prior to the shut-in. The right plot shows the size of the largest pressure decrease as a function of distance from the injection well.**

pore pressures decreased in the region surrounding the injection well to a distance of roughly 4 km following the Jan.-Apr. 2013 shut-in. At a distance of 0.5 km from the well, the model indicates that the pore pressure experienced a maximum decrease of 406 psi and that reduced pore pressures persisted for 1145 days before the pressure recovered to its previous maximum value (lowest plot, Figure 3-6). The decrease, or fall-off, in pressure occurred relatively rapidly, and the subsequent pressure increase, or build-up, was much more gradual. With increasing distance from the well, both the magnitude and duration of the reduced pore pressures substantially lessen. The following patterns are also observed: the initial onset of the reduction in pore pressure is delayed with increasing distance from the well, the time at which the pressure recovers to its previous maximum value occurs earlier, and the rates of change of pressure during the fall-off and build-up periods become more similar. After the pore pressures have recovered to their previous maximum values, the pressures exhibit a continuous increase at all distances examined (0.5 to 5.0 km).

The patterns in pore-pressure perturbation as a function of time and distance from the well following the 2013 shut-in and subsequent change in injection operations are summarized in the plots presented in Figure 3-7. The plot on the left indicates the beginning (dashed red curve) and end (solid red curve) of the period of reduced pore pressures as a function of time (x axis) and distance from the well (y axis). Consistent with the pore pressure curves just discussed, this plot indicates that pore pressures at distances  $\geq 1 \text{ km}$  had recovered to their pre-shut-in maximum values by late 2014. Pressures very close to the well take substantially longer to recover. This model indicates that pore pressures at a distance of 0.5 km from the well recovered in early 2016.

The plot on the right in Figure 3-7 shows that the magnitude of the pressure decrease following the 2013 operational changes was greatest very close to the injection well and decreased rapidly with increasing distance from the well. This initial model indicates that the magnitude of the pore pressure decrease was less than 50 psi at distances  $\geq \sim 1.8 \text{ km}$ .

The spatial pattern of pore-pressure perturbations are further explored with a series of figures showing pore pressures as a function of distance from the well at specific times (Figure 3-8 to Figure 3-13). For these plots, the total pore pressure was computed by adding the pre-injection downhole pressure to the pressure changes computed from the pressure diffusion model. The first figure compares the pore pressures on the day before the January 2013 injection well shut-in (1/22/2013) to the pressures on the day before injection resumed (4/16/2013; Figure 3-8). The upper plot shows pore pressure as a function of distance from the well on these two days, and the lower plot shows the change in pore pressure as a function of distance from the well from 1/22/2013 to 4/16/2013. These results indicate that pressures decreased to a distance of about 2 km during the Jan.-Apr. 2013 injection well shut-in. The plots in Figure 3-9 compare the pore pressures at the end of 2013 (12/31/2013) to those prior to the shut-in (1/22/2013). These plots indicate that the zone of decreased pressure extended to about 3.5 km at the end of 2013, but that the pressures beyond 3.5 km were continuing to increase. By June, 2014, the zone of decreased pore pressure had shrunk back to about 2 km (Figure 3-10). Over time, as the zone of decreased pressure continued to contract, the pore pressures beyond this zone continued to increase, as indicated by the plots showing the pressures at the end of 2014, 2015, and 2016 (Figure 3-11 to Figure 3-13). The results from this initial model indicate that at the end of 2016 the zone of decreased pressure only extended to a distance of ~300 m from the well and that pressures beyond this zone were approximately 30 to 50 psi higher than they were before the shut-in and operational changes implemented in 2013 (Figure 3-13).

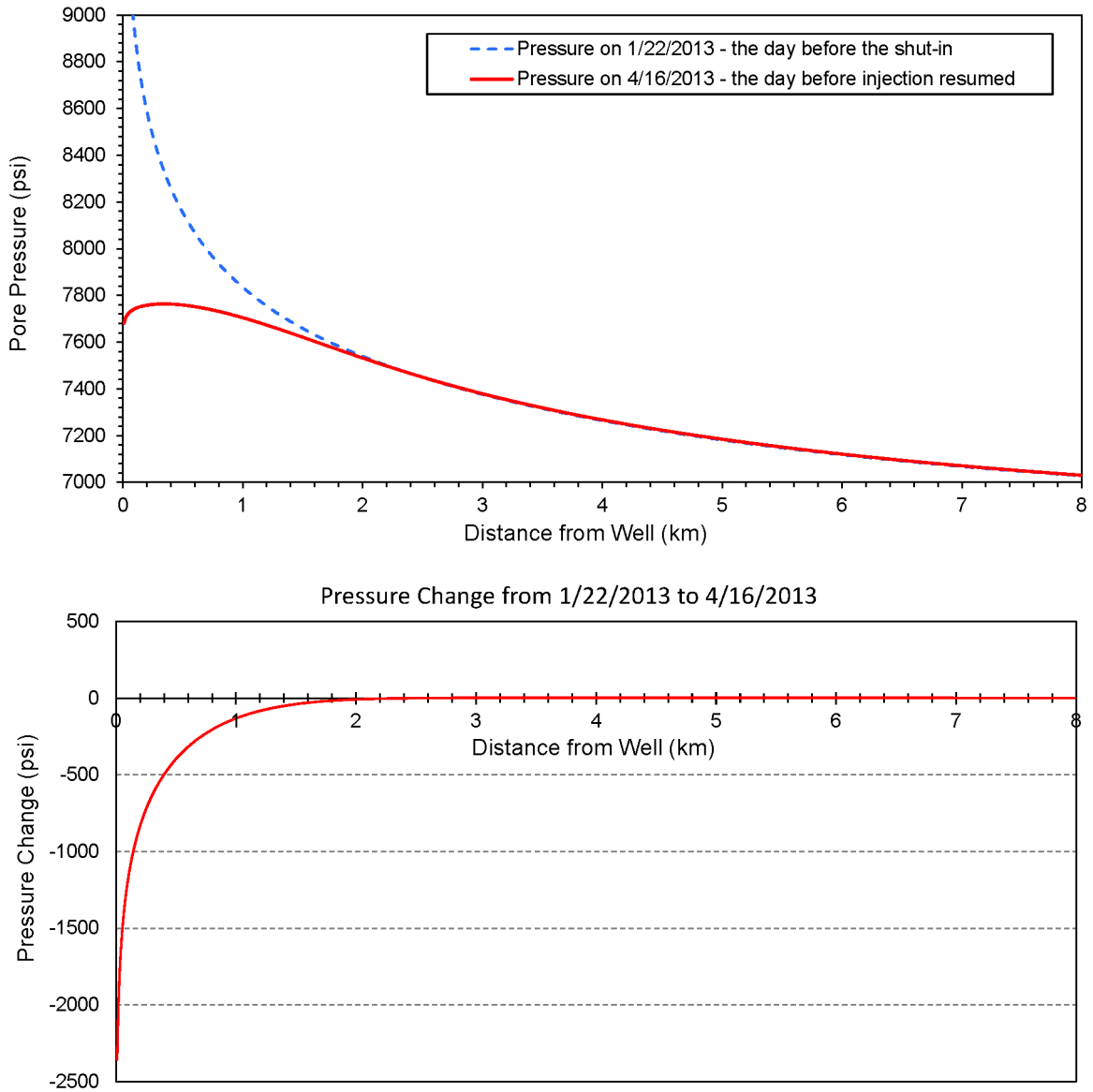


**Figure 3-8: Pore pressures as a function of distance from the well on the day before the January 2013 injection well shut-in (1/22/2013) and on the day before injection resumed (4/16/2013) (upper plot) and the difference between these two curves (lower plot). These results are from the initial diffusion model with  $D = 0.115 \text{ m}^2/\text{s}$  and  $r_w = 10 \text{ cm}$ .**

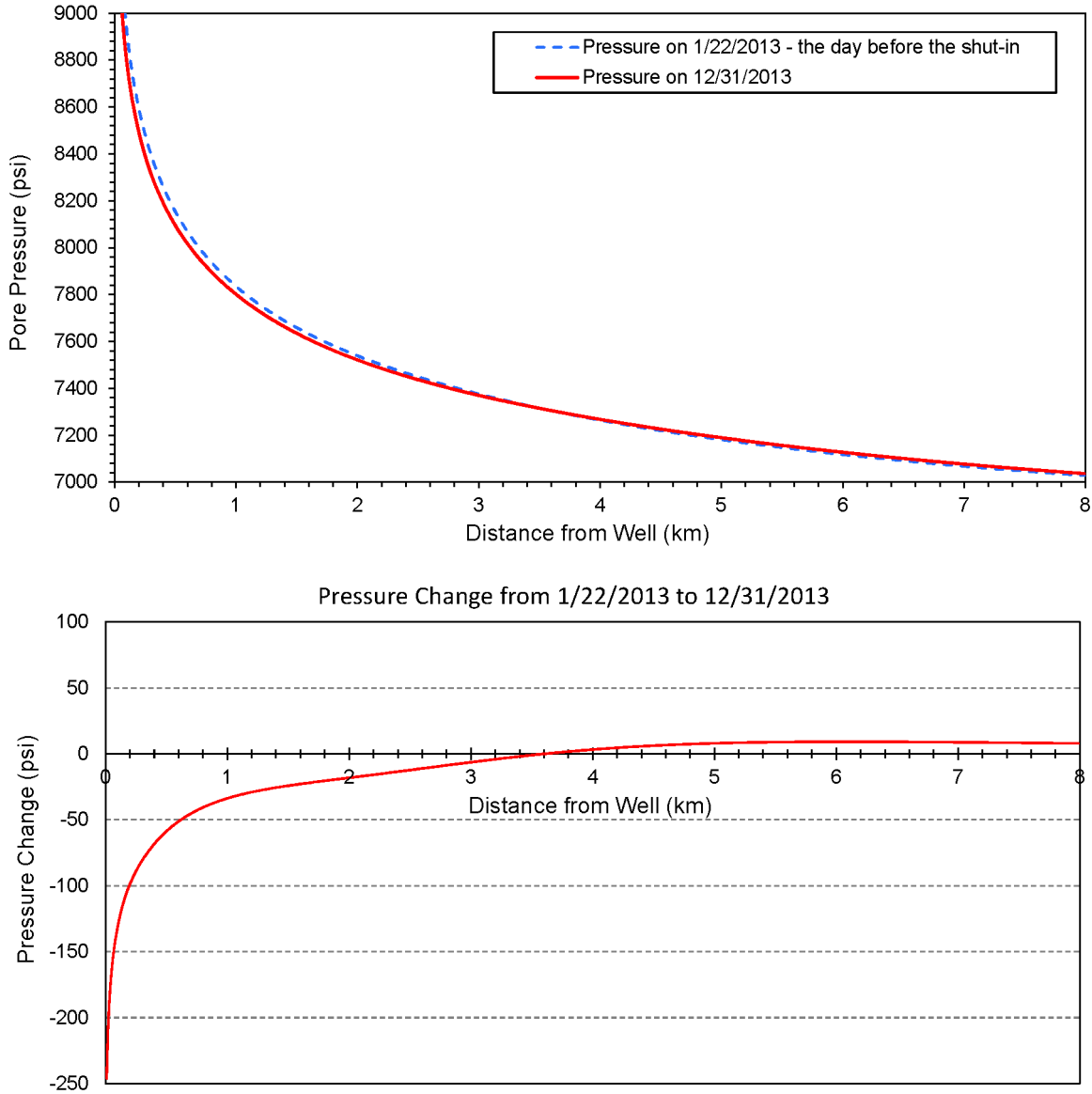


**Figure 3-9: Pore pressures as a function of distance from the well on the day before the January 2013 injection well shut-in (1/22/2013) and on 12/31/2013 (upper plot) and the difference between these two curves (lower plot). These results are from the initial diffusion model with  $D = 0.115 \text{ m}^2/\text{s}$  and  $r_w = 10 \text{ cm}$ .**

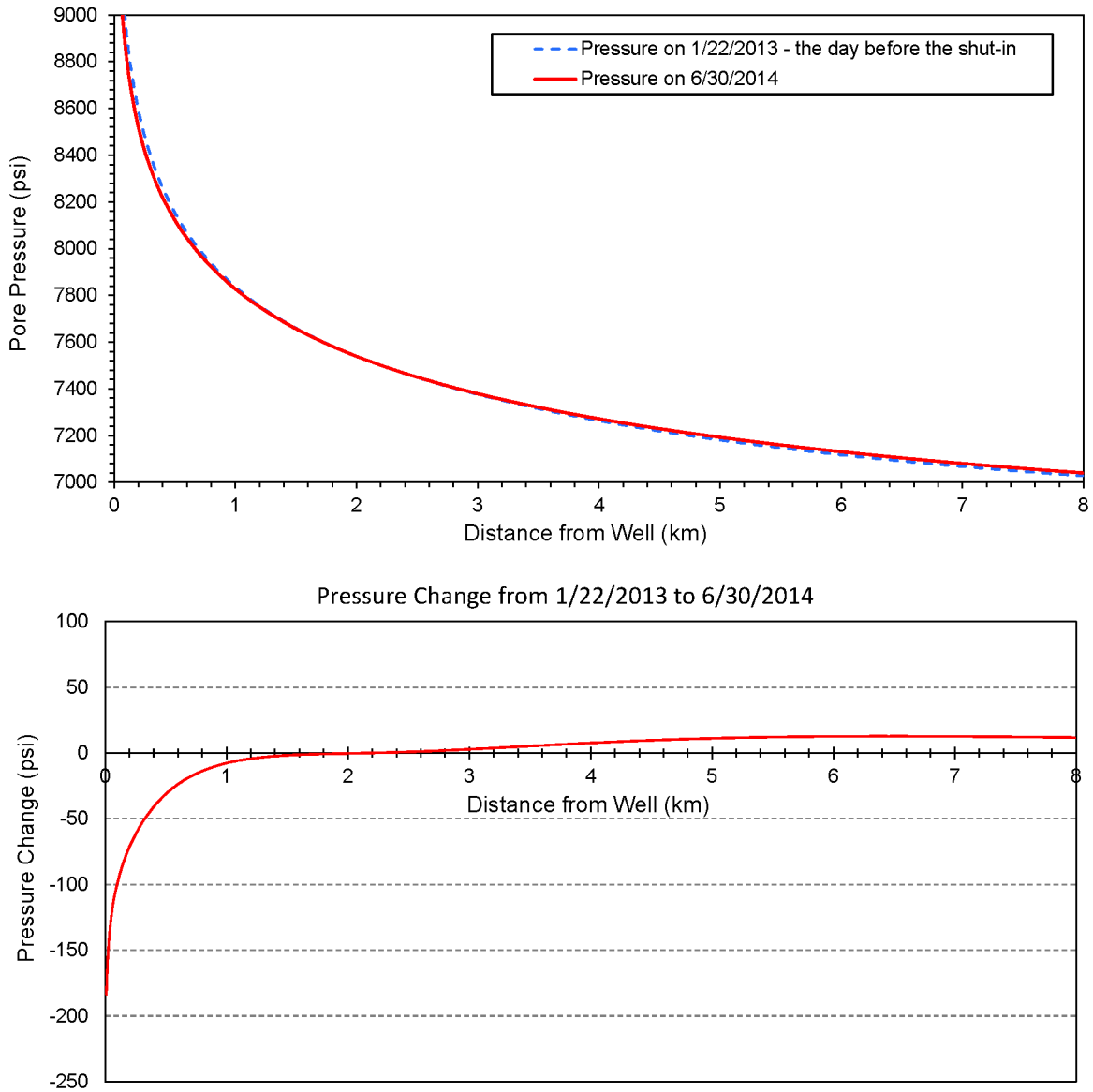


**Figure 3-10: Pore pressures as a function of distance from the well on the day before the January 2013 injection well shut-in (1/22/2013) and on 6/30/2014 (upper plot) and the difference between these two curves (lower plot). These results are from the initial diffusion model with  $D = 0.115 \text{ m}^2/\text{s}$  and  $r_w = 10 \text{ cm}$ .**

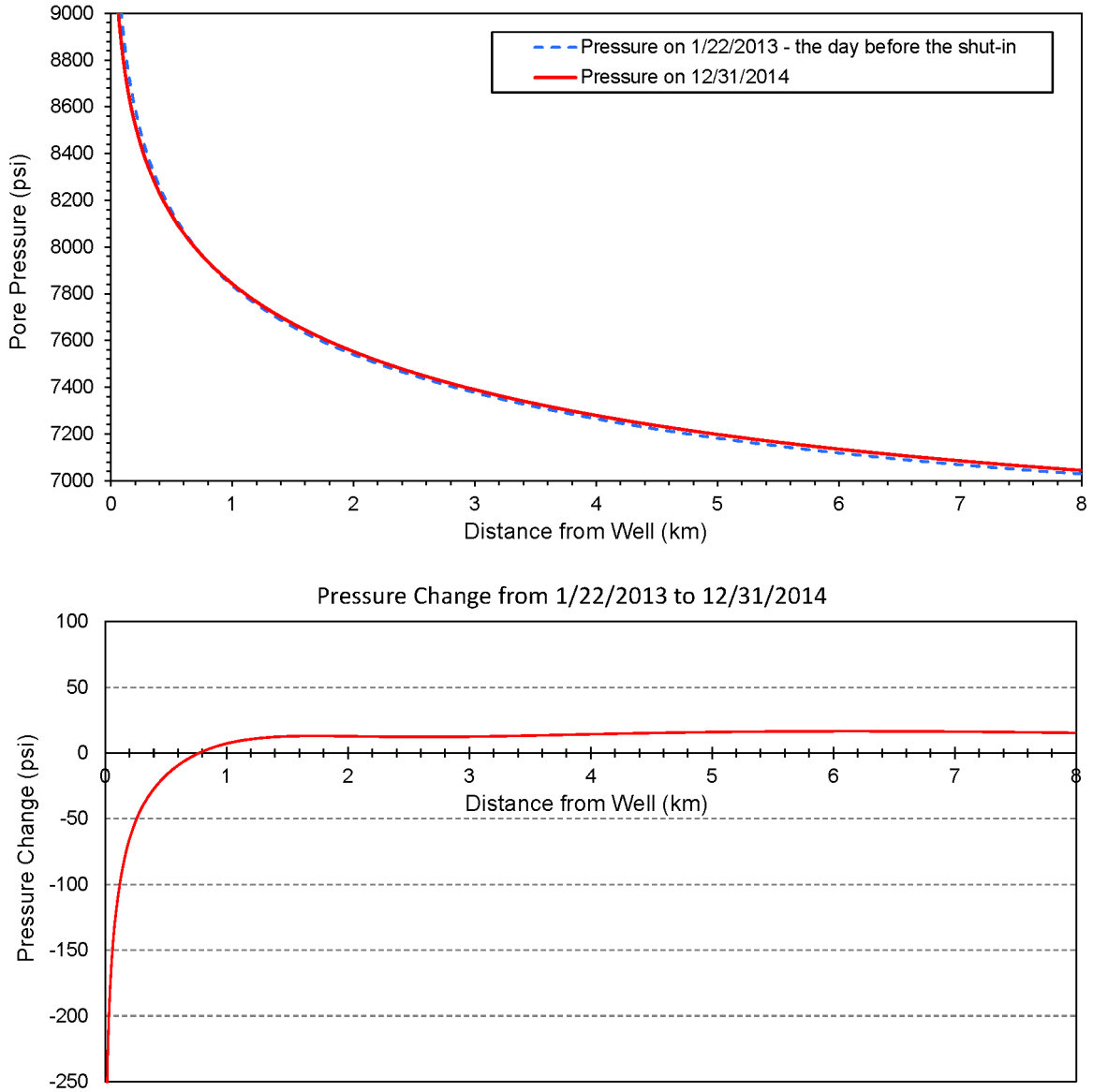


**Figure 3-11: Pore pressures as a function of distance from the well on the day before the January 2013 injection well shut-in (1/22/2013) and on 12/31/2014 (upper plot) and the difference between these two curves (lower plot). These results are from the initial diffusion model with  $D = 0.115 \text{ m}^2/\text{s}$  and  $r_w = 10 \text{ cm}$ .**

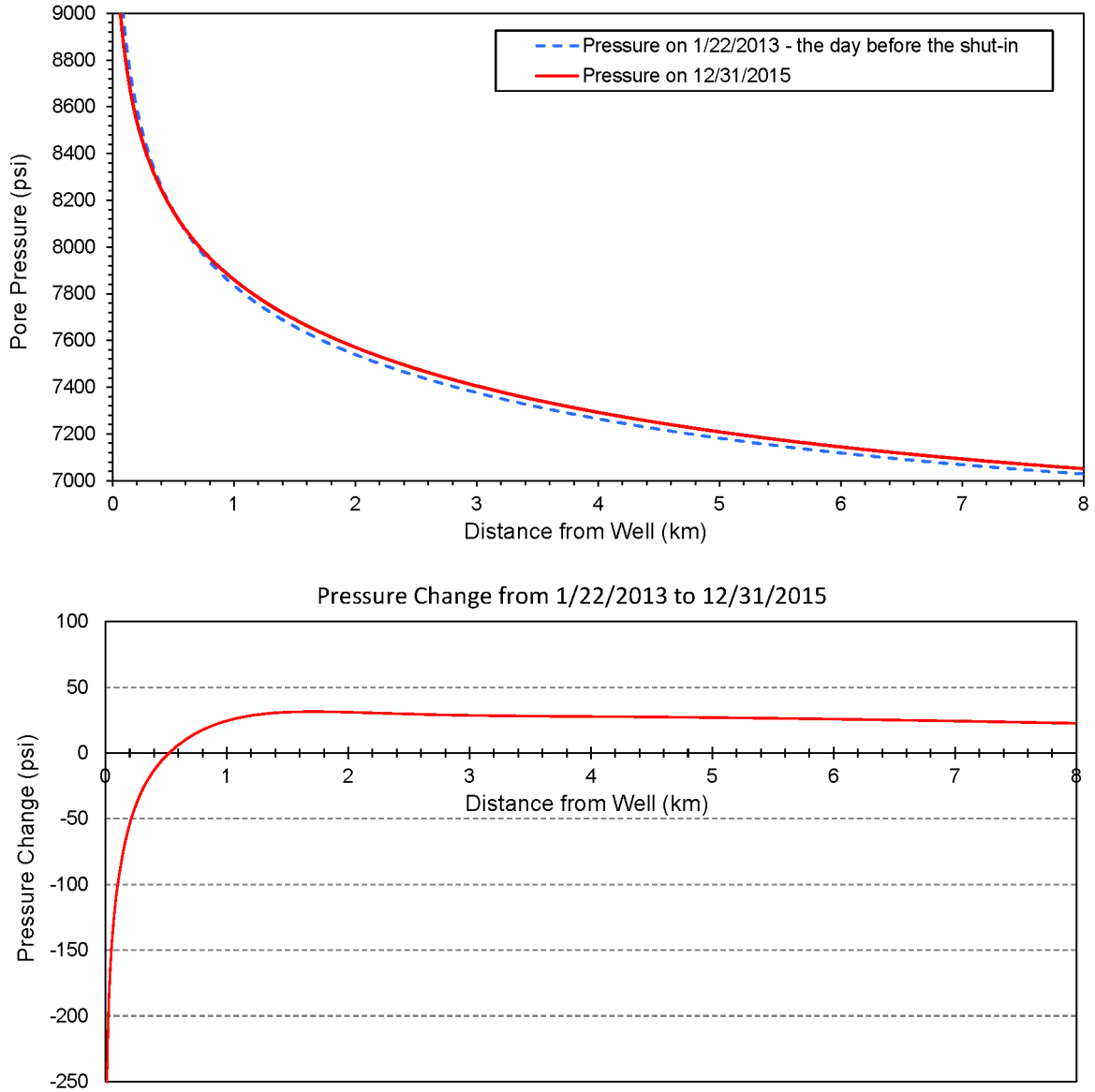


**Figure 3-12: Pore pressures as a function of distance from the well on the day before the January 2013 injection well shut-in (1/22/2013) and on 12/31/2015 (upper plot) and the difference between these two curves (lower plot). These results are from the initial diffusion model with  $D = 0.115 \text{ m}^2/\text{s}$  and  $r_w = 10 \text{ cm}$ .**

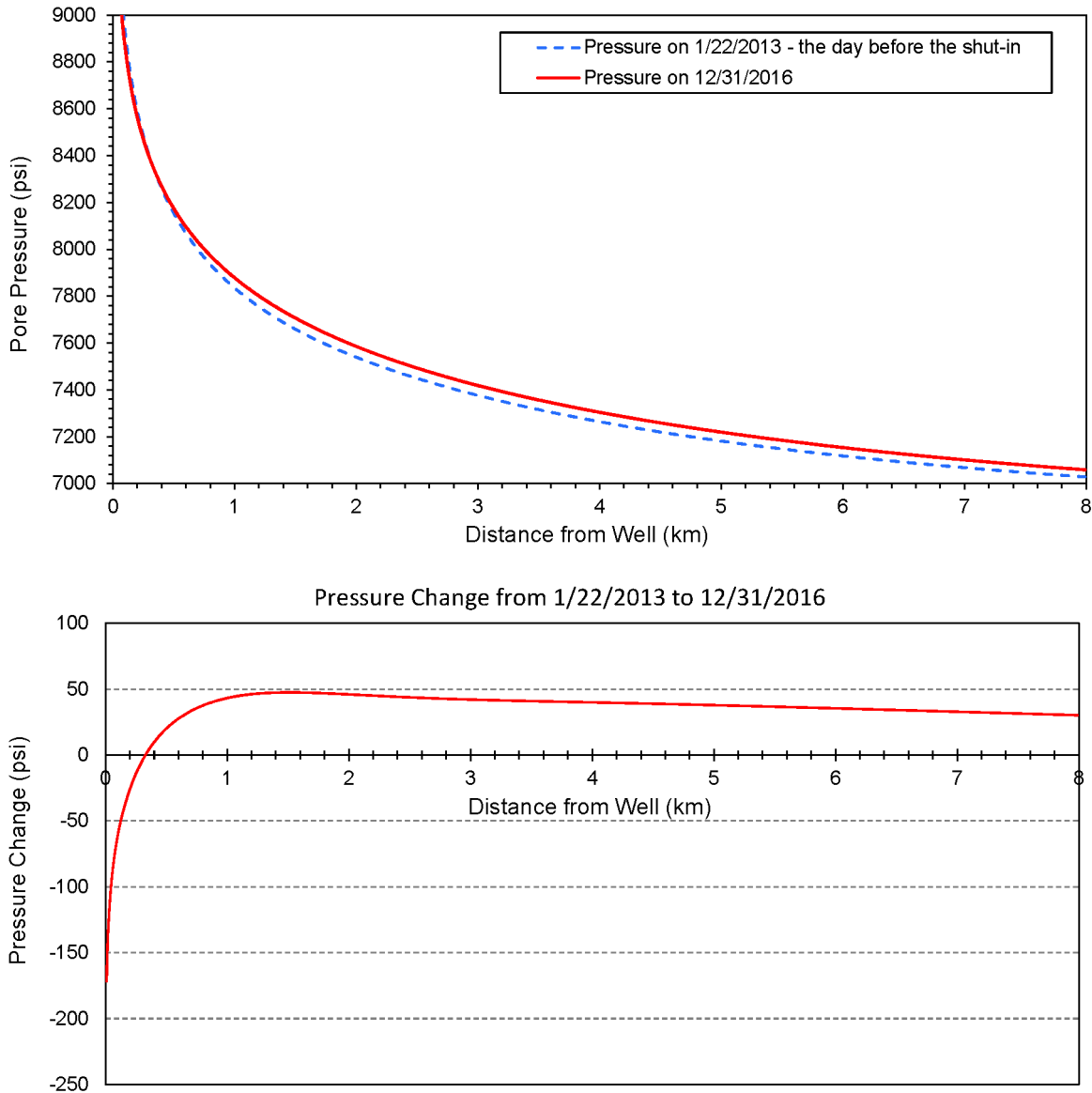


**Figure 3-13: Pore pressures as a function of distance from the well on the day before the January 2013 injection well shut-in (1/22/2013) and on 12/31/2016 (upper plot) and the difference between these two curves (lower plot). These results are from the initial diffusion model with  $D = 0.115 \text{ m}^2/\text{s}$  and  $r_w = 10 \text{ cm}$ .**

### 3.2.2 Additional Models

To evaluate the dependence of the model results on the assumed values of diffusivity and effective borehole radius, we computed pore pressures using several additional pressure diffusion models with different values of  $D$  and  $r_w$ . Below we compare the results of these models to each other and to the results from the initial model presented above.

### 3.2.2.1 Varying Effective Borehole Radius

The diffusivity of the region immediately surrounding the injection well has likely increased to some extent since the injection well was drilled. Reasons for believing that a higher-diffusivity zone has developed around the well include: acid stimulation was performed in the PVU well in 1993; injection has occurred at pressures above the fracture propagation pressure for extended periods of time (years), which should cause fractures parallel to the direction of maximum horizontal stress to lengthen; the 180°F difference in temperature between the in-situ reservoir rock and the injected fluid should cause the rock matrix to cool and shrink, thereby opening microfractures; and an aseismic zone developed around the well between distances of ~400 m and ~1100 m after the injection flow rate was reduced in 2000 (and has persisted despite increased pressures), which may be an indication of increased diffusivity near the well (King and Block, 2016).

The simple diffusion model used here does not allow for spatially varying diffusivity. However, the extreme case – in which the diffusivity in the immediate region around the borehole is so high that it experiences pore pressure perturbations introduced at the well almost instantaneously – can be easily modeled by increasing the value of the effective borehole radius,  $r_w$ . This would be an appropriate approximation for the case of significantly increased fracture permeability near the well. Below we examine results of several diffusion models with  $r_w$  ranging from 10 cm (the initial model) to 500 m. These models use the same value of  $D$  as the initial model,  $0.115 \text{ m}^2/\text{s}$ .

Figure 3-14 shows summary plots of the results from pressure diffusion models with  $r_w$  equal to 10 cm (initial model), 10 m, 100 m, 250 m, and 500 m for the time period following the shut-in of the injection well and change in flow rate implemented in 2013. The plot on the left shows that as  $r_w$  increases, the zone of reduced pressure that occurred after the shut-in extends farther from the well. The model with the largest value of  $r_w$  (500 m) indicates that pore pressures experienced a decrease to a maximum distance of about 5.8 km from the well, compared to a distance of about 4.4 km for the model with the smallest value of  $r_w$  (10 cm). As  $r_w$  increases, the duration of the time period of reduced pressure also increases, with pressures decreasing slightly sooner and recovering later. The model with  $r_w = 10 \text{ cm}$  indicates that pressures at distances  $\geq 0.5 \text{ km}$  from the well recovered to their pre-shut-in maximum values by early 2016, whereas the model with  $r_w = 500 \text{ m}$  indicates that, at the beginning of 2016, pressures were still reduced to a distance of ~1.8 km. The plot on the right in Figure 3-14 indicates that the magnitude of the maximum pore pressure reduction at a given distance from the well increases for larger values of  $r_w$ . For example, the model with an  $r_w$  of 500 m indicates a 450 psi maximum reduction in pore pressure at a distance of 2 km from the well, compared to a maximum reduction of less than 50 psi at the same distance for the model with an  $r_w$  of 10 cm. For the model with an  $r_w$  of 500 m, reductions in pore pressure  $\geq 50 \text{ psi}$  are predicted to distances of 4 km, whereas the model with  $r_w = 10 \text{ cm}$  indicates that reductions in pore pressure  $\geq 50 \text{ psi}$  extend to only ~1.8 km.

The plots in Figure 3-15 compare pore pressures as a function of distance from the injection well for the model with the smallest effective borehole radius, 10 cm (left plots in Figure 3-15) and the model with the largest value of  $r_w$ , 500 m (right plots in Figure 3-15). Pressures are shown for

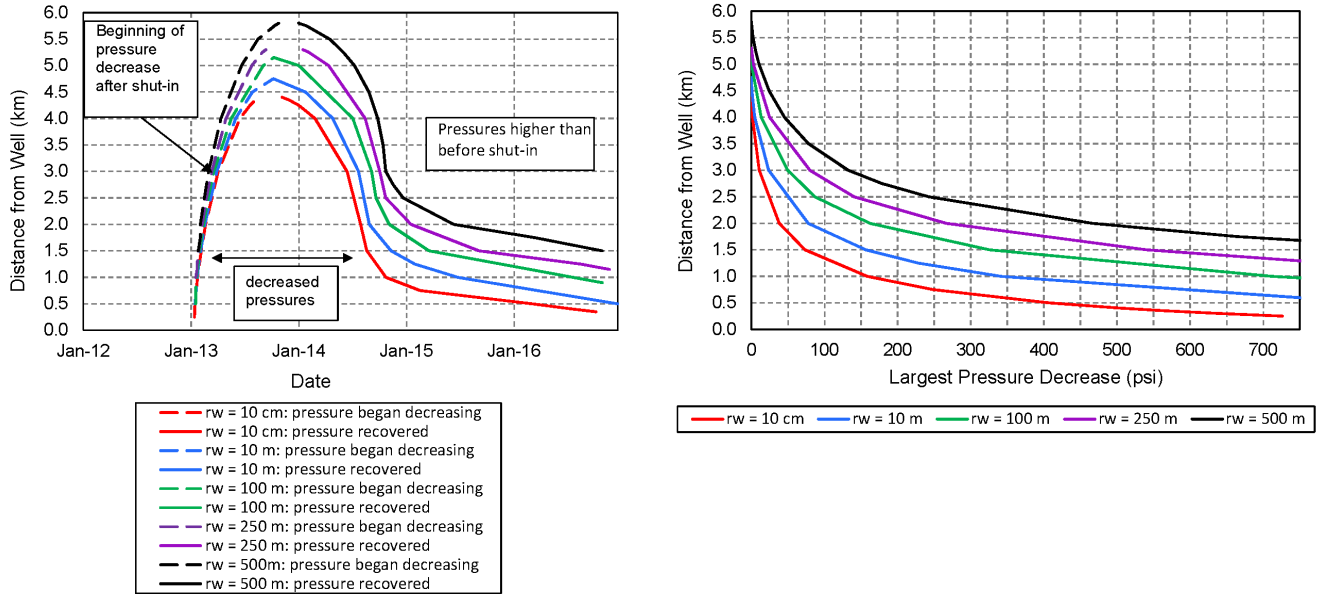


**Figure 3-14: Summary plots of the results from pressure diffusion models with  $D = 0.115 \text{ m}^2/\text{s}$  and  $r_w = 10 \text{ cm}$ ,  $10 \text{ m}$ ,  $100 \text{ m}$ ,  $250 \text{ m}$ , and  $500 \text{ m}$  for the time period following the injection well shut-in and reduced flow rate implemented in 2013. The left plot shows the dates when pore pressures began decreasing following the injection well shut-in, as a function of distance from the well (dashed lines), and the dates when the pressures recovered to their previous maximum values (solid lines). For dates to the right of the solid lines, the models predict that pressures are higher than they were prior to the shut-in. The right plot shows the size of the largest pressure decrease as a function of distance from the injection well for each model.**

two days: January 22, 2013, the day before the injection well was shut in, and December 31, 2016 (Figure 3-15, upper plots). The differences in the pressures on these two days, as a function of distance from the well, are also included (Figure 3-15, lower plots). (The plots shown here for the model with  $r_w = 10 \text{ cm}$  are the same ones shown previously in Figure 3-13.) Both models indicate the same absolute pressures and pressure differences at the wellbore. Away from the wellbore, however, the pressures are substantially different. The absolute pore pressures are higher everywhere away from the well in the model with the larger value of  $r_w$  compared to the model with the smaller value of  $r_w$  (upper plots in Figure 3-15). The differences in pressures between 1/22/2013 and 12/31/2016 indicate that reduced pressures extended to a larger distance at the end of 2016 for the model with the larger  $r_w$  (to  $\sim 1.2 \text{ km}$ ) than for the model with the smaller  $r_w$  (to  $\sim 0.4 \text{ km}$ ) (lower plots in Figure 3-15). However, beyond this near-well zone of decreased pressure, the model with  $r_w = 500 \text{ m}$  indicates a significantly larger increase in pore pressures at the end of 2016 compared to their pre-shut-in maximum values ( $\sim 100 \text{ psi}$ ) than does the model with  $r_w = 10 \text{ cm}$  ( $\sim 30\text{-}50 \text{ psi}$ ).

The effect of  $r_w$  on the model results is seen in more detail in the plots presented in Figure 3-16. These plots show the differences in pore pressure as a function of distance from the well from the day prior to the injection well shut-in (1/22/2013) to several later dates: 4/16/2013 (the day before injection resumed), 12/31/2013, 12/31/2014, 12/31/2015, and 12/31/2016. Each plot

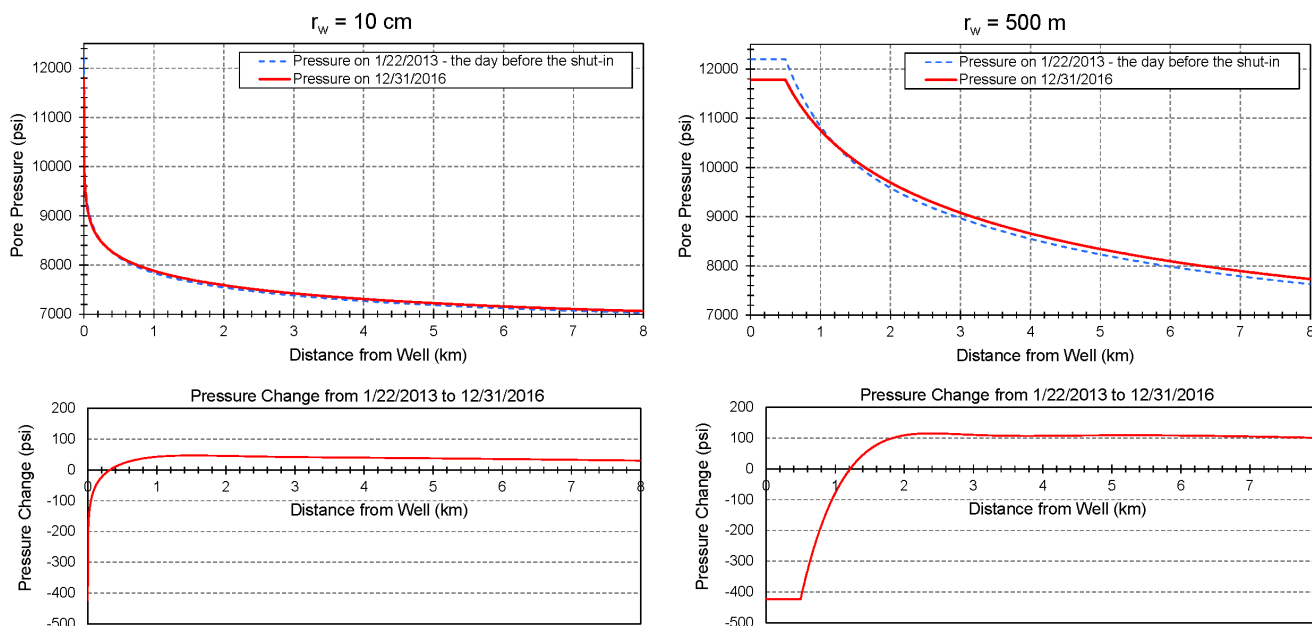


**Figure 3-15: Pore pressures as a function of distance from the well on the day before the January 2013 injection well shut-in (1/22/2013) and on 12/31/2016 (upper plots) and the difference between these two curves (lower plots). Results are shown for pressure diffusion models using  $D = 0.115$  m<sup>2</sup>/s and  $r_w = 10$  cm (left plots) and  $r_w = 500$  m (right plots).**

shows the pressure differences from a model with  $r_w = 10$  cm (dashed blue curves) and from a model with  $r_w = 500$  m (solid red curves). Substantial differences in the pore pressure trends for the two models are observed for all time periods examined. During the shut-in period, pore pressures decline to a greater distance for the model with  $r_w = 500$  m (to  $\sim 3.2$  km) than for the model with  $r_w = 10$  cm (to  $\sim 2.2$  km) (uppermost plot in Figure 3-16). Beyond this near-well area of decreased pressure, pore pressures show no noticeable change during the shut-in period compared to their pre-shut-in values for either model. By the end of 2013 (second plot from the top in Figure 3-16), the model with  $r_w = 500$  m predicts reduced pore pressures to a distance of almost 5 km from the well. The model with  $r_w = 10$  cm predicts reduced pore pressures to a distance of  $\sim 3.5$  km. Beyond this zone of decreased pressures, pore pressure have begun to increase compared to their pre-shut-in values. The model with the larger  $r_w$  shows a more rapid increase in pressure at these distances. During subsequent time periods, the zone of reduced pressures begins to shrink. For any given time period, the model with  $r_w = 500$  m shows larger pressure changes than the model with  $r_w = 10$  cm, with pressures in the near-well zone showing a bigger decrease and pressures beyond this zone showing a larger increase. Pressure trends for models with intermediate values of  $r_w$  would show pressure changes greater than those for  $r_w = 10$  cm but less than those for  $r_w = 500$  m.

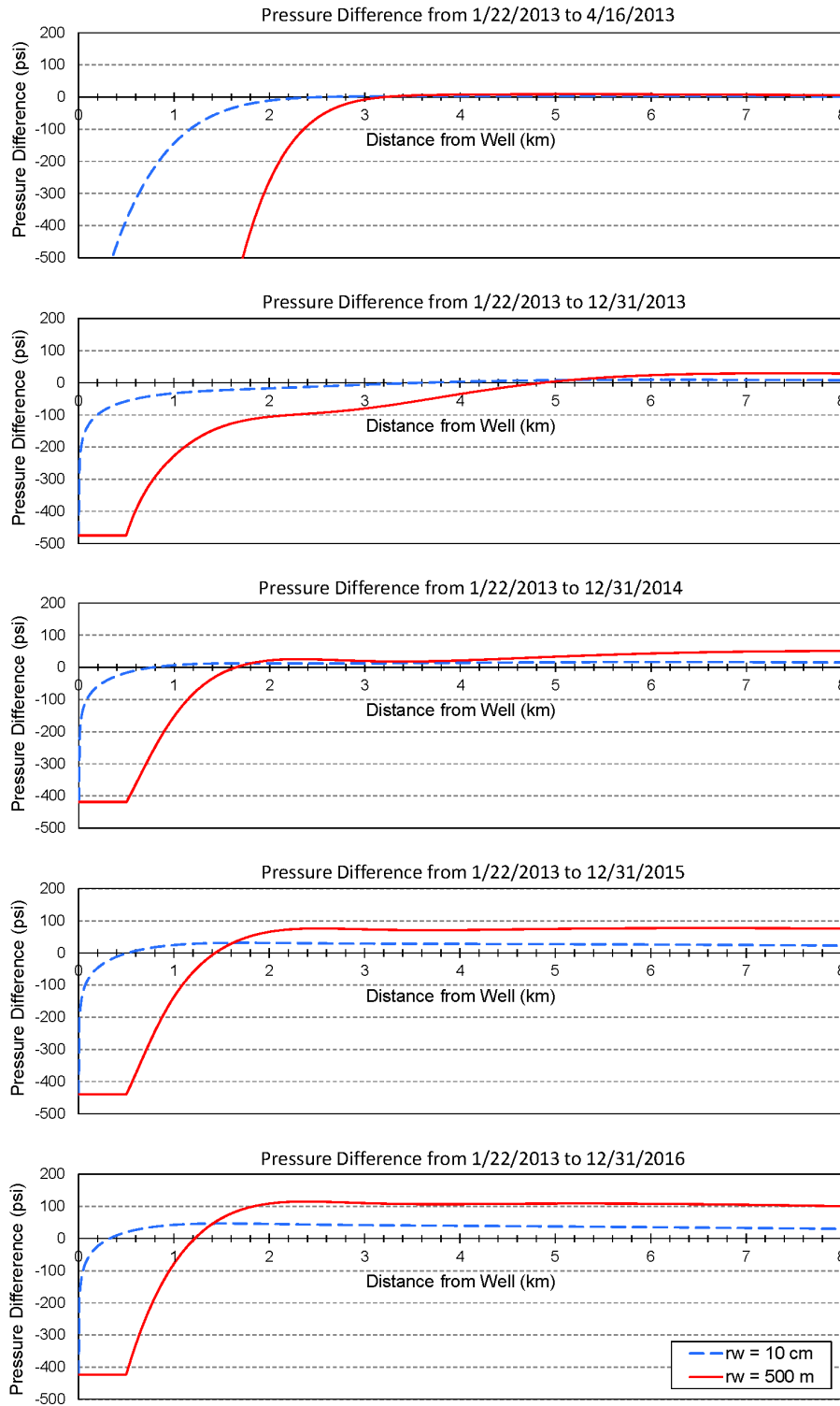


**Figure 3-16: Differences in pore pressure, as a function of distance from the well, from the day before the injection well was shut in (1/22/2013) to (from top to bottom): the day before injection resumed (4/16/2013), 12/31/2013, 12/31/2014, 12/31/2015, and 12/31/2016. Results are shown for pore pressure diffusion models with  $r_w = 10$  cm (dashed blue curves) and  $r_w = 500$  m (solid red curves). The diffusivity,  $D$ , is  $0.115 \text{ m}^2/\text{s}$  for all models.**

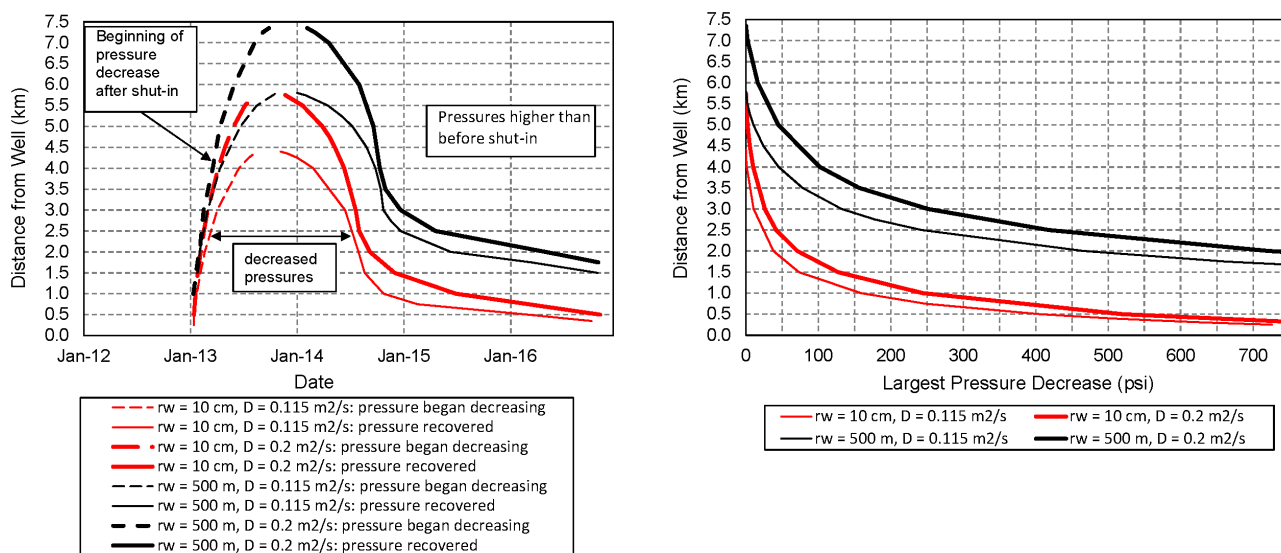


**Figure 3-17: Summary plots of the results from pressure diffusion models with  $D = 0.115\text{ m}^2/\text{s}$  and  $D = 0.2\text{ m}^2/\text{s}$  and  $r_w = 10\text{ cm}$  and  $r_w = 500\text{ m}$  for the time period following the injection well shut-in and reduced flow rate implemented in 2013. The left plot shows the dates when pore pressures began decreasing following the injection well shut-in, as a function of distance from the well (dashed lines), and the dates when the pressures recovered to their previous maximum values (solid lines). For dates to the right of the solid lines, the models predict that pressures are higher than they were prior to the shut-in. The right plot shows the size of the largest pressure decrease as a function of distance from the injection well for each model.**

### 3.2.2.2 Varying Diffusivity

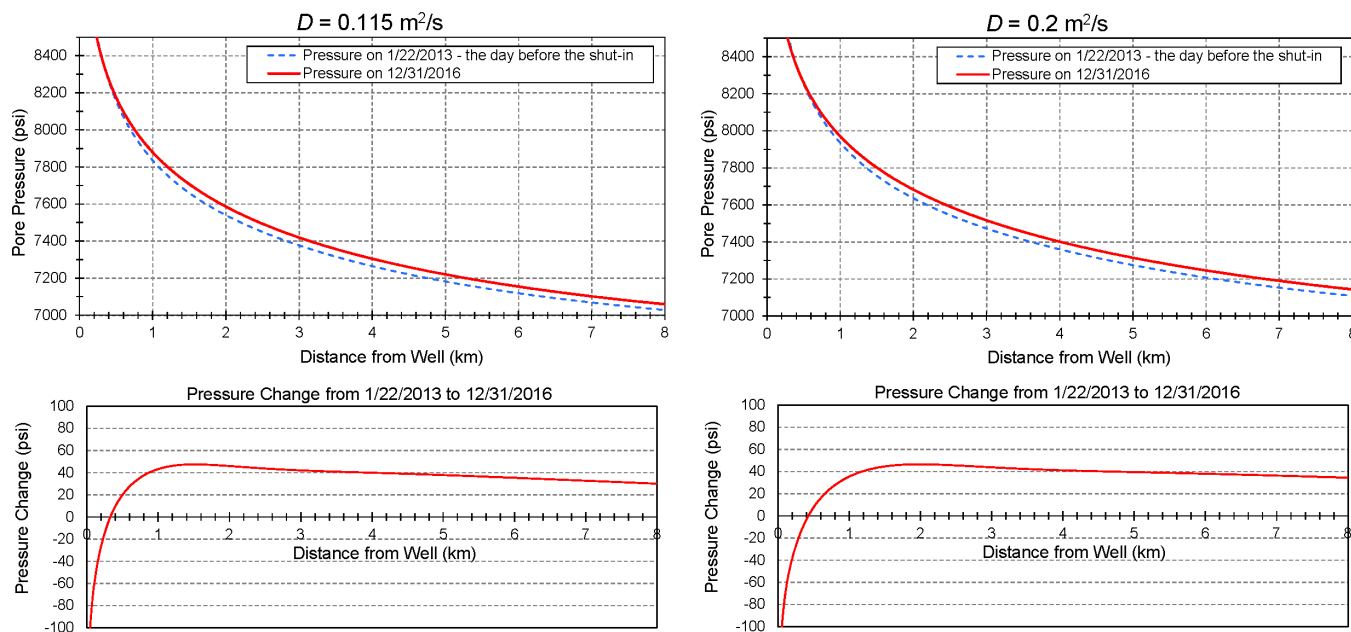
The value of diffusivity used in all of the above models is  $0.115\text{ m}^2/\text{s}$ , the value obtained from the move-out of the initial onset of induced seismicity as a function of distance from the injection well to about 10 km. A somewhat higher value of  $D$ ,  $0.2\text{ m}^2/\text{s}$ , was obtained when fitting the initial onset of induced seismicity at greater distances (King and Block, 2016). To see how much the results of the pressure diffusion models vary with a reasonable variation in the value of diffusivity, we recomputed the results using  $D = 0.2\text{ m}^2/\text{s}$  and compared them to the results obtained previously using  $D = 0.115\text{ m}^2/\text{s}$ .

Figure 3-17 shows summary plots of the results from pressure diffusion models with  $D = 0.115\text{ m}^2/\text{s}$  and  $D = 0.2\text{ m}^2/\text{s}$  for the time period following the shut-in of the injection well and change in flow rate implemented in 2013. Results are shown using two values of  $r_w$ : 10 cm and 500 m. The plot on the left shows that as  $D$  increases, the zone of reduced pressure that occurred after the shut-in extends farther from the well. For the model with  $r_w = 10\text{ cm}$ , the model with the larger value of  $D$  ( $0.2\text{ m}^2/\text{s}$ ) indicates that pore pressures experienced a decrease to a maximum distance of about 5.7 km from the well, compared to a distance of about 4.4 km for the model with the smaller value of  $D$  ( $0.115\text{ m}^2/\text{s}$ ). Similarly, for the model with  $r_w = 500\text{ m}$ , the model with the larger value of  $D$  indicates that pore pressures experienced a decrease to a maximum distance of about 7.4 km from the well, compared to a distance of  $\sim 5.8\text{ km}$  for the model with the smaller value of  $D$ . As  $D$  increases, the duration of the time period of reduced pressure also

increases, with pressures decreasing slightly sooner and recovering later. However, the effect on the duration of pressure decrease is not nearly as substantial as the effect on the maximum distance of pressure decrease. The right plot in Figure 3-17 shows that models with larger values of  $D$  predict larger pressure decreases at a given distance from the well. However, this effect is relatively modest. Hence, the main impact of using a model with a higher diffusivity is that operational changes at the injection well are predicted to impact pore pressures at greater distances from the well than comparable models with lower diffusivity values.

The plots in Figure 3-18 compare pore pressures as a function of distance from the injection well for the model with the smaller value of diffusivity,  $0.115 \text{ m}^2/\text{s}$  (left plots in Figure 3-18) and the model with the larger value of diffusivity,  $0.2 \text{ m}^2/\text{s}$  (right plots in Figure 3-18). Pore pressures are shown for two days: January 22, 2013, the day before the injection well was shut in, and December 31, 2016 (Figure 3-18, upper plots). The differences in the pressures on these two days, as a function of distance from the well, are also included (Figure 3-18, lower plots). The plots shown in Figure 3-18 were computed using an effective borehole radius,  $r_w$ , of 10 cm; Figure 3-19 presents the same types of plots computed using  $r_w = 500 \text{ m}$ . The plots in these two figures show that the pore pressures are not very sensitive to the value of  $D$  used in the modeling. The models with the higher value of  $D$  predict very slightly higher pore pressures (upper plots in Figure 3-18 and Figure 3-19). Furthermore, the changes in predicted pore pressures from 1/22/2013 to 12/31/2016 are also not very sensitive to the value of  $D$  used in the models. The models with the higher value of  $D$  indicate decreased pore pressures at the end of 2016 extending to slightly greater distances than the models with the lower value of  $D$ , but the magnitudes of the pressure changes beyond this near-well zone are almost identical (lower plots in Figure 3-18 and Figure 3-19).

The effect of  $D$  on the model results is seen in more detail in the plots presented in Figure 3-20 and Figure 3-21. These plots show the differences in pore pressure as a function of distance from the well from the day prior to the injection well shut-in (1/22/2013) to several later dates: 4/16/2013 (the day before injection resumed), 12/31/2013, 12/31/2014, 12/31/2015, and 12/31/2016. Each plot shows the pressure differences from a model with  $D = 0.115 \text{ m}^2/\text{s}$  (dashed blue curves) and from a model with  $D = 0.2 \text{ m}^2/\text{s}$  (solid red curves). Results for  $r_w = 10 \text{ cm}$  are presented in Figure 3-20, while the results for  $r_w = 500 \text{ m}$  are presented in Figure 3-21. These plots illustrate that the value of diffusivity used in the models only has a substantial impact on the computed pressures for the time period during and shortly after the injection well shut-in. Pore pressures decrease to a substantially greater distance during the shut-in period for the models with the higher value of  $D$  (uppermost plots in Figure 3-20 and Figure 3-21). Noticeable differences are still seen at the end of 2013, especially in the model with  $r_w = 500 \text{ m}$  (second plot in Figure 3-21). For later times, however, the effect of the value of  $D$  used in the modeling is very small.



**Figure 3-18: Pore pressures as a function of distance from the well on the day before the January 2013 injection well shut-in (1/22/2013) and on 12/31/2016 (upper plots) and the difference between these two curves (lower plots). Results are shown for pressure diffusion models using  $r_w = 10 \text{ cm}$  and  $D = 0.115 \text{ m}^2/\text{s}$  (left plots) and  $D = 0.2 \text{ m}^2/\text{s}$  (right plots).**

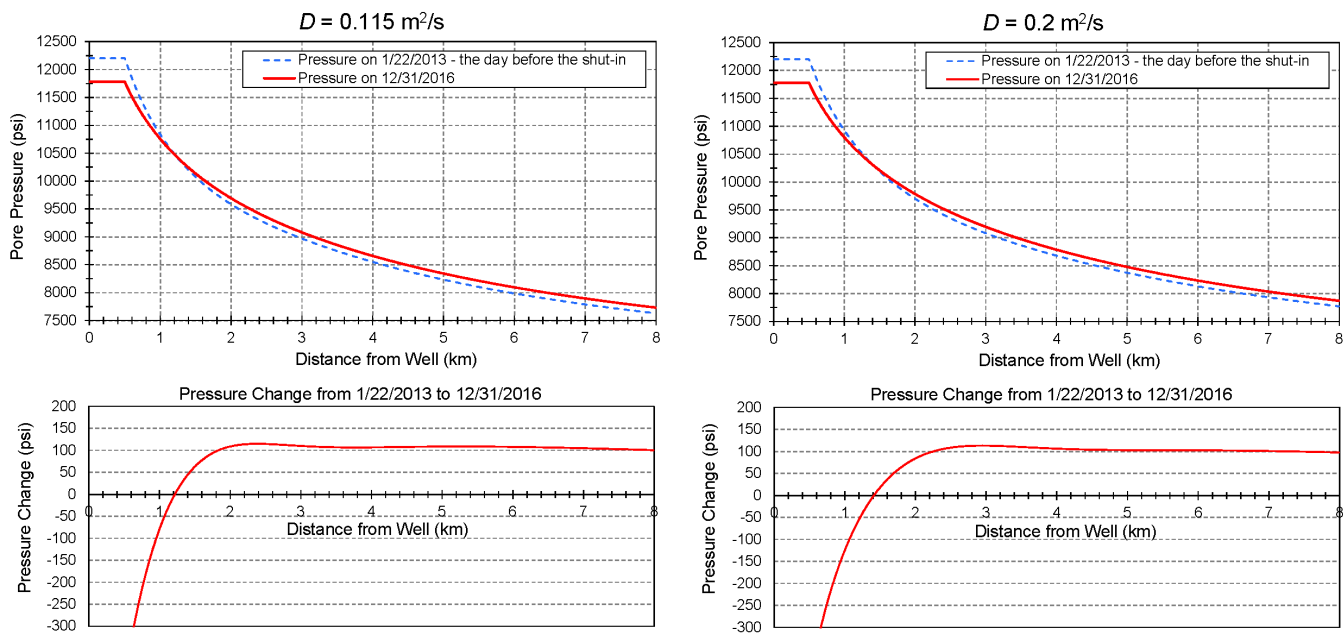


**Figure 3-19: Pore pressures as a function of distance from the well on the day before the January 2013 injection well shut-in (1/22/2013) and on 12/31/2016 (upper plots) and the difference between these two curves (lower plots). Results are shown for pressure diffusion models using  $r_w = 500 \text{ m}$  and  $D = 0.115 \text{ m}^2/\text{s}$  (left plots) and  $D = 0.2 \text{ m}^2/\text{s}$  (right plots).**

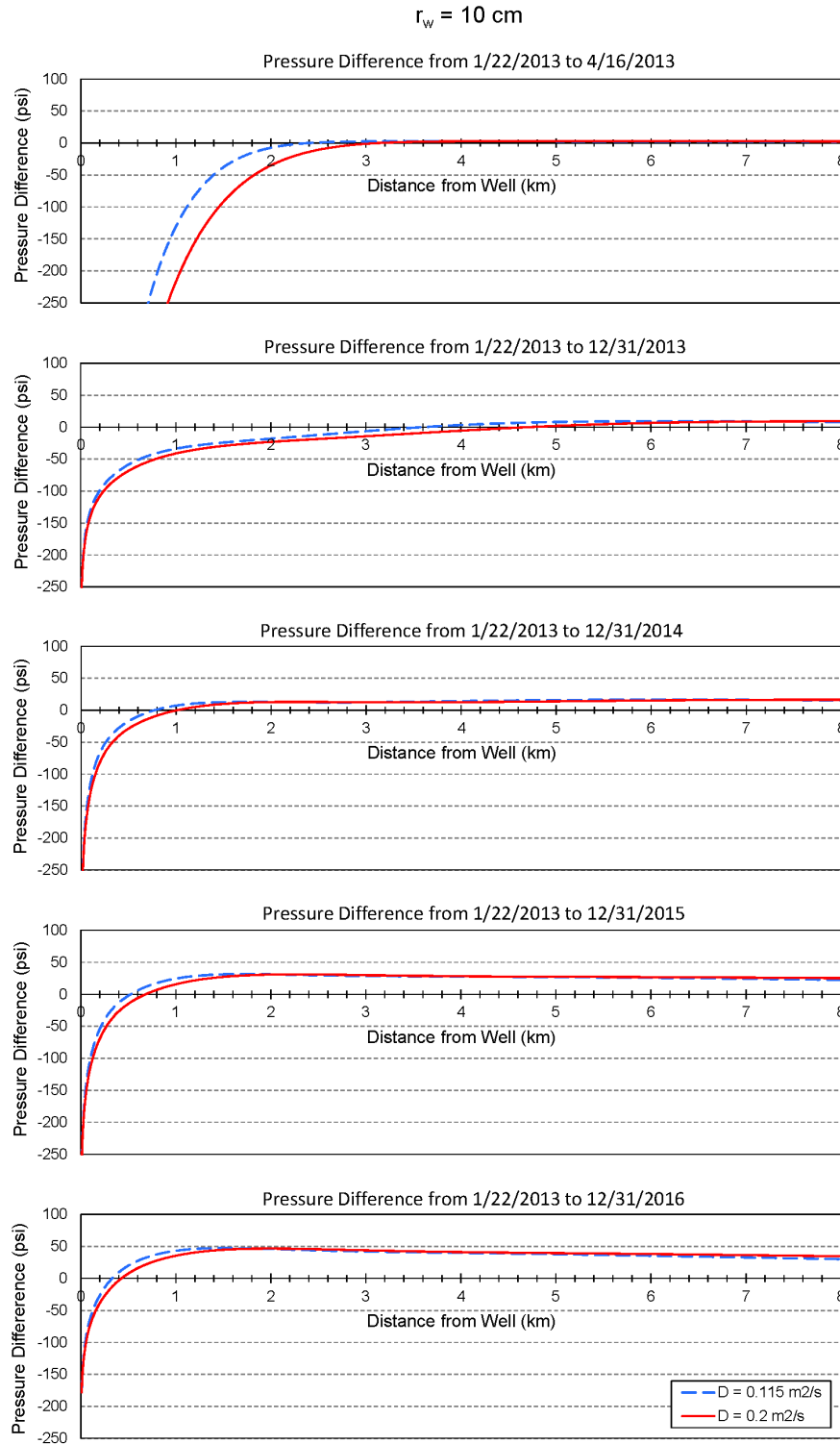


**Figure 3-20: Differences in pore pressure, as a function of distance from the well, from the day before the injection well was shut in (1/22/2013) to (from top to bottom): the day before injection resumed (4/16/2013), 12/31/2013, 12/31/2014, 12/31/2015, and 12/31/2016. Results are shown for pore pressure diffusion models with  $D = 0.115 \text{ m}^2/\text{s}$  (dashed blue curves) and  $D = 0.2 \text{ m}^2/\text{s}$  (solid red curves). The effective borehole radius,  $r_w$ , is 10 cm for all models.**

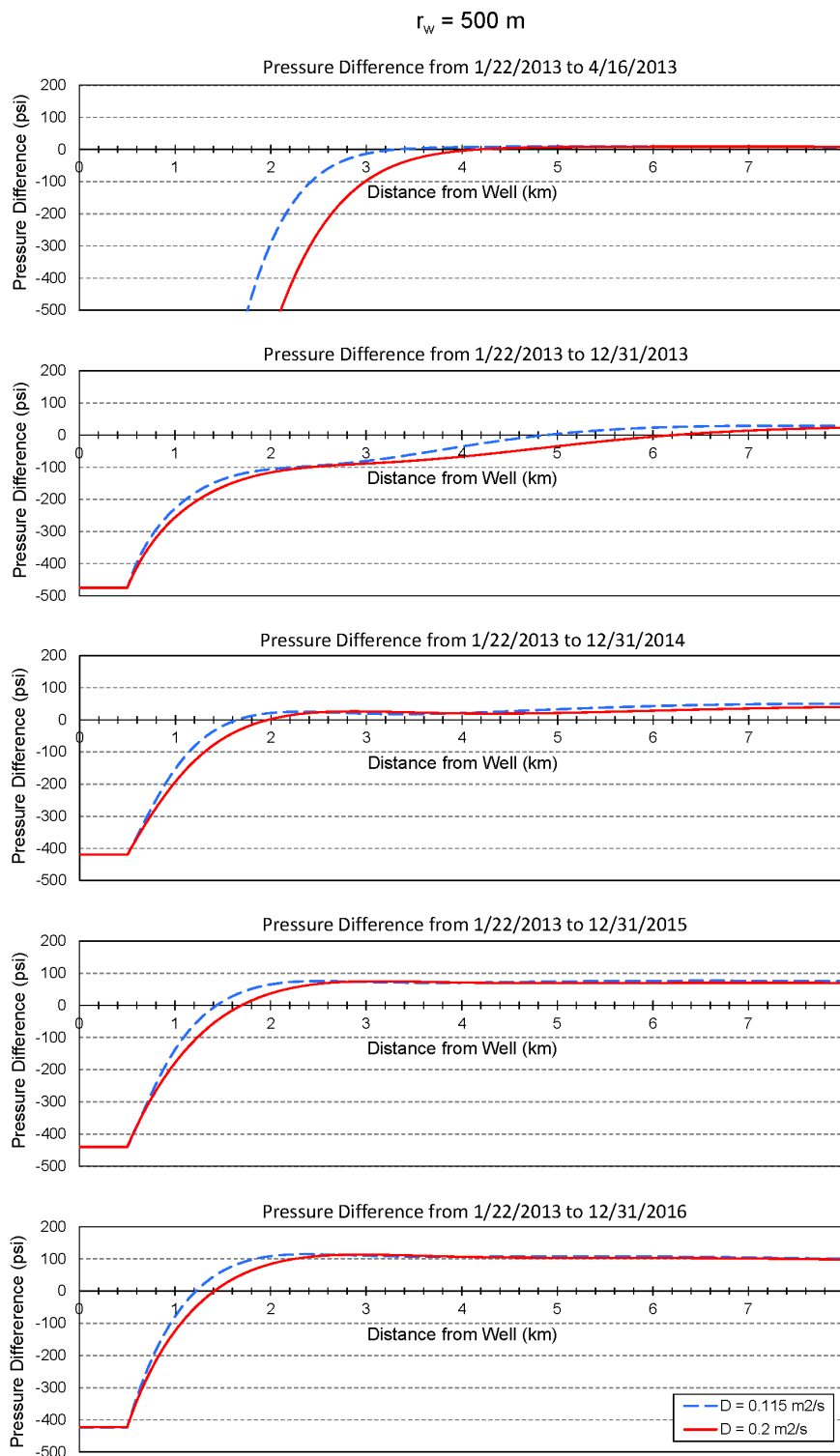


**Figure 3-21: Differences in pore pressure, as a function of distance from the well, from the day before the injection well was shut in (1/22/2013) to (from top to bottom): the day before injection resumed (4/16/2013), 12/31/2013, 12/31/2014, 12/31/2015, and 12/31/2016. Results are shown for pore pressure diffusion models with  $D = 0.115 \text{ m}^2/\text{s}$  (dashed blue curves) and  $D = 0.2 \text{ m}^2/\text{s}$  (solid red curves). The effective borehole radius,  $r_w$ , is 500 m for all models.**

### 3.3 Summary

At the end of 2016, the maximum injection pressure at the PVU well was still ~300 psi lower than the peak value reached just prior to January 2013  $M_L$  4.4 earthquake. However, the trend in injection pressure changed in early 2016, showing a more consistent and steeper increase over time during 2016 compared to the previous two years. In addition, pore pressure diffusion modeling indicates that pore pressures away from the well were higher at the end of 2016 than they were prior to the occurrence of the January 2013 earthquake and subsequent change in injection protocol.

The pore pressure diffusion models examined here indicate that pore pressures decreased to a distance of several km from the PVU injection well following the extended shut-in of the well in early 2013 and subsequent resumption of injection at a decreased flow rate. Depending on the model parameters assumed, pore pressures are estimated to have decreased to a distance of 4.4 to 7.4 km from the well, with the magnitude of the pressure decrease greatly diminishing with distance. Pore pressures began increasing again at all distances by late 2013. As the pressures gradually increased, they eventually reached and then exceeded their pre-shut-in maximum values. This recovery to pre-shut-in pressures was achieved earlier at larger distances from the well and later at closer distances. The models indicate that, by the end of 2016, pore pressures at distances greater than ~0.3 – 1.4 km from the injection well were approximately 30 to 100 psi higher than prior to the January 2013  $M_L$  4.4 earthquake.



## 4 Conclusions

Injection pressures, subsurface pore pressures, and rates of induced seismicity decreased substantially following the January-April 2013 shut-in of the PVU injection well and subsequent change in injection protocol. These operational changes were made in response to a  $M_L$  4.4 earthquake that occurred 8.2 km northwest of the injection well in January 2013. Wellhead pressures have remained several hundred psi lower since injection resumed in April 2013, compared to the peak value reached just prior to the earthquake. Pressure diffusion modeling indicates that pore pressures decreased to a distance of roughly 4 to 7 km from the well following the changes in injection operations. Rates of induced earthquakes within 10 km of the injection well began decreasing approximately 4 to 6 months after the injection well was shut in. Rates of earthquakes within 5 km of the well decreased 72% after mid-2013, compared to the previous 2.5 years. Rates of earthquakes 5 to 10 km from the well decreased 81%.

The decrease in seismicity rates within 5 km of the well following the operational changes implemented in 2013 is consistent with past observations and theoretical models. For example, near-well seismicity rates decreased substantially following an extended shut-in of the well in mid-2000 and subsequent resumption of injection at a decreased flow rate and following an extended shut-in in late 2005-early 2006. These decreased near-well seismicity rates persisted for 2.5 to 3 years before rebounding. During these periods of decreased near-well seismicity rates, average injection pressures were also relatively low, suggesting a cause-and-effect relationship between pressure and induced seismicity. Results of pore pressure diffusion modeling are consistent with such a relationship, since they indicate that pore pressures decreased to a distance of ~4-7 km from the well following the 2013 operational changes. In addition, a causal relationship between pressure and induced seismicity is consistent with theoretical models, since an increase in pore pressure reduces the effective normal stress across pre-existing faults, allowing slip to occur. Conversely, decreasing the pore pressure allows the effective normal stresses to recover and help prevent fault slip. In addition, an increase in pore pressure causes deformations (strains), which in turn generate stresses that can trigger fault slip. Decreasing the pore pressures causes these strains and associated stresses to relax, reducing the likelihood of slip. Changes in these stresses can occur beyond the region that experiences significant changes in pore pressure and in overlying or underlying geologic layers (Denlinger and Roeloffs, 2016).

A substantial change in rates of earthquakes occurring 5 to 10 km from the injection well following major changes in injection operations has not been observed in the past. No change was observed following the operational changes implemented in mid-2000. A hint of decreased seismicity rates can be seen in the rates of earthquakes with  $M_D < 2.0$  following the 2005-2006 injection well shut-in. However, several stations were intermittently offline during the winters of 2005-2006 and 2006-2007 due to failing power supplies, making variations in the rates of smaller-magnitude events less robust. (This was especially true for areas at greater distances from the well, where the station density was less than near the well.) Hence, the marked decrease in rates of earthquakes in the 5-to-10 km distance range following the operational changes implemented in 2013 was not expected. This observation may indicate that the response time of

seismicity in this distance range to operational changes has decreased, perhaps because of increased diffusivity within the target injection formations or because of how spatial patterns of pressures and stresses have evolved over time. The length of the shut-in implemented in 2013 may also play a role, since it was three times as long as the 2000 shut-in and about 50% longer than the 2005-2006 shut-in. Alternatively, since many of the earthquakes that occurred prior to 2013 in this distance range were in seismicity clusters near the January 2013 earthquake (6 to 8 km northwest of the well), re-distribution of stress from the occurrence of the  $M_L$  4.4 earthquake could have contributed to the subsequent decrease in seismicity rate in this distance range. More in-depth analyses, such as modeling of stress redistribution caused by the rupture of the  $M_L$  4.4 earthquake fault plane or geomechanical modeling of pressure and stress changes caused by PVU fluid injection, would be required to better understand the observed decrease in the 5-to-10 km seismicity rate.

Recent trends of pressures and seismicity rates indicate that the beneficial effects of the operational changes made in 2013 are diminishing. Wellhead pressures, which had fluctuated in 2014-15 with little steady increase, have been increasing more consistently and more steeply since early 2016. Pressure diffusion modeling indicates that pore pressures were increasing at all distances from the well by late 2013. By the end of 2016, pore pressures at distances greater than ~0.3 – 1.4 km had fully recovered and exceeded their previous maximum values by 30 to 100 psi. The rates of induced seismicity within 5 km of the well abruptly rebounded in early 2016, and the average seismicity rate for the year was comparable to that experienced during the two years prior to the 2013 change in operations (2011-2012). Similarly, rates of induced earthquakes 5 to 10 km from the well substantially increased in mid-2016, and rates for the second half of the year were comparable to those experienced prior to 2013. In addition, new seismicity clusters formed in this distance range during 2016, most notably two clusters within Paradox Valley, 5 to 7 km north of the injection well. The rebound in pressures and induced seismicity beginning in early 2016 is consistent with patterns observed after previous major operational changes, which also display rebounds 2.5 to 3 years after the change was implemented.

While the seismicity rates within 10 km of the well decreased after mid-2013 and remained low through 2015, rates of induced earthquakes occurring at greater distances showed no response to the 2013 operational changes. In addition, the geographical distribution of the seismicity induced by PVU injection continued to evolve during this time. The distant seismicity expanded in some azimuthal directions, especially to the southeast, and seismicity is now occurring up to 17-20 km from the well in most directions. Some areas that were experiencing scattered seismicity prior to 2013 developed distinct seismicity clusters, such as within and north of Paradox Valley. The continued evolution of the distant induced seismicity and its insensitivity to operational changes at the well were anticipated. Pressure perturbations introduced at the injection well by operational changes are modulated with distance, with the effects of modest changes become negligible at distances beyond ~10 km. Pore pressures and associated deformational strains and stresses at these large distances will continue to increase over time as injection continues, and the distant seismicity could continue to evolve and expand for several years even if injection were to cease.

## 5 References

- Block, L., and C. Wood, 2009, *Overview of PVU-Induced Seismicity from 1996 to 2009 and Implications for Future Injection Operations*, Technical Memorandum No. 86-68330-2009-22, Bureau of Reclamation, Denver, Colorado, 16 pp.
- Block, L. V., C. K. Wood, W. L. Yeck, and V. M. King, 2014, The 24 January 2013  $M_L$  4.4 earthquake near Paradox, Colorado, and its relation to deep well injection, *Seismological Research Letters*, v. 85, no. 3, 609-624.
- Block, L. V., C. K. Wood, W. L. Yeck, and V. M. King, 2015, Induced seismicity constraints on subsurface geological structure, Paradox Valley, Colorado, *Geophysical Journal International*, v. 200, 1172-1195.
- Block, L., Meremonte, M., Wood, C., and G. Besana-Ostman, 2017, *2016 Annual Report, Paradox Valley Seismic Network, Paradox Valley Unit, Colorado*, Technical Memorandum No. TM-85-833000-2017-22, Bureau of Reclamation, Denver, CO, 110 pp.
- Denlinger, R. P., and E. Roeloffs, 2016, Analysis of seismicity induced by deep brine disposal beneath Paradox Basin, Colorado, in preparation.
- Excel Geophysical Services and International Reservoir Technologies, Inc., 2017, *Paradox Valley Unit 2D Phase 3 Seismic Report, Detailed Site Interpretation*, Report to the Bureau of Reclamation, Solicitation No. R16PS01490, Purchase Order No. R16PX00760, 114 pp.
- King, V. M., L. V. Block, W. L. Yeck, C. K. Wood, and S. A. Derouin, 2014, Geological structure of the Paradox Valley Region, Colorado, and relationship to seismicity induced by deep well injection: *Journal of Geophysical Research*, v. 119, 4955-4978.
- King, V., and L. Block, 2016, *Evidence for Far-Field Reservoir Pressurization, Paradox Valley, Colorado*, Technical Memorandum No. TM-85-833000-2014-42, Bureau of Reclamation, Denver, CO, 97 pp.
- King, V. M., Block, L. V., and C. K. Wood, 2016, Pressure/flow modeling and induced seismicity resulting from two decades of high-pressure deep-well brine injection, Paradox Valley, Colorado, *Geophysics*, v. 81, no. 5, B119-B134.
- Wood, C., V. King, L. Block, and W. Yeck, 2016, The  $M_L$  4.4 Earthquake of January 24, 2013, Near Paradox, Colorado, and Implications for Near-term Injection Operations, Technical Memorandum No. 86-68330-2013-12, Bureau of Reclamation, Denver, Colorado, 151 pp.



# **Appendix A**

## **Pressure**

### **Modeling Methods**



# Introduction

The pressure diffusion modeling performed for this study is based on a simple analytical radial flow model proposed by a previous Consultant Review Board (CRB) (Wang et al., 2015). The CRB recommended that the long-term injection history at PVU and its measured pressure response be used to evaluate the suitability of this model for predicting future wellhead pressures and estimating reservoir pore pressures away from the well. The model as originally presented computes pore pressures as a function of time and distance from the well based on input flow rates. Analysis of the PVU data indicates that this simple radial flow model with constant model parameters is inadequate to match the decades-long pressure trends observed at the PVU injection well. However, incorporating the temporal variation in injected fluid viscosity and the development of a substantial stimulated zone around the borehole into the model (with a radius of at least 100 m) produces a fair fit to the observed pressures.

While more advanced geomechanical models that can accommodate the complex geologic structure at PVU are currently being pursued, the simple analytical modeling approach used for this study is useful for understanding the general trends of pore pressures as a function of time and distance from the well. It is especially useful for computing estimates of how changes in injection operations affect the pore pressure trends within a few km of the injection well over relatively short time periods of a few months to a few years. Having a simple model that can be used to quickly estimate recent pore pressures within a few km of the injection well is important for operational decision-making in the absence of observation wells, since the pressures observed at the wellhead may be quite different than those only a few hundred meters into the injection formation. This is especially true when frequent shut-ins of the well occur, as has been the case since early 2013.

To enable us to more easily use a simple analytical model for evaluating historical pore pressure trends at PVU, we recast the model into one that uses only the observed pressures at the wellhead. Flow rate data are not used; formation pore pressures are simply computed from observed wellhead pressures assuming radial pressure diffusion. Hence, the model can be used to estimate historical pore pressures as a function of time and distance from the well but cannot be used for predicting future pressure trends. Because this model still assumes simple layered geology, its applicability decreases with distance from the well, as impermeable faults may be substantially altering pore pressure patterns at greater distances.

Below we present a mathematical description of the original radial flow model and some results from that model using the injection history at PVU. We then present a mathematical description of the modified model that uses only pressure data. Results from the revised model are presented in the main body of this report.

## Original Radial Flow Model

The original flow model is presented in detail in Wang et al. (2015) and summarized here. The model assumes a pie-shaped semi-infinite reservoir with angle  $\alpha$  and thickness  $H$ , with the injection well at the vertex. The injection flow rate history is discretized into uniform time increments of length  $\Delta t$  and normalized by a nominal or average flow rate,  $Q_o$ . Let  $Q_i$  denote the normalized average flow rate from time  $t_{i-1}$  to time  $t_i$ , where  $t_i = i \Delta t$ . The pore pressure change at radial distance  $r$  and time  $t_j$  after the start of injection is then given by

$$\Delta p(r, t_j) = p^* \sum_{i=1}^j (Q_i - Q_{i-1}) E_1 \left( \frac{r^2}{4D(t_j - t_{i-1})} \right). \quad (\text{A-1})$$

$D$  is the hydraulic diffusivity of the injection formation (reservoir), and  $p^*$  is the characteristic pressure, defined as  $p^* = Q_o / 2\alpha\kappa H$ , where  $\kappa$  is the reservoir mobility.  $E_1$  is the exponential integral function:

$$E_1(x) = \int_x^{\infty} \frac{e^{-u}}{u} du. \quad (\text{A-2})$$

When fitting equation A-1 to the observed pressure history at a well, the values of the diffusivity  $D$  and characteristic pressure  $p^*$  can be varied to try to obtain a good match of the observed and computed pressures. It is not necessary to explicitly define values for  $\alpha$ ,  $\kappa$ , or  $H$ . All model parameters are assumed to remain constant over time.

Changes in pressure computed with the above model using two different values of  $p^*$  and two values of  $D$  are compared to the observed PVU wellhead pressure changes in Figure A-1. The range of  $D$ , 0.1 to 0.2 m<sup>2</sup>/s, is consistent with diffusivity estimates derived from the initial onset of the induced seismicity as a function of distance from the well and with results of early PVU injection tests (King and Block, 2016). The values of  $p^*$  were chosen to obtain a general fit to the observed data. A borehole radius of 10 cm, approximately corresponding to the radius of the wellbore at the depth of the primary injection horizon, was used for the calculations. The daily average PVU flow rate data from 1991 to 2014 were normalized by the average flow rate from July 10, 1991 to December 31, 2014 (248,966 gal/day) and then binned into 30-day intervals to use as input for these models.

The model results presented in Figure A-1 show a poor fit to the observed data. The models using the lower value of  $p^*$ , 130 psi, fit the observed pressures for early times fairly well but substantially underestimate the pressures for all times after mid-2000. The models using the higher value of  $p^*$ , 150 psi, overestimate the early pressures by as much as 1500 psi and

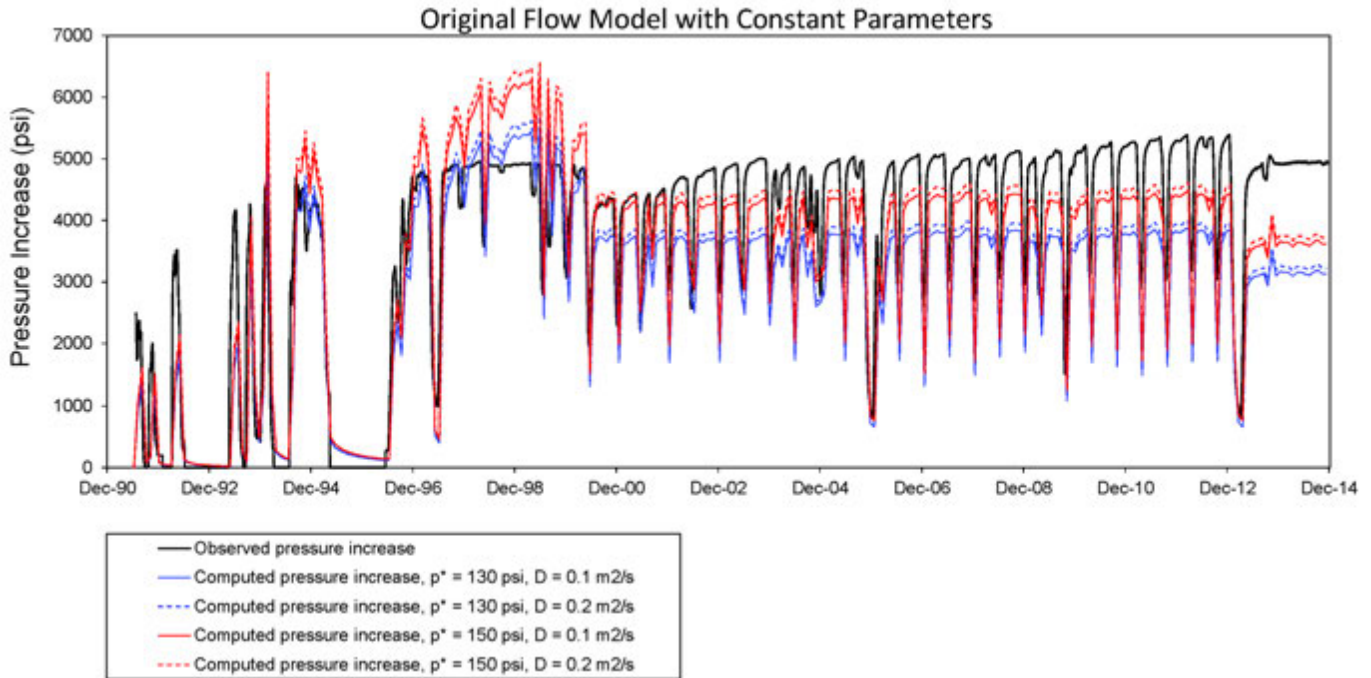


**Figure A-1: Pressure changes computed with the original flow model using two values of  $D$ , 0.1 and 0.2 m<sup>2</sup>/s, and two values of  $p^*$ , 130 and 150 psi. A 30-day running average of the changes in observed wellhead pressure over time is shown in black.**

underestimate pressures for times after 2001. The misfit for all models generally increases with time after 2001.

## Radial Flow Model with Time-Varying Viscosity

One of the reasons that the fit of the original model to the PVU data is so poor is that a substantial change in the viscosity of the injected fluid occurred in January 2002, and this change is not taken into account in the original model. On January 7, 2002, the fluid injected at PVU changed from a 70% brine: 30% fresh water mixture to 100% brine. This change resulted in an increase in fluid viscosity of approximately 31%.

Two parameters in equation A-1 are dependent on the fluid viscosity,  $p^*$  and  $D$ . Recalling that  $p^* = Q_o / 2\alpha\kappa H$ , we can illustrate its dependence on fluid viscosity  $\mu$  by substituting  $\kappa = k / \mu$ , where  $k$  is the reservoir permeability:

$$p^* = \frac{Q_o \mu}{2\alpha k H}. \quad (\text{A-3})$$

This equation illustrates that  $p^*$  is directly proportional to fluid viscosity. In contrast, the diffusivity  $D$  is inversely proportional to fluid viscosity:

$$D = \frac{k}{\mu \phi c_t}, \quad (\text{A-4})$$

where  $\phi$  is the reservoir porosity and  $c_t$  is the total reservoir compressibility. (The remaining parameters in the above equations,  $Q_o, \alpha, k, H, \phi,$  and  $c_t$  are independent of  $\mu$ .)

Given the above relations, we can accommodate the 31% increase in fluid viscosity in the modeling by changing the parameters for times since January 7, 2002 as follows:

$$p^{*'} = 1.31 p^* \quad (\text{A-5})$$

$$D' = \frac{D}{1.31} \quad (\text{A-6})$$

The summation for computing the pressure changes is thus separated into two parts, one for early times when the brine: fresh water mixture was injected and one for later times when 100% brine was injected:

$$\Delta p(r, t_j) = p^* \sum_{i=1}^{ibr-1} (Q_i - Q_{i-1}) E_1 \left( \frac{r^2}{4D(t_j - t_{i-1})} \right) + p^{*'} \sum_{i=ibr}^j (Q_i - Q_{i-1}) E_1 \left( \frac{r^2}{4D'(t_j - t_{i-1})} \right). \quad (\text{A-7})$$

In the above equation,  $ibr$  is the index of the data interval or bin that contains the start date for 100% brine injection (1/7/2002).

The change to 100% brine implemented in 2002 resulted in a decrease to the fluid compressibility of approximately 10%. This change in fluid compressibility also affects the pressures because it alters the total compressibility of the reservoir and hence the diffusivity (equation A-4). However, because the average porosity of the PVU reservoir is low ( $< \sim 5\%$ ), changes in fluid compressibility have a relatively small effect on the total reservoir compressibility and associated diffusivity. For the analyses presented in this report, this effect is ignored.

Results from flow models that incorporate the 2002 change in fluid viscosity are presented in Figure A-2. Compared to results from the original model (Figure A-1), the fit to the observed pressures has improved. However, the modeled pressures still do not fit the observed data well. The model curves show an abrupt increase in pressure in 2002 when the fluid viscosity changes, and subsequent maximum modeled pressures from 2002 to 2012 are fairly constant. In contrast, the increase in observed pressures in 2002 is more gradual than the models predict, and the observed pressures continue to gradually increase through 2012. Furthermore, similar to results

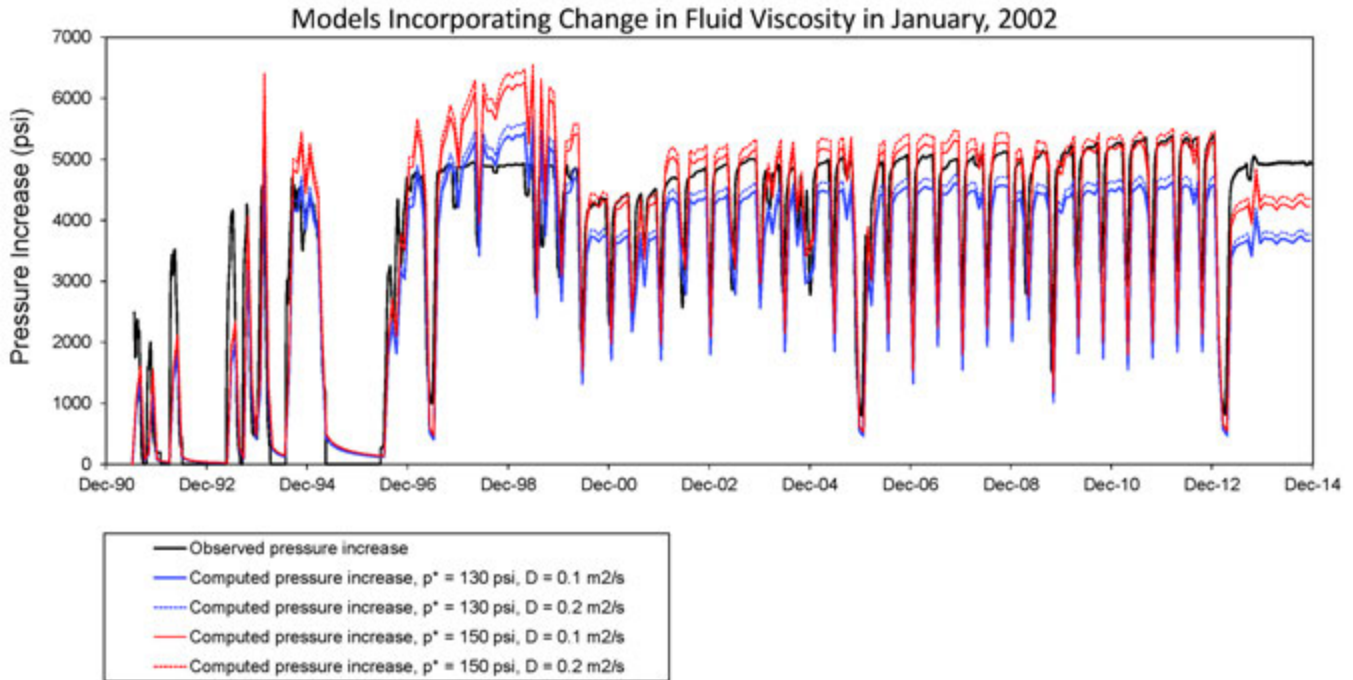


**Figure A-2: Pressure changes computed with the flow model that incorporates time-varying viscosity of the injected fluid. Results were computed using two values of  $D$ , 0.1 and 0.2 m<sup>2</sup>/s, and two values of  $p^*$ , 130 and 150 psi. A 30-day running average of the changes in observed wellhead pressure over time is shown in black.**

for the original model, the revised model still predicts pressures that are too high for most times prior to mid-2000 and too low for times after early 2013.

## Effective Borehole Radius

One other parameter that can be altered to try to improve the model fit is the radius for which the pressures are computed. If the borehole radius has decreased due to scale build-up, a radius smaller than that of the original borehole may be appropriate. In models that explicitly incorporate the borehole, this effect is represented by using a positive skin factor. Conversely, if there is a stimulated zone around the borehole (a region with increased diffusivity), a larger borehole radius would be appropriate. This case would correspond to using a negative skin factor in models that include a borehole. A modeled radius that is either smaller or larger than the actual borehole radius is referred to as an effective (or apparent) borehole radius.

Previous modeling of the PVU pressure-flow data indicate a negative skin factor for the PVU well (King and Block, 2016), corresponding to an increased effective borehole radius. The presence of a stimulated zone around the wellbore is consistent with other information, including: acid stimulation was performed in the PVU well in 1993; injection has occurred at pressures above the fracture propagation pressure for extended periods of time (years), which should cause fractures parallel to the direction of maximum horizontal stress to lengthen; the

180°F difference in temperature between the in-situ reservoir rock and the injected fluid should cause the rock matrix to cool and shrink, thereby opening microfractures; and an aseismic zone has persisted around the well since the injection flow rate was reduced in 2000 (despite increased wellhead pressures), which may be an indication of increased diffusivity near the well (King and Block, 2016).

The use of an increased effective borehole radius, like the use of a negative skin factor in models that include a borehole, is a mathematical way to account for a smaller change in pressure across the zone of increased diffusivity around the well than would be expected if the stimulated zone were not present. Because the magnitude of this pressure change depends on both the spatial extent (diameter) of the stimulated zone and the degree of diffusivity increase within this zone, the effective borehole radius does not have a strict physical meaning. The same effective borehole radius could represent a large stimulated zone with a relatively small increase in diffusivity or a smaller stimulated zone with a relatively large increase in diffusivity.

Models computed with effective borehole radii ranging from 0.1 m (10 cm) to 500 m are presented in Figure A-3. When computing these models, we used a value of 0.115 m<sup>2</sup>/s for the diffusivity, which is the value that fits the move-out of the initial onset of induced seismicity to a distance of about 10 km from the well (King and Block, 2016). The value of  $p^*$  was manually adjusted for each model to try to obtain a good fit to the observed pressures. These values are shown in the labels at the upper right of each plot and range from 150 psi to 625 psi. These models incorporate the 2002 change in fluid viscosity as described above.

Increasing the effective borehole radius improves the fit of the modeled and observed pressure trends at the PVU well. Even a relatively modest increase in effective borehole radius, such as an effective radius of 10 m, causes the computed pressures to increase gradually from 2002 to 2012, better matching the trend in observed pressures. However, a relatively large effective borehole radius is needed to match the pressure trends in 2000 and 2013, when reductions in flow rate and corresponding decreases in wellhead pressures occurred. Models with relatively small radii (0.1 – 10 m) produce curves that predict a larger decrease in pressure than was observed. Models with relatively large radii (250 – 500 m) show pressure trends that better match the data during these transition periods. For the models with large effective borehole radii, the pressures for the early years of injection (prior to ~ 1998-1999) are underestimated, which makes sense if the effective borehole radius took several years to develop. These models do not fit the pressures observed during the injection well shut-in times, when the observed pressures decrease substantially more than the computed pressures (>1000 psi). Such a discrepancy could potentially be caused by fractures around the wellbore that close when pressures fall, decreasing the effective wellbore radius. However, the discrepancy could also indicate that the effective borehole radii used in these models are too large.

We can compare the effective borehole radii used in these models to the skin factors computed from previous PVU pressure-flow modeling by considering the following relation (Mian, 1992):

$$r_{effective} = r_{actual} e^{-skin} \quad (A-8)$$

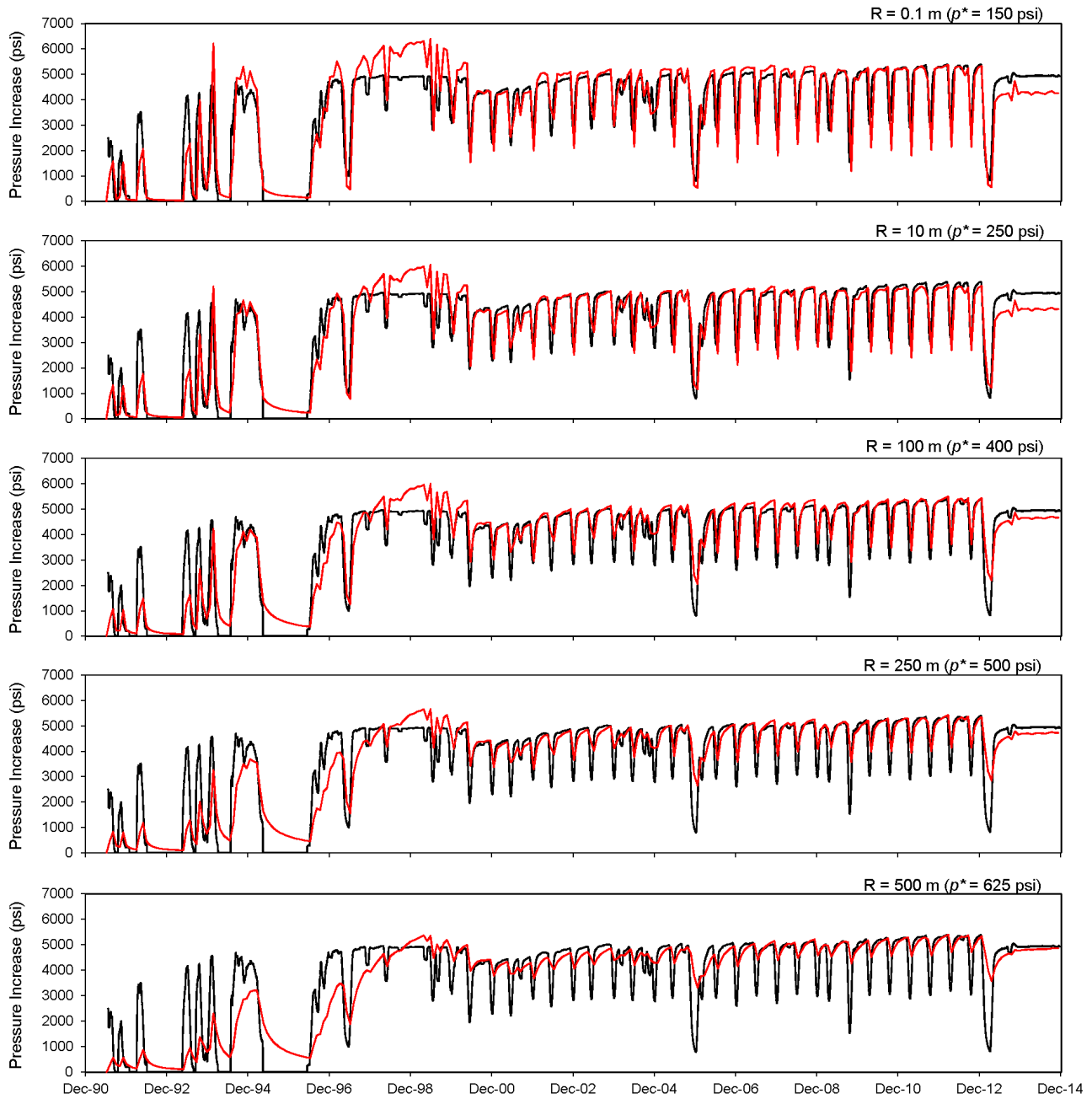


**Figure A-3: Pressure changes computed with the flow model that incorporates time-varying fluid viscosity, for a range of effective borehole radii (red curves). Results were computed using  $D = 0.115 \text{ m}^2/\text{s}$ . For each model, the value of  $p^*$  was manually set to try to fit the observed pressures. The radius (R) and  $p^*$  values are given in the upper right label of each plot. Thirty-day running averages of the changes in observed wellhead pressure over time are shown in black.**

During the previous PVU pressure-flow modeling, model parameters were determined by fitting the computed pressures to the observed pressures independently for the build-up period of each injection cycle (King and Block, 2016). For the time period from mid-2000 through 2012 (the latest build-up period analyzed), the computed values of skin range from -6 to -2, with a median value of -4.6. These computed skin values have large uncertainty because there was strong trade-off between values of skin and values of permeability in the model. Using an actual wellbore radius of 0.1 m (10 cm), equation A-8 yields an effective wellbore radius of 10 m for the median skin value (-4.6) and 40 m for the smallest skin value (-6). An effective borehole radius of 100 m would correspond to a skin value of -6.9. The largest effective wellbore radius assumed in the models presented in Figure A-3, 500 m, would correspond to a skin factor of -8.5.

## Pressure Diffusion Model

To simplify the pressure calculations for historical time periods, we recast the analytical radial flow model described above into a pressure diffusion model that only uses observed wellhead pressures as input instead of flow rates. Doing this eliminates the  $p^*$  parameter, and therefore the only parameters that need to be specified in the modeling are the values of diffusivity and effective wellbore radius. This method is useful for exploring the changes in pressures that have occurred within several km of the injection well in response to changes in injection operations. We derived this alternative formulation from the original flow model as described below. For simplicity, we ignore the change in fluid viscosity during the derivation and subsequently describe how it is accommodated.

First, let  $\Delta p(r, t_j)_i$  represent the pressure increase at radius  $r$  and time  $t_j$  due to the fluid that was injected from time  $t_{i-1}$  to time  $t_i$ . The total pressure increase since the start of injection can then be represented as the summation of the contributions from all past incremental fluid injections:

$$\Delta p(r, t_j) = \sum_{i=1}^j \Delta p(r, t_j)_i . \quad (\text{A-9})$$

By comparing equations A-9 and A-1, we can see that the pressure increase due to the fluid that was injected from time  $t_{i-1}$  to time  $t_i$  is given by:

$$\Delta p(r, t_j)_i = p^* (Q_i - Q_{i-1}) E_1 \left( \frac{r^2}{4D(t_j - t_{i-1})} \right) . \quad (\text{A-10})$$

Similarly, the contribution to the pressure increase observed at the injection well, at an effective wellbore radius  $r_w$  and time  $t_j$  due to the fluid that was injected from time  $t_{i-1}$  to time  $t_i$  is given by:

$$\Delta p(r_w, t_j)_i = p^* (Q_i - Q_{i-1}) E_1 \left( \frac{r_w^2}{4D(t_j - t_{i-1})} \right). \quad (\text{A-11})$$

Solving equation A-11 for  $p^* (Q_i - Q_{i-1})$  and substituting the result into equation A-10 yields:

$$\Delta p(r, t_j)_i = \Delta p(r_w, t_j)_i \frac{E_1 \left( \frac{r^2}{4D(t_j - t_{i-1})} \right)}{E_1 \left( \frac{r_w^2}{4D(t_j - t_{i-1})} \right)}, \quad (\text{A-12})$$

and the total pressure increase since the start of injection at radius  $r$  and time  $t_j$  is then given by:

$$\Delta p(r, t_j) = \sum_{i=1}^j \Delta p(r_w, t_j)_i \frac{E_1 \left( \frac{r^2}{4D(t_j - t_{i-1})} \right)}{E_1 \left( \frac{r_w^2}{4D(t_j - t_{i-1})} \right)}. \quad (\text{A-13})$$

The contributions to the observed pressure increase at the injection well from the incremental fluid injections,  $\Delta p(r_w, t_j)_i$ , are computed from the observed changes in wellhead pressure using a recursive algorithm. To derive this algorithm, we first consider the increase in wellhead pressure observed at time  $t_1$ . From equation A-11 (with  $i = 1$  and  $j = 1$ ), this pressure increase is:

$$\begin{aligned} \Delta p(r_w, t_1)_{obs} &= \Delta p(r_w, t_1)_1 = p^* (Q_1 - Q_0) E_1 \left( \frac{r_w^2}{4D(t_1 - t_0)} \right) \\ &= p^* (Q_1 - Q_0) E_1 \left( \frac{r_w^2}{4D\Delta t} \right). \end{aligned} \quad (\text{A-14})$$

Hence, the first contribution to the wellhead pressures that we need to know ( $\Delta p(r_w, t_1)_1$ ) is simply equal to the observed wellhead pressure increase after the first incremental fluid injection ( $\Delta p(r_w, t_1)_{obs}$ ).

We now consider the increase in wellhead pressure observed at time  $t_2$ . From equation A-11 (with  $i = 1$  to 2 and  $j = 2$ ), this pressure increase is:

$$\Delta p(r_w, t_2)_{obs} = \Delta p(r_w, t_2)_1 + \Delta p(r_w, t_2)_2, \quad (A-15)$$

where

$$\begin{aligned} \Delta p(r_w, t_2)_1 &= p^* (Q_1 - Q_0) E_1 \left( \frac{r_w^2}{4D(t_2 - t_0)} \right) \\ &= p^* (Q_1 - Q_0) E_1 \left( \frac{r_w^2}{4D(2\Delta t)} \right) \end{aligned} \quad (A-16)$$

and

$$\begin{aligned} \Delta p(r_w, t_2)_2 &= p^* (Q_2 - Q_1) E_1 \left( \frac{r_w^2}{4D(t_2 - t_1)} \right) \\ &= p^* (Q_2 - Q_1) E_1 \left( \frac{r_w^2}{4D\Delta t} \right). \end{aligned} \quad (A-17)$$

We can compute the first term,  $\Delta p(r_w, t_2)_1$ , using values that we already know. Solving for  $p^* (Q_1 - Q_0)$  in equation A-14 and substituting the result into equation A-16 gives:

$$\Delta p(r_w, t_2)_1 = \Delta p(r_w, t_1)_{obs} \frac{E_1 \left( \frac{r_w^2}{4D(2\Delta t)} \right)}{E_1 \left( \frac{r_w^2}{4D\Delta t} \right)}. \quad (A-18)$$

Furthermore, the general formula for computing the increase in pressure at time  $t_j$  due to the fluid injection from time  $t_0$  to time  $t_1$  can be derived in the same way and found to be:

$$\Delta p(r_w, t_j)_1 = \Delta p(r_w, t_1)_{obs} \frac{E_1 \left( \frac{r_w^2}{4Dj\Delta t} \right)}{E_1 \left( \frac{r_w^2}{4D\Delta t} \right)}. \quad (A-19)$$

We can compute the second term in equation A-15,  $\Delta p(r_w, t_2)_2$ , by simply subtracting the first term from the observed pressure increase at time  $t_2$ :

$$\Delta p(r_w, t_2)_2 = \Delta p(r_w, t_2)_{obs} - \Delta p(r_w, t_2)_1. \quad (\text{A-20})$$

We now consider the increase in wellhead pressure observed at time  $t_3$ :

$$\Delta p(r_w, t_3)_{obs} = \Delta p(r_w, t_3)_1 + \Delta p(r_w, t_3)_2 + \Delta p(r_w, t_3)_3. \quad (\text{A-21})$$

We have already derived a general formula for computing the first term,  $\Delta p(r_w, t_3)_1$  (equation A-19). From equation A-11 (with  $i=2$  and  $j=3$ ), the second term is:

$$\begin{aligned} \Delta p(r_w, t_3)_2 &= p^* (Q_2 - Q_1) E_1 \left( \frac{r_w^2}{4D(t_3 - t_1)} \right) \\ &= p^* (Q_2 - Q_1) E_1 \left( \frac{r_w^2}{4D(2\Delta t)} \right). \end{aligned} \quad (\text{A-22})$$

We solve equation A-17 for  $p^* (Q_2 - Q_1)$  and substitute the result into equation A-22 above to get:

$$\Delta p(r_w, t_3)_2 = \Delta p(r_w, t_2)_2 \frac{E_1 \left( \frac{r_w^2}{4D(2\Delta t)} \right)}{E_1 \left( \frac{r_w^2}{4D\Delta t} \right)}. \quad (\text{A-23})$$

Since we calculated  $\Delta p(r_w, t_2)_2$  previously, we can now compute  $\Delta p(r_w, t_3)_2$ . Similarly, the general formula for computing the increase in pressure at time  $t_j$  due to the fluid injection from time  $t_1$  to time  $t_2$  is:

$$\Delta p(r_w, t_j)_2 = \Delta p(r_w, t_2)_2 \frac{E_1 \left( \frac{r_w^2}{4D(j-1)\Delta t} \right)}{E_1 \left( \frac{r_w^2}{4D\Delta t} \right)}. \quad (\text{A-24})$$

The third term in equation A-21 can now be computed by subtracting the first two terms from the observed wellhead data:

$$\Delta p(r_w, t_3)_3 = \Delta p(r_w, t_3)_{obs} - \Delta p(r_w, t_3)_1 - \Delta p(r_w, t_3)_2. \quad (A-25)$$

By repeating these steps, we can similarly determine the individual contributions to the wellhead pressure increase due to later fluid injection increments. The recursive algorithm can be written as follows:

1. Compute the pressure increase at all times  $t_j$  due to the fluid injection from time  $t_0$  to time  $t_1$ . For  $j = 1, N$ , where  $N$  = the number of time increments:

$$\Delta p(r_w, t_j)_1 = \Delta p(r_w, t_1)_{obs} \frac{E_1\left(\frac{r_w^2}{4Dj\Delta t}\right)}{E_1\left(\frac{r_w^2}{4D\Delta t}\right)} \quad (A-26)$$

2. Recursively compute contributions for later fluid injection increments. For  $k = 2, N$ :

$$\left\{ \Delta p(r_w, t_k)_k = \Delta p(r_w, t_k)_{obs} - \sum_{i=1}^{k-1} \Delta p(r_w, t_k)_i \right. \quad (A-27)$$

For  $j = k+1, N$ :

$$\left. \Delta p(r_w, t_j)_k = \Delta p(r_w, t_k)_k \frac{E_1\left(\frac{r_w^2}{4D(j-k+1)\Delta t}\right)}{E_1\left(\frac{r_w^2}{4D\Delta t}\right)} \right\} \quad (A-28)$$

After the incremental contributions to the observed wellhead pressure increase (for all times) have been computed, then equation A-13 can be used to compute the pressures at an arbitrary radius  $r$  from the well.

To accommodate the 31% increase in fluid viscosity that occurred in January, 2002, the value of  $D$  is simply replaced with  $D'$  ( $= D/1.31$ ) for time periods starting in January 2002 in equations A-28 and A-13. Hence, if  $ibr$  is the index of the time increment that contains the start date for 100% brine injection (1/7/2002),  $D'$  is used when  $j \geq ibr$  in equation A-28 and when  $i \geq ibr$  in equation A-13.

## References

- King, V., and L. Block, 2016, *Evidence for Far-Field Reservoir Pressurization, Paradox Valley, Colorado*, Technical Memorandum No. TM-85-833000-2014-42, Bureau of Reclamation, Denver, CO, 97 pp.
- Mian, M. A., 1992, *Petroleum Engineering Handbook for the Practicing Engineer, Volume 2*, PennWell Publishing Company Tulsa, OK, 688 pp.
- Wang, H., Detournay, E., Dusseault, M., Fehler, M., and C. Frohlich, 2015, *Report from the Consultant Review Board on Paradox Valley Unit – MASIP/Induced Seismicity Meeting No. 1, January 28-31, 2015, Grand Junction, Colorado*, for the Bureau of Reclamation, 35 pp.